Using Electrospray Ionization Mass Spectrometry for Understanding Metal-Ligand Interactions: Silver and Copper Complexes with Organophosphorus Pesticides, and Uranium, Vanadium and Iron Complexes with Amidoxime Ligands

A Dissertation

Presented in Partial Fulfillment of the Requirements for the

Degree of Doctorate of Philosophy

with a

Major in Chemistry

in the

College of Graduate Studies

University of Idaho

by

Adetayo Musbau Mustapha

Major Professor: Sofie P. Pasilis, Ph.D.

Committee Members: Chien M. Wai, Ph.D.; I. Francis Cheng, Ph.D.; Armando McDonald, Ph.D.

Department Administrator: Ray von Wandruszka, Ph.D.

October 2015

Authorization to Submit Dissertation

This dissertation of Adetayo M. Mustapha, submitted for the degree of Doctorate of Philosophy with a Major in Chemistry and titled "Using Electrospray Ionization Mass Spectrometry for Understanding Metal-Ligand Interactions: Silver and Copper Complexes with Organophosphorus Pesticides, and Uranium, Vanadium and Iron Complexes with Amidoxime Ligands," has been reviewed in final form. Permission, as indicated by the signatures and dates below, is now granted to submit final copies to the College of Graduate Studies for approval.

Major Professor: _____ Date: _____
Sofie P. Pasilis, Ph.D.

Committee Members: _____ Date: _____
Chien M. Wai, Ph.D.

_____ Date: _____
I. Francis Cheng, Ph.D.

_____ Date: _____
Armando McDonald, Ph.D.

Department Administrator: _____ Date: _____
Ray von Wandruszka, Ph.D.

Abstract

Metal-ligand interactions are important in such diverse areas as environmental remediation, drug development, and biochemistry. Potentiometric and spectroscopic techniques, including UV-Visible, infrared, Raman, and NMR spectroscopies, are commonly used to investigate metal-ligand interactions. However, ESI-MS is a valuable technique for accurate determination of complex stoichiometric ratios, and for the study of the gas-phase chemistry of metal complexes with organic ligands. This dissertation presents two broad areas where ESI-MS has been used to study such complexes.

In the first area, I investigated the analytical importance of transition metal interactions with phosphorothioate and phosphorodithioate pesticides. These pesticides are important subclasses of organophosphorus pesticides commonly used in agriculture to control pests in fruits and vegetables. Using ESI-MS, I examined how the interactions of three phosphorothioate pesticides (fenitrothion, parathion, and diazinon) and one phosphorodithioate pesticide (malathion) with silver and copper ions affects the mass spectral detection of the resulting complexes. My results show that each pesticide forms silver and copper complexes that significantly improve their detection using ESI-MS. I also found that these metal-pesticide complexes do not undergo the thiono-thiolo rearrangement reaction during collision-induced dissociation, unlike protonated phosphorothioate ions.

In the second part of the dissertation I explore the use of ESI-MS for characterization of gas-phase complexes that arise from uranyl(VI), vanadium(V) and iron(III) interactions with 2,6-dihydroxyiminopiperidine (DHIP) and N^1, N^5-dihydroxypentanediimidamide (DHPD) in aqueous solutions. I also investigated uranyl(VI) interactions with N^1, N^5-dihydroxyethanediimidamide (DHED). Uranium is an important fuel for nuclear power

generation, and there is much interest in the possibility of its extraction from seawater using amidoxime-functionalized sorbents. Vanadium and iron can compete with uranium for binding sites on these sorbents. My results show that DHIP binds uranyl(VI) more effectively that DHPD or DHED, forming ions having uranyl(VI):DHIP stoichiometric ratios of 1:1, 1:2, and 2:3. Vanadium(V) forms 1:1 and 1:2 vanadium(V):DHIP complexes, while iron(III) forms only a 1:2 iron(III):DHIP complex. With DHPD, vanadium(V) forms only a 1:2 vanadium(V):DHPD complex, while iron(III) forms both 1:2 and 1:3 complexes with DHPD. I also observed that gas-phase uranyl(VI)-DHIP complexes are less likely to form in the presence of either vanadium(V) or iron(III).

Acknowledgements

It would not have been possible to pursue this doctoral program or even dream of writing a doctoral dissertation without the approval and support of God Almighty and the kind people around me. It is not be possible to mention everyone here, but I am extremely grateful to everyone who contributed one way or the other towards my being able to obtain a Ph.D. degree.

First I would like to express my sincere appreciation to my Ph.D. advisor, Dr. Sofie P. Pasilis for her support during my program. Your advice and mentoring has made me develop into a better research scientist. I am very lucky to have had you as my major advisor, thank you for your patience and understanding.

I would also like to thank my committee members Drs. Chien M. Wai, I. Francis Cheng, and Armando McDonald, for serving on my committee. I am so fortunate to have had each of you on my committee and to have had the advantage of your wealth of experience. Your suggestions have been invaluable to my research work.

To all the students I have worked with in the lab: Ruma Joshi, Jacob Donton and Justin Anast, and all the chemistry departmental staff, Cindy Bogar, Deb Cissell, Ashley Bogar, Terry Evans, Dave Sergent, and others, I thank you all for your help and contributions to the success of this dissertation

I would like to acknowledge all the people and organizations that provided me with funding support during my time at UI. I would like to thank Dr. and Mrs Renfrew for the Malcolm Renfrew summer scholarships I received each summer, as well as the Graduate and Professional Students Associations of the University of Idaho (GPSA-UI) and the

National Society of Black Engineers, University of Idaho Chapter (NSBE-UI) for travel grant awards. Thank you all for your generosity.

Finally, I have to specially thank my parents Alidu Tapha and Mojisola Mustapha, who are also my mentors, for guiding, protecting, and providing for me. To my lovely wife Jokotade Mustapha, I thank you more for the patience, love, and the perseverance you showed throughout my program. I hope that my quest for more success would not prevent me from making it up to you. I also thank my brothers and my sister for their constant love, prayers and support, as well as all my friends here in Moscow Idaho, for their support and encouragement. Thank you everyone!!!

Dedication

This dissertation is dedicated to my parents, Alidu and Mojisola, and my wife, Tade. Thank you all for your prayers.

Table of Contents

List of Figures

List of Tables

List of Abbreviations

CID	Collision-Induced Dissociation
CRM	Charged Residue Model
DES	Desferrioxamine B
DESI	Desorption Electrospray Ionization
DFT	Density Functional Theory
DHED	N^1,N^2-dihydroxyethanediimidamide
DHIP	2,6-dihydroxyiminopiperidine
DHPD	N^1,N^5-dihydroxypentanediimidamide
DZ	Diazinon
EDTA	Ethylenediaminetetraacetic acid
EPR	Electron Paramagnetic Resonance
ESI	Electrospray Ionization
ESI-MS	Electrospray Ionization Mass Spectrometry
FN	Fenitrothion
FO	Fenitrooxon
GC	Gas Chromatography
GC-MS	Gas Chromatography/Mass Spectrometry
HPLC	High Performance Liquid Chromatography
HSAB	Hard-Soft Acid-Base
IEM	Ion Evaporation Model
LC-ESI-MS	Liquid Chromatography Electrospray Ionization Mass Spectrometry
LOD	Limit of Detection
MT	Malathion
m/z	Mass-to-charge ratio
NMR	Nuclear Magnetic Resonance
NTA	Nitrilotriacetic acid
OP	Organophosphorus Pesticides
PT	Parathion

QqQ	Triple quadrupole
Q-TOF	Quadrupole – Time of Flight
S/B	Signal-to-Background ratio
TOF/MS	Time of Flight-Mass Spectrometry
UV-Vis	Ultraviolet-Visible

Chapter 1

Introduction and Literature Review

1.1 Importance of Metal-Ligand Interactions

Metal-ligand interactions are of major interest due to their important role in many environmental and biochemical systems. The chemistry of metal-ligand systems is important to environmental remediation, to metal transport in the body, and to the development of therapeutic drugs, to name a few. In environmental remediation, for example, heavy metals such as cadmium, lead, arsenic, mercury, etc. in contaminated soil may be removed based on favorable interactions between the metals and organic ligands that preferentially chelate with them.[1, 2, 3] Common examples of such chelating agents include ethylenediamine-tetraacetic acid, tartaric acid, citric acid, and oxalic acid.

In biochemical processes, many important metal-ligand interactions have been identified.[4, 5] For example, the interactions between iron and hemoglobin make oxygen transport in the body possible, and the presence of zinc in carbonic anhydrase enzyme allows the enzyme to perform its catalytic function. Protein folding, which is very important in understanding the structure and function of a given protein can be induced by interactions with a metal.[6, 7] The actions of many common drugs are also based on metal-ligand interactions. Cisplatin, for example, is a cancer treatment drug containing platinum metal, which interacts with the guanine bases of the DNA of cancerous cells.[8, 9]

All these diverse applications mean that metal-ligand interactions have a great importance, and there is need to fully understand the basic solution equilibria of metal-ligand systems. Understanding the solution equilibrium chemistry allows the behavior of metals and ligands in environmental or biochemical systems to be modeled, and provides a better interpretation of the present and future large scale effects of these systems.

1.2 General Overview of my Dissertation

In this dissertation, I discuss metal-ligand interactions in two very different systems of environmental importance. First, I examine how metal-ligand interactions in silver or copper organophosphorus pesticide complexes can be exploited to improve the detection of poorly ionized pesticides during analysis using electrospray ionization mass spectrometry (ESI-MS). Secondly, I discuss the use of ESI-MS to study the gas-phase interactions between uranyl(VI), vanadium(V) and iron(III) with 2,6-dihydroxyiminopiperidine (DHIP) and N^1, N^5-dihydroxypentanediimidamide (DHPD) in aqueous solutions. I will also compare uranyl(VI)-DHPD complexes with the complexes uranyl(VI) forms with N^1, N^5-dihydroxyethanediimidamide (DHED). Uranyl(VI) is an important metal for nuclear power generation, and there is much research on the feasibility of its extraction from seawater using amidoxime-functionalized sorbents. Iron(III) and vanadium(V) are among the elements that could compete with uranyl(VI) for sites on the sorbent. By investigating the gas-phase interactions between these metal ions (uranyl(VI), iron(III) and vanadium(V)) and the amidoxime ligands mentioned above, I hope to add to the current understanding of uranyl(VI)-amidoxime chemistry.

In Section 1.3, I first discuss the most common techniques for investigating metal-ligand systems, and then I discuss how and why ESI-MS can be a powerful tool for the study of metal-ligand complexation chemistry, as well as some of the difficulties with using ESI-MS for this purpose.

1.3 Common Techniques for Studying Metal-Ligand Chemistry

In other to fully understand the solution chemistry of metal-ligand systems, information about the number of complexes formed in solution, the stoichiometric ratios of these complexes, and their formation constants is essential. Determining stoichiometric ratios is important for understanding complexation chemistry and structure, while the formation constant provides information about the strength or affinity of the ligand for the metal ion. In addition, investigating the effects of pH and metal-to-ligand mole ratios on speciation for a particular metal-ligand system is important for a complete understanding of the metal-ligand equilibrium chemistry. Common techniques used to obtain this type of information are potentiometry, UV-Visible spectroscopy, nuclear magnetic resonance (NMR) spectroscopy, Raman spectroscopy, and infrared spectroscopy.

1.3.1 Potentiometry

Potentiometry is an electroanalytical technique that is used to measure the electrode potential of a solution as a function of an analyte's activity. The activity of an analyte taking part in a reversible electrochemical reaction at an electrode is related to the cell potential (E) by the Nernst equation (Equation 1.1)

$$E = E^o + \frac{RT}{nF} \ln \frac{a_{red}}{a_{ox}}$$ Equation 1.1

where E is the standard cell potential at T = 25°C, R is the gas constant, F is the Faraday constant, n is the number of electrons involved, and a_{red} and a_{ox} are the activities of reduced and oxidized analyte species respectively.

A potentiometry setup for metal-ligand studies consists of two electrodes: a reference electrode, and an indicator (or measuring) electrode. The electrodes, which are half-cells, produce a cell potential when placed in a solution. This cell potential is the difference in potential between the two half cells. The electrode potential of the reference electrode is known, and independent of the analyte concentration. Reference electrodes commonly used in metal-ligand studies are the saturated calomel electrode and the silver/silver chloride electrode. An indicator electrode, on the other hand, is a half cell electrode whose electrode potential varies with the concentration of a given analyte in solution. Examples of indicator electrodes include metal electrodes, membrane electrodes (e.g. the pH electrode), and ion selective electrodes.

In metal-ligand studies, potentiometric techniques are often used to determine complex formation constants and stoichiometric ratios. The formation constant is determined using a potentiometric titration. During a potentiometric titration, the variation in solution electrode potential with stepwise addition of a titrant is measured. A computer program is used in order to estimate the formation constants and determine the stoichiometric ratios of the complexes in solution from the titration data. Common examples of computer programs used are HYPERQUAD,[10] MINIQUAD,[11] PSEQUAD,[12] and BEST.[13]

Potentiometry is the most accurate technique for determining formation constants of metal complexes. It can be used for metal-ligand systems that form colored or turbid complexes in solution. The titration process, which can be automated, allows detection of complexes of different stoichiometries in solution. However, the major disadvantage of the potentiometric technique is that it is an indirect measurement, because data has to be subjected to computation methods before the complex stoichiometric ratios and formation constants can be determined. These computation methods can be tedious and require multiple assumptions.[14] As pointed out by Pistolis et al.,[15, 16] some of these experimental assumptions may not be correct. In addition, potentiometric data does not give information about the various modes of coordination between the ligand and the metal ion. Such information can only be obtained using NMR or other spectroscopic techniques, such as UV-Visible spectroscopy, infrared spectroscopy, or Raman spectroscopy.

1.3.2 UV-Visible spectroscopy

The metal-ligand chemistry can also be investigated by monitoring the interaction of the metal-ligand containing solutions with electromagnetic radiation. In UV-Visible spectroscopy, the compound absorbs light at a particular wavelength. The absorption observed is due to electronic transitions of σ, π or non-bonding (n) electrons within the ligand molecule from ground states to excited states, or within the *d*, and *f* orbitals of the metal. Common examples of electronic transitions that could result in UV-Visible absorption spectra of a metal complex are σ to σ*, n to σ*, π to π* and n to π* within the ligand molecule, *d-d* and *f-f* transitions within the metal ion, and charge transfer across the metal and ligand. The wavelength at which a compound absorbs light is a function of the

chromophore it contains, while the amount of absorbance is a measure of the concentration of the analytes in the solution and is governed by Beer's law. Different chromophores have different absorbing wavelengths and this is due to the different electronic transitions between the various states.

In metal-ligand studies, UV-Visible spectroscopy can be used to determine the number of species in solution, complex stoichiometric ratios, and formation constants. The complex must contain a chromophore that absorbs light in the UV-Visible region before this technique can be use to investigate its solution equilibrium chemistry.

The number of metal-ligand species in a solution is determined using UV-Visible spectroscopy by acquiring spectra for a number of solutions containing a fixed concentration of the metal but increasing ligand concentrations at a particular pH. The acquired spectra are superimposed on each other to determine if there is an isosbestic point (a point where the superimposed spectra intersect). The presence of one isosbestic point indicates that there are two species in solution: free ligand and one metal-ligand complex, while the presence of two isosbestic points indicate the presence of free ligand and two metal-ligand complexes of different stoichiometric ratios, etc.[17]

Stoichiometric ratios of metal-ligand complexes can be determined using the method of continuous variation, mole ratio, or slope ratio. The most common method is the method of continuous variation, and this involves mixing solutions containing equal concentrations of metal and ligand at different volumetric ratios, while keeping the total volume and solution pH constant. The absorbances of a series of prepared solutions are measured and a graph is plotted showing measured absorbances as a function of volume mole fraction of

metal added. The volume mole fraction that gives the maximum absorbance corresponds to the complex stoichiometric ratio.

Compared to potentiometry, UV-Visible spectroscopy is not an accurate technique for the determination of complex formation constants. However, it is still used to estimate complex formation constants because of its simplicity and capability for fast data generation compared to potentiometry. In UV-Visible spectroscopy, formation constants are usually determined using titrations. The absorbance of the solution containing a metal is monitored while it is being titrated with the ligand at constant pH. Apart from spectrophotometric titrations, complex formation constants can also be estimated with UV-Visible spectroscopy using the method of corresponding solutions and the competitive method, each of which has been explained in detail in references 17 and 18.

UV-Visible spectroscopy is a convenient method for investigating metal-ligand interactions. Spectra are easy to collect and mostly simple to interpret. However, the technique is limited to metal-ligand systems that contain a chromophore. Also, low analyte concentrations must be used due to the fact that the Beer's law relationship does not hold at high concentrations. UV-Visible absorption spectra are highly dependent on solvent polarity, as this affects molecular absorption. UV-Visible spectroscopy is most effectively used to determine complex stoichiometry when a single complex is formed in solution, as formation of multiple complexes makes data interpretation difficult. In addition, the determination of the complex formation constant is limited to metal-ligand complexes having a 1:1 stoichiometric ratio. Determination of formation constants for metal-ligand complexes having higher stoichiometric ratios can be difficult to achieve.[17, 18]

1.3.3 Infrared spectroscopy

Infrared and Raman spectroscopies can also be used to investigate metal-ligand interactions. Infrared spectroscopy measures the changes in vibrational and rotational energies of the bonds in a molecule when it is exposed to infrared radiation. A molecule can undergo different types of vibrations, such as symmetric/asymmetric stretching or bending (in-plane bending: rocking, scissoring, or out-of-plane bending: twisting, wagging). Absorption of IR radiation occurs when there is a change in the dipole moment during vibration. Infrared spectroscopy is used to identify the type of bonding and the functional groups in a molecule.

In metal-ligand studies, infrared spectroscopy is generally used to investigate the degree of interaction between a metal ion and a ligand. This is achieved by monitoring the effect of metal ion addition on the vibrational mode of a given bond or ligand functional group. Infrared spectroscopy, unlike potentiometry, can be used to determine which bond or atom in a ligand coordinates with the metal ion. Infrared spectroscopy can be used to determine complex formation constants, but its application is limited by low sensitivity compared to potentiometry. This is due to the relatively low molar absorptivities of molecules in the infrared region, meaning that solutions having relatively high analyte concentrations have to be prepared. In addition, absorption by solvents, especially water, in the infrared region makes infrared measurement difficult.

1.3.4 Raman spectroscopy

Unlike infrared spectroscopy, Raman spectroscopy measures the scattering of light by a substance when that substance is exposed to visible, ultraviolet, or infrared radiation emitted from a laser. Laser irradiation leads to excitation of molecules to a virtual state after absorption of a photon of energy from the source. The absorbed photon causes a brief distortion of electrons around the molecule's bond. The distorted electrons return to their normal state by subsequently reemitting a photon, which is known as scattered radiation. A large percentage of the scattered radiation has energy equal to the energy of the excitation radiation, and this is referred to as Rayleigh scattering. Only a small amount of the emitted radiation is due to inelastic scattering, in which the energy of the emitted radiation is higher or lower than the energy of the exciting radiation. When the energy of the emitted (scattered) radiation is of lower energy than the excitation energy, it is called Stokes scattering. Anti-stokes scattering is observed when the energy of the emitted scattered radiation is higher than the energy of the excitating radiation. Raman measurements are based on inelastic scattering of radiation, and the energies of scattered radiation are characteristics of the vibrational energy of the bonds present in the molecule.

The applications of Raman spectroscopy are similar to those of infrared spectroscopy, as it can be used to investigate and determine the mode of coordination between a metal and a ligand. The technique is not sensitive because only a small fraction of the emitted radiation is due to Raman scattering. Thus, solutions to be investigated have to contain high concentrations of both metal and ligand. In addition, the technique suffers from high background due to solvent vibrational modes. Solvent vibrational modes may have to

be identified and subtracted from a spectrum before spectral intensity can be correlated with the analyte concentration. Despite these disadvantages, Raman spectroscopy has been used to determine formation constants of some complexes, though with low reproducibility.

1.3.5 Nuclear magnetic resonance spectroscopy

NMR spectroscopy is another technique that can be used to investigate metal-ligand interactions. NMR spectroscopy measures the nuclear spin of an atom in the presence of a magnetic field.[19] NMR is a powerful tool for structural characterization and identification of organic and inorganic compounds.

In metal-ligand interaction studies, NMR is used to investigate the binding mode of a metal ion to the ligand. This can be done using the changes in the ^{1}H, ^{13}C, ^{15}N, etc. ligand chemical shifts due to changes in the chemical environment induced by the presence of the metal ion. NMR can be used to determine the stoichiometric ratio and formation constant of a metal-ligand complex. For a metal-ligand system under slow exchange conditions (i.e. the exchange between the free and bound ligands occurs at a very slow rate such that two peaks are observed in the spectrum), the formation constants can be determined by first determining the concentrations of the free and bound components in solution. This can be achieved by first integrating the intensities of the relevant signals, then creating a calibration plot of intensity vs. concentration. The concentrations of the free and bound components can then be estimated from the calibration plot. The formation constant of a metal-ligand complex under fast exchange conditions (i.e. the exchange between free and bound ligands occurs rapidly, such that a single peak is observed in the spectrum) can be determined using

any of several methods: a graphical method for weak complexes, a chemical shift titration, competitive techniques, and relaxation time techniques.[19]

One of the advantages of NMR over other techniques in metal-ligand studies is its specificity. Different nuclei do not interfere with each other. This is because of the large resonance range of the nuclei that makes it impossible for signals from two different nuclei to be observed simultaneously.[19] In addition to formation constants, NMR can be used to determine metal-ligand reaction kinetics and exchange, complex structure, and metal-ligand coordination modes.

NMR, like other techniques discussed above, does not give direct information about the stoichiometric ratios of complexes in solution, and the complex formation constant determination is usually limited to 1:1 and 1:2 metal-complexes.[19] In systems that contain mixed metal complexes or polynuclear species, accurate determination of the formation constants and stoichiometric ratios becomes even more challenging.

1.4 Electrospray Ionization Mass Spectrometry

In electrospray ionization mass spectrometry (ESI-MS), many of the difficulties in determining stoichiometric ratios of multiple complexes are overcome. ESI-MS has many other advantages and disadvantages for the study of complex equilibria. These will be discussed in this section. ESI-MS is used to measure the mass-to-charge ratio (*m/z*) of ions arising from species in solution. The *m/z* values can provide direct information about the stoichiometric ratios of solution complexes. The mechanism of ion generation in ESI-MS, the advantages and disadvantages of the technique over the techniques discussed earlier

(potentiometry, UV-Visible spectroscopy, infrared and Raman spectroscopies, and NMR), and various applications to metal-ligand studies are presented in the following sections.

1.4.1 History

ESI-MS is a useful tool for studying metal-ligand interactions. It was first introduced in 1968 by Malcolm Dole while he was trying to determine the molecular mass of polystyrene dissolved in a mixture of benzene and acetone.[20] He discovered that spraying a solution through a narrow capillary to which a voltage was applied produced charged droplet ions. This process, which is called electrospray, will be discussed in detail later in Section 1.4.2. Dole's apparatus consisted of a hollow needle through which the polystyrene solution was sprayed, and a spray chamber where the solution underwent solvent evaporation. The spray chamber consisted of an inlet and an outlet for nitrogen nebulizing gas, and a collimating lens that directed the gaseous analytes towards nozzle and skimmer apertures. The nozzle and skimmer chamber were under a pressure of 1×10^{-4} torr, maintained by mechanical and diffusion pumps. Charged ions were detected using a Faraday cage and grid system. He found that the gas-phase polystyrene ions had molecular masses in the kilodalton range. Using his apparatus, Dole was unable to distinguish between doubly-charged dimers and singly-charged monomers and had difficulties in determining *m/z* from the detector output. The *m/z* of the polymer was estimated using equations that incorporated the current and voltage values from the orifices, needle tip, Faraday cage, and grid detector systems.

John Fenn developed the method further by incorporating a quadruople mass analyzer into the instrumental setup. He demonstrated that electrospray ionization could be used to generate both positive and negative gas-phase ions by analyzing salt solutions

containing LiCl, NaI, or $(NH_4)_2CO_3$ dissolved in a mixture of methanol and water.[21, 22] Subsequent work by Fenn and coworkers demonstrated the effectiveness of ESI-MS for the analysis of peptides and proteins, which have molecular masses in the kilodalton range. They showed that proteins and other compounds of high molecular mass can be analyzed using mass analyzers of modest *m/z* range, due to the fact that many large molecules can become multiply charged during electrospray.[23-25] Fenn was awarded a Nobel Prize in 2002 for his contribution towards the development of ESI-MS.

1.4.2 Gas-phase ion formation during electrospray ionization

In ESI, the formation of gas-phase ions from a solution containing ionic or neutral species follows three major steps: 1) the production of a plume containing charged droplets, 2) solvent evaporation from the charged droplets, and 3) the ejection of ions from the charged droplets (Figure 1.1).[26, 27] In the first step, a solution is passed through a stainless steel or silica capillary (also called a spray needle) which is under an applied voltage of ~2-5 kV. According to Kebarle et al,[27] the applied voltage generates an electric field which penetrates the liquid around the capillary tip.

For an electrospray process operating in positive ion mode (a positive voltage applied to the capillary), the electric field will result in the separation of ions, with positively charged ions drifting towards the liquid surface, and negatively charged ions moving away from the surface. The accumulated positively charged ions around the liquid surface at the capillary tip are drawn towards an oppositely charged metal plate (which acts as a counter electrode), resulting in the formation of a cone-shaped region of liquid at the capillary tip, called a Taylor cone (Figure 1.1). At a sufficiently high electric field, the surface tension can

no longer hold the liquid together because of the increased charge density at the Taylor cone, resulting in ejection of positively-charged ion-enriched droplets from the cone's tip. The ejected charged droplets move downstream towards the counter electrode based on a potential gradient. The polarity of the voltage applied at the capillary tip and metal plate can be switched so that either positive or negative analyte ions in solution can be investigated. The continuous production of charged droplets is sustained by electrochemical reactions at the metal-solution interface at the capillary tip and at the metal electrodes at the mass analyzer entrance. The electrochemistry of the electrospray process will be discussed in detail in the next section.

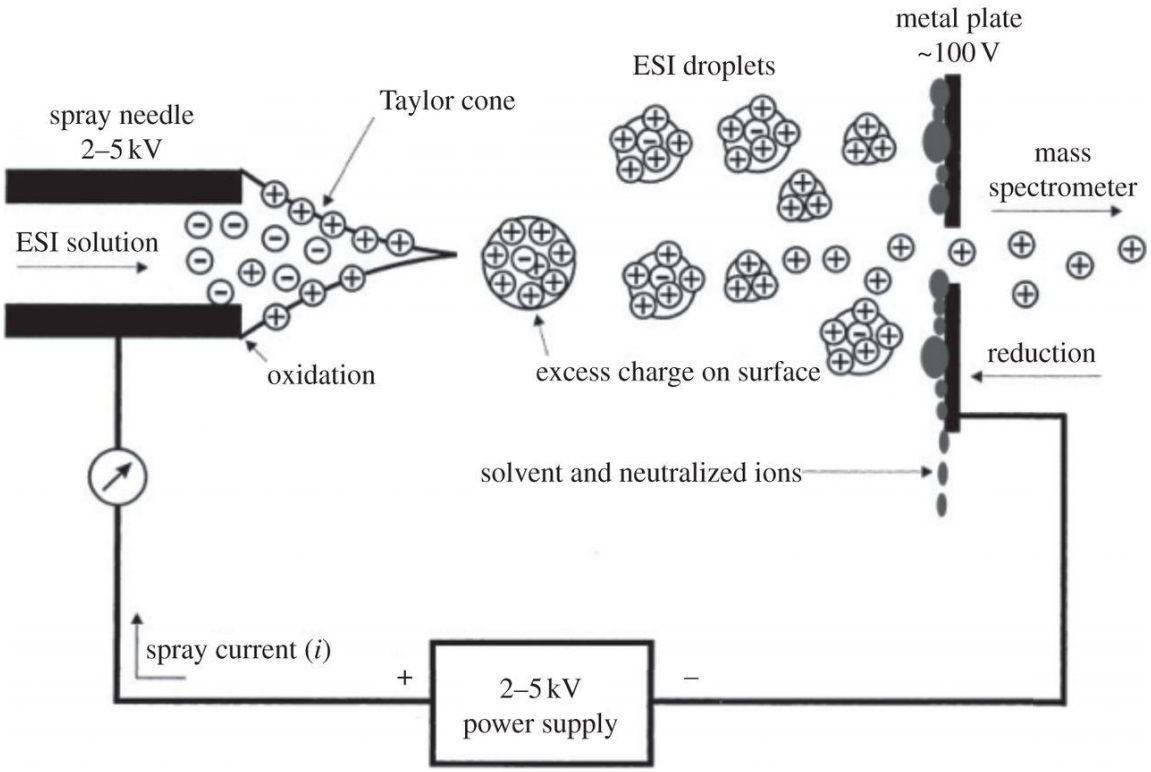

Figure 1.1 Mechanism of gas phase ion formation during electrospray ionization. Figure reproduced with permission from Reference 29.

The charged droplets in the plume undergo solvent evaporation, forming smaller droplets. The continuous evaporation of solvent from the charged droplets leads to an increase in the charge density in the droplet. The high-density charged droplets undergo coulombic explosions when the repulsive forces between the ions within the droplet are higher than the surface tension, forming smaller charged droplets. This solvent evaporation process is continuously repeated until the charged droplets reach ~10 nm in diameter.

There is some debate as to whether the gas-phase ions from these nano-sized charged droplets are formed following the charged residue model (CRM) or the ion evaporation model (IEM). In the CRM, which was developed by Dole,[20] the charged droplet will continue to experience solvent evaporation until bare singly (or multiply) charged gas-phase ions are formed. In the IEM, developed by Iribarne and Thomson,[28] singly (or multiply) charged ions are ejected from the charged droplet's surface, leaving behind a solvent droplet. In general, it was concluded that either of the models may be applicable, with large ions such as proteins or dendrimers following the CRM, while smaller analytes probably follow the IEM. Whatever model is used, the gas-phase ions formed are accelerated towards the mass analyzer by the cone voltage that is applied between the capillary or spray needle and metal endplate (Figure 1.1). Neutral species and excess solvent molecules, which are unaffected by the electric field, are swept out of the spray chamber by the nebulizing gas, usually nitrogen. The gas-phase ions formed are separated based on their *m/z*, and later passed to a detector, where the ion intensities are measured. The intensities of the ions are plotted against their *m/z* to give a mass spectrum. In the mass spectrum, the peak due to the ion with the highest intensity is called the base peak, and its abundance is set to 100. The

relative abundances of other ions in the spectrum are thereafter given as a percentage of the base-peak height.

1.4.3 Electrochemistry of electrospray ionization

The electrochemical process that takes place during electrospray ionization has been extensively discussed.[26, 27, 30-35] According to Blades et al.,[36] the electrospray apparatus can be seen as a special form of electrolytic cell, where ion transfer occurs through the gas phase instead of through the solution phase as in a conventional electrolytic cell. Van Berkel et al.[30, 35] noted that the typical configuration for electrospray ionization is one of a two-electrode system, where one electrode is the metal capillary of the ion source (the working electrode), and the second electrode is the sampling aperture metal plate (the counter electrode).

During an electrospray ionization process where positive voltage is applied to the ESI capillary tip, electrochemical oxidation reactions can occur at the solution-metal interface of the capillary tip. The oxidation reactions inject positive ions into the solution, thus preventing a charge imbalance that would be created by the migration of positive ions to the liquid surface of the Taylor cone. The oxidation reactions at the capillary tip can take many forms. However, they mostly involve the conversion of metal atoms and neutral molecules in solution to positive ions with production of electrons, and/or removal of negative ions from solution by converting them to neutral molecules with production of free electrons.[27, 30, 35, 36]

Apart from the analyte solution, electrochemical oxidation reactions at a metal capillary have also been observed to occur. Blades et al.[36] observed the release of Zn^{2+} into the solution when a zinc capillary was used for electrospray. Similar results were also observed when a stainless steel capillary was used, as Fe^{2+} was released into the solution.

Electrochemical oxidation reactions that occur at the ESI capillary depend on the analyte ions present in solution, the solvent used, and the composition of the capillary. However, the reactions that will dominate the electrospray ionization process will be the reactions with lowest oxidation potentials.[35] Van Berkel et al.[30] gave a list of possible electrochemical reactions that can occur in a given metal capillary in both positive and negative modes. Some of the most common reactions are given in Table 1.1. The implications of a few of these reactions will be discussed later in this chapter. As pointed out by Cole et al.,[31] it is the electrochemical reactions at the capillary tip that keep the electrospray ionization process going.

Table 1.1 Major electrochemical reactions occurring at a metal electrospray capillary. Table reproduced from Reference 30.

Positive ion mode		**Negative ion mode**	
Oxidation reactions	E^0 (V) vs. SHE	Reduction reactions	E^0 (V) vs. SHE
$2H_2O \rightarrow O_2 + 4H^+ + 4e^-$	1.23	$2H_2O + O_2 + 4e^- \rightarrow 4OH^-$	0.40
$4OH^- \rightarrow 2H_2O + O_2 + 4e^-$	0.40	$CH_3OH + 2H^+ + 2e^- \rightarrow CH_4 + H_2O$	0.58
$2NH_4^+ \rightarrow N_2H_5^+ + 3H^+ + 2e^-$	1.28	$2NH_4^+ + 2e^- \rightarrow 2NH_3 + H_2$	− 0.55
$Fe \rightarrow Fe^{3+} + 3e^-$	− 0.03	$Fe(OH)_3 + e^- \rightarrow Fe(OH)_2 + OH^-$	− 0.56

As mentioned earlier, the electrochemical oxidation reactions at the ESI capillary prevent a charge imbalance from occurring, thus ensuring continuous production of charged droplets having one polarity. The electrochemical reactions at the metal endplate ensure a complete electrolytic circuit is formed.[35, 36] The ions and neutral molecules arriving at the metal plate undergo reduction reactions in positive ion mode or oxidation reactions in negative ion mode. Electrochemical reduction of solvent molecules results in production of negative ions or of neutral molecules that cannot be detected using mass spectrometry.

One major consequence of electrochemical reactions during electrospray is the alteration of the solution pH.[30, 37] Reactions listed in Table 1.1 show that the electrochemical oxidation or reduction reactions at the spray capillary result in the production of H^+ or OH^-, affecting the pH of the electrosprayed solution. This can change the equilibrium composition of the pH-sensitive species in the original solution. Van Berkel et al.[37] noted that the nature and extent of compositional change of the solution due to pH changes will depend on the current emitted from the spray capillary (i_{ES}), solution flow rate (v_f), and redox characteristics of the metal capillary and solution species. The extent of this change can be calculated using Equation 1.2

$$pH_{final} = -\log([H^+]_{elec} + [H^+]_{initial})$$

Equation 1.2

$$\text{where } [H^+]_{elec} = \frac{i_{ES}}{nFv_f}$$

where n is the molar equivalent of electrons involved in producing one mole of H^+, and F is the Faraday constant. $[H^+]_{initial}$ is the initial concentration of H^+ in the solution before any electrochemical reactions have occurred, while $[H^+]_{elec}$ is the concentration of H^+ produced

as a result of electrochemical reactions occurring during the electrospray process. This change in solution pH is one of the major chemical changes in the spray solution observed during the electrospray ionization process. Other possible solution perturbations will be discussed later in Section 1.4.4.

1.4.4 Advantages and drawbacks of using ESI-MS for the analysis of metal-ligand complexes

The major advantage of ESI-MS over other techniques for the investigation of metal-ligand systems is its ability to allow fast, accurate, and direct determination of the stoichiometric ratios for metal-ligand complexes. ESI-MS mass spectra acquired for metal-ligand complexes in solution can be simple, due to the production of mainly singly- or doubly-charged ions. The *m/z* of these ions relates directly to the stoichiometric ratios of the metal-ligand complexes. The stoichiometric ratios of all the complexes formed in solution can be simultaneously determined, unlike in spectroscopic techniques, where multiple complexes of different stoichiometric ratios often cannot be distinguished from each other. Electrospray ionization is a "soft" technique, meaning that there is little or no fragmentation of the complex. This results in simple and clean mass spectra with peaks that can be easily assigned. In addition, the soft ionization nature of the technique makes it possible for a complex formed in solution to be gently transferred to the gas phase and analyzed.

Another advantage of ESI-MS over other techniques in studying metal-ligand speciation and equilibria is its relatively low detection limits for complexes that form gas-phase ions from solution efficiently during electrospray. ESI-MS can be used to analyze

solutions with analyte concentrations as low as 1 μM.[38] This high sensitivity allows investigation of solutions with analyte concentrations close to those usually encountered in biological and environmental samples. Other techniques such as UV-Visible spectroscopy, infrared spectroscopy and Raman spectroscopy, and NMR spectroscopy cannot be used to investigate metal-ligand interactions at such low analyte concentrations. ESI-MS is also very fast in data generation and requires lower sample volumes compared to other techniques.

While the simplicity and high sensitivity of ESI-MS makes it a very attractive tool in studying metal-ligand interactions, the potential limitations and drawbacks should also be kept in mind. Di Marco et al.[38] and Keith-Roach et al.[39] highlighted in separate reviews some of the drawbacks of this technique. They emphasized that the main strength of ESI-MS lies in obtaining information about the stoichiometric ratios of metal-ligand complexes in solution and that the results obtained usually agreed with results from other techniques. An ideal ESI-MS technique for metal-ligand equilibrium studies should be able to identify all the metal complexes in solution, their stoichiometric ratios, and their concentrations. However, ESI mass spectra do not always represent the true composition of the species present in the solution before the measurement due to perturbations occurring in solution, at the liquid-gas phase interface during ionization, and in the gas phase before ion detection.

The gas-phase complexes observed in ESI mass spectra are assumed to be the same as those in solution, but perturbations during the ionization process can make this assumption unreliable. These perturbations can lead to equilibrium shifts (i.e. changes in concentration and/or speciation) of the complexes in the droplets as a result of volume changes due to solvent evaporation during electrospray. Changes in droplet volume can

affect both the concentration of the species and ionic strength of the solution.[40] Perturbation of solution complexes during electrospray can also be caused by electrochemical reactions that take place at the capillary. As previously discussed, the electrochemical oxidation of solvent results in the production of H^+ or OH^-. The H^+ or OH^- produced leads to changes in the solution pH of the charged droplets, thus resulting in pH-related changes in the distribution of the species.[37, 41, 42]

The relative differences in transfer efficiencies of metal-ligand complexes from the droplets to the gas-phase is the major reason why observed gas-phase species do not necessarily reflect solution species. The transfer efficiency is highly dependent on the droplet equilibrium partition constant.[43] The equilibrium partition constant is a measure of the distribution of an ionic species between the surface of the liquid droplet and the bulk phase. This measure depends on properties such as the droplet's surface activity, charge density, hydrophobicity, and solvent polarity. For example, in a charged droplet of low surface activity (i.e. analyte ions within the droplet have less affinity for the droplet surface than for the bulk), the transfer of the ions from the liquid phase to gas phase will be less efficient than for a droplet with high surface activity.

After the electrospray ionization process, the gas phase ions formed may undergo further changes before reaching the mass analyzer. These changes which can be due to gas-phase reactions, such as solvent or metal adduct formation, oligomerization, or fragmentation, contribute to the discrepancy between species observed in mass spectra and those actually present in solution. Water, methanol, and acetonitrile are the most common electrospray solvents, and H_2O, CH_3OH, and CH_3CN adducts are commonly observed in the mass spectra. Solvent molecules can coordinate to the metal centre in the gas phase, and

may be present due to incomplete solvent evaporation. Sodium and potassium adducts are also commonly observed in mass spectra. These alkali metal ions can come from glassware, solvent, or from an instrument contaminated by previous ESI-MS analysis of salt-containing solutions. Sodium and potassium ions react with the analyte ion during desolvation to form adducts before the ion reaches the mass analyzer. The adducts formed during gas-phase reactions do not affect the stoichiometries of the metal-ligand systems being studied, but do complicate peak assignments.

Gas-phase reactions of analyte ions can also include the formation of dimers, trimers, or oligomers. These cluster ions can be formed as a result of reactions in the gas-phase. Despite the soft nature of ESI, fragmentation reactions of metal complexes in gas phase are also observed due to the instability of the complex at certain instrumental parameters. For example, certain capillary temperatures or cone voltages can lead to equilibrium shifts, decomposition of complexes, chemical reactions, etc.

One of the major factors that has limited the use of ESI-MS for quantitative studies is the high sensitivity of the mass spectra to instrumental parameters. Electrospraying a solution containing metal-ligand complexes under different instrumental conditions will give different results. These differences are due to perturbations in solution, at liquid-gas phase interface, and gas-phase reactions which are affected by certain instrumental parameters. Some common ESI-MS instrumental parameters that significantly affect mass spectra are solution flow rate, capillary voltage, cone voltage, and capillary temperature. The effects of these parameters on the mass spectra are discussed in the following paragraphs.

Electrospraying solutions at high flow rates results in the formation of droplets with large radii. According to Di Marco et al.[44, 45] droplets with increased radii are susceptible to solution perturbations because of the increased residence time of the analyte ion in the droplets relative to the gas phase. The increased residence time is due to the increased number of solvent evaporation and droplet fission cycles that will be required before a gas phase ion is formed. Because of the increased residence time in the droplets, analyte ions can be more severely affected by changes in ionic strength or pH, or can undergo gas-phase reactions such as oligomerization (cluster ion formation), fragmentation, or rearrangement reactions. In addition, the effect of droplet radius on the efficiency of analyte ion transfer to the gas phase for analytes of different surface activity was investigated by Schmidt et al.[46] and Benkestock et al.[47] They observed that, for a solution that forms droplets with low surface activity, if the initial droplet radius is large as a result of high solution flow rate, fewer analyte ions in the droplet will be transferred into the gas phase and made available for analysis by the mass analyzer and ion detection systems.

Another instrumental parameter that has an effect on mass spectra is the capillary voltage. Capillary voltage describes the amount of electric field applied to the tip of a capillary. Kebarle et al.[27] observed that applying a large voltage to the electrospray capillary results in the production of droplets containing a large number of charges, thus enhancing droplet surface activity. As reported by Sherman el at.,[48] the ion abundances detected by the mass spectrometer are proportionally related to the surface activity of the droplets. Thus, changing the capillary voltage value of an ESI capillary will affect the intensities of analyte ions in the mass spectrum.

Cone voltage is by far the most important instrumental parameter having an effect on mass spectra. It is mostly used for structural elucidation, and also to eliminate or reduce adducts. Cone voltage is the voltage applied between the spray capillary and the metal endplate containing the orifice that leads to the mass analyzer (Figure 1.1). An increase in cone voltage will lead to an increase in intramolecular collisions, and collisions with nebulizing gas molecules. The increased number of collisions will result in fragmentation of the parent ions.[44] Thus, acquiring spectra at different cone voltages will lead to differences in the relative abundances of peaks in the mass spectrum, and sometime to the appearance of fragment ions. Varying the cone voltage is a common method for investigation of the structural detail and fragmentation patterns of a compound. Variation in cone voltage significantly affects the ion intensities. For example, Miao et al.[49] showed how ion intensities of protonated ginsenosides, and their sodium, ammonium and potassium adducts vary with cone voltage.

Capillary temperature is another parameter that has a major effect on the relative abundances of ions observed in mass spectra because of its effect on solvent evaporation and gas-phase reactions. High capillary temperatures increase the rate of solvent evaporation from the charged droplet, thus reducing the probability of solvent adduct formation, and improving the signal intensity of the analyte ion. High capillary temperatures also increase the rate of gas phase reactions, thus increasing the relative abundances of ions formed as a result of such reactions. Equilibrium constants of most metal complexes are temperature dependent. Changes in the capillary temperature during ESI can shift the equilibrium reaction left, towards the reactants, or right, towards the products. This shift in the

equilibrium position will lead to differences in the relative ion abundances of the metal complexes.

1.4.5 Applications of electrospray ionization mass spectrometry

Although ESI-MS was introduced in the 1960's, the first application of the technique to the study of metal-ligand interactions was reported by Katta et al.[50] in 1990. In that study, Katta et al. characterized the complexes formed between rubidium(II) and a 2,2'-bypyridyl ligand. Since Katta et al. were focused on using ESI-MS for complex characterization, they did not discuss the applicability of this technique to metal-ligand equilibrium chemistry. Cheng et al.[51] later demonstrated that ESI-MS could also be used to investigate the equilibrium that exists in solutions, while investigating aqueous solutions of metal salts such as CdI_2, $CuSO_4$, and ZnI_2, among others. Their results suggested that the ions observed in the mass spectrum depend on the aqueous chemistry of the salt solutions. Despite the drawbacks highlighted earlier, the application of ESI-MS to metal-ligand solution studies has been on the rise in the last decade. In the following sections, the broad areas in which this technique is applied will be reviewed in detail, while outlining some of the major difficulties encountered.

1.4.5.1 Qualitative studies: Characterization of metal-ligand complexes

ESI-MS is widely used for the investigation of metal-ligand complexes of biological, environmental, and medicinal importance. The technique is used to identify the complexes formed and determine their stoichiometric ratios. In many cases, complex identification can be aided by examining the isotopic distribution of the metal in the complex.

ESI-MS is mostly used as a stand-alone technique, but because of the drawbacks cited earlier, results from the technique are sometimes compared with those from other techniques, such as potentiometry, UV-Visible spectroscopy, NMR spectroscopy, and infrared or Raman spectroscopy. In most cases, ESI-MS results are in agreement with results obtained using these techniques, and when they are not, gas-phase reactions and artifact production are generally cited as the probable cause.

In using ESI-MS as a stand-alone technique, researchers aim at understanding the number and stoichiometric ratios of complexes formed in solution between a metal and ligand. The effects of changes in solution conditions, such as changing metal-ligand mole ratios and pH values, and the effect of changing instrumental parameters are then investigated in other to understand the solution chemistry of the metal-ligand system. A few examples of the use of ESI-MS as a stand alone technique have been reported.[52-60]

Given the possibility that changes in solution chemistry occur during ESI, it is generally a good idea to compare the results obtained using ESI-MS with results obtained from other techniques. In most cases, the results obtained using ESI-MS are in agreement with results obtained using other established techniques. As one example, Lodyga-Chruscinska et al.[61] characterized the complexes formed between vanadium(IV) oxide, VO^{2+}, and cis-2,4,6-trimethoxycyclohexane-1,3,5-triamine (tmca) using potentiomentry, UV-Vis spectroscopy, electron paramagnetic resonance (EPR), density functional theory (DFT), and ESI-MS. The EPR and potentiomentric data revealed that a 1:2 non-oxido V(IV):tmca complex was present in aqueous solution at pH > 10. This result was in

agreement with spectra obtained using ESI-MS, which showed a peak corresponding to the ion $[V+2(tmca)-4H]^+$.

In cases where there is some ambiguity in results obtained using traditional techniques, ESI-MS can be used to remove some ambiguity or confirm the existence of the proposed complexes. For example Enyedy et al.[62] investigated the interaction of an anticancer drug, triapine (3-amino-pyridine-2-carbaldehyde thiosemicarbazone), with Cu^{2+}, Zn^{2+}, and Fe^{2+} using potentiomentry, UV-Visible spectroscopy, EPR, DFT, and ESI-MS. Data from potentiometric and EPR techniques showed the formation of a copper dinuclear complex $[Cu_2L_3]^+$ in addition to the 1:1 and 1:2 metal:ligand complex, where the third ligand is assumed to form a bridge linking two $[CuL]^+$ complexes (L = 3-amino-pyridine-2-carbaldehyde thiosemicarbazone). This dinuclear complex was also observed in ESI-MS spectra, along with $[CuL]^+$ and $[CuL_2]^+$. The formation of the 1:1 and 1:2 complexes ($[CuL]^+$ and $[CuL_2]^+$) when the dinuclear ion was subjected to collision-induced dissociation confirmed that the dinuclear complex was not an artifact. The observation of the dinuclear complex in both the solution phase and the gas phase shows that the possible solution perturbations usually experienced during electrospray ionization were not significant enough to alter the speciation in this case.

Caudle and coworkers[63, 64] studied the complexes formed between iron(III) and dihydroxamic acid and between iron(III) and rhodotorulic acid. Data from potentiometry and UV-Visible spectroscopy allowed the authors to propose two possible stoichiometries for the complex formed in solution: $[FeL(H_2O)_2]^+$ or $[Fe_2L_2(H_2O)_4]^{2+}$, where L = either dihydroxamic acid or rhodotorulic acid. The use of ESI-MS allowed the stoichiometry of the

complex to be confirmed. Other studies where ESI-MS has been used to confirm results obtained using other equilibrium techniques have been reported.[65-67]

Results from ESI-MS and other techniques are not always in agreement. Matsumoto et al.[68] studied the interaction between Cu^{2+} and 2-(5-bromo-2-pyridylazo)-5-diethylaminophenol using UV-Visible spectroscopy and ESI-MS techniques. Only a 1:1 metal-ligand complex was observed in UV-Visible spectra, while 1:2 and 2:2 metal-ligand complexes, in addition to the 1:1 complex, were observed in ESI-MS spectra. The reason for this difference was attributed to gas phase reactions such as dimerization and ligand addition reactions. Dimerization of the 1:1 complex after solvent evaporation during ESI was thought to lead to the formation of the 1:2 and 2:2 metal-ligand complexes.

As previously mentioned, fragmentation of the ligand during the ESI process sometimes contributes to the discrepancies between ESI-MS results and those from solution phase techniques. This was illustrated by Murner et. al.,[69] in their study of interactions between metal ions Cd^{2+}, Fe^{2+}, and Zn^{2+}, and bis-[4,5]-pineno-2,2'-bipyridines. Some fragment ion peaks, in addition to peaks due to metal complexes, were observed in the ESI mass spectrum. In a related study, Jezowska-Bojezuk et. al.,[70] while studying the coordination of copper to lincomycin and H_2O_2, noticed the presence of fragment ion peaks in the ESI mass spectra, in addition to some peaks which were believed to be due to metal-ligand complexes. However, the proposed stoichiometric ratios of these metal-ligand complexes could not be confirmed using potentiometry, UV-Visible, EPR, or NMR techniques. These metal-ligand complexes peaks were therefore considered to be artifacts

arising from ions formed during electrospray ionization. In cases where the number of unassigned peaks is relatively high, the ESI-MS data is discarded.

1.4.5.2 Quantitative applications

While the qualitative applications of ESI-MS to metal-ligand system are focused on determining the numbers and stoichiometric ratios of solution complexes, quantitative applications of ESI-MS aim at determining the concentrations, and thus the formation constants, of the complexes formed in solution. However, there has been much debate on the suitability of ESI-MS for such quantitative studies because relative ion intensities in the mass spectra may not represent the true concentrations of the species in solution. The solution perturbations that occur during ESI (discussed earlier) and the different response factors of the various solution species all have an effect on the ion intensities of species observed in mass spectra. For example, Murariu et al.[71] observed that an uncomplexed peptide gives a higher relative abundance than the metal-peptide complex, because the peptide has a higher response factor than the metal complex. A similar observation was made by Groenewold et al.[72] in their investigation of uranyl(VI)-desferrioxamine B complexes. The uncomplexed desferrioxamine B was observed as the most abundant peak in the mass spectrum. This was attributed to the higher liquid-to-gas phase transfer efficiency of desferrioxamine B compared to the uranyl(VI)-desferrioxamine B complexes.

As mentioned earlier, the ESI-MS signal is highly dependent on instrumental parameters. Using solutions containing Al^{3+} and 2,3-dihydroxypyridine, Di Marco et al.[44] studied the effects on ESI mass spectra of changes in such instrumental parameters as capillary temperature, spray voltage, solution flow rate, and nebulizer gas flow rate. They

observed that, of all the instrumental parameters investigated, capillary temperature had the greatest effect on the ion signal intensities for the Al^{3+}/2,3-dihydroxypyridine system under investigation. As discussed earlier, capillary temperature has an effect on the rate of gas phase reactions during the ESI process. In the study by Di Marco et al.,[44] the increase in capillary temperature was observed to lead to an increase in the relative ion abundances of AlL and AlL_2 complexes (where L = 2,3-dihydroxypyridine), and to a decrease in the relative ion abundances of AlL_3 complexes. The decrease in the relative ion abundances of AlL_3 complexes was found to be due to the increase in the extent of fragmentation of AlL_3 (at high capillary temperature), which produced AlL and AlL_2 species. In another related study, Clark and co workers.[73] studied the speciation of the Nd-acetate system under different solution conditions (pH, solvent composition, metal:ligand mole ratio) and instrumentation parameters (cone voltage). They observed that, in addition to cone voltage, the pH changes that occur due to electrochemical redox reactions, and rapid ligand exchange in the metal-ligand complexes, are some of the factors that alter the solution speciation during ESI. This affects the signal intensities of ions arising from the various metal-ligand species.

In order to correct for this discrepancy between concentration and gas-phase ion intensities, and to further the application of ESI-MS for quantitative studies of metal-ligand systems, Bombi and coworkers[74] derived an equation (Equation 1.3) that correlates the ion intensity in the mass spectrum to the analyte equilibrium concentration in the solution:

$$i = kC^0 f \qquad \text{Equation 1.3}$$

where i = ion intensity, k = response factor, C^0 = analyte equilibrium concentration, and f = fraction of complex with the same protonation state as ions detected in the mass spectrum.

Equation 1.3 takes into account the acid/base properties of metal-ligand complexes, which affect the transfer efficiency of an ion from solution to the gas phase. The validity of the equation was tested by acquiring mass spectra of solutions containing aluminium(III) and any of the following ligands at various pH values: citric acid, ethylenediamine-tetramethylene phosphonic acid, 3,4-dihydroxybenzoic acid, and 3-hydroxy-2-(1H) pyridinone. The ESI-MS ion intensities, i, and the corrected analyte equilibrium concentrations, C^0f, were observed to be correlated in a majority of the systems investigated. The authors used the term "correlate" to indicate that both the ion intensity, i, and the corrected analyte equilibrium concentration, C^of, show the same trend when the solution pH was varied.

Because of these concerns, there have been few studies where ESI-MS has been employed for quantitation. As mentioned by Di Marco and Bombi in their review,[38] the agreement between results from ESI-MS and results obtained using other techniques generally ranges from fair to poor. Di Marco et al.,[75] in one of their works, investigated complex formation between Al^{3+} and several hydroxypyridine-carboxylic acids at differing pH values and metal-ligand mole ratios. They compared their results to results previously obtained using potentiometry.[76] While there is excellent agreement in the qualitative data obtained from ESI-MS data and potentiometric titrations, there were differences in the quantitative data (concentrations of detected complexes) obtained. These differences were attributed to the differences in solvent composition and solution ionic strength used in each

technique. The absence of supporting electrolytes and the use of water/methanol mixtures in the ESI-MS experiment, instead of only water, was believed to lead to the destabilization of highly charged species. This resulted in the reduction of the response factors of the aluminum complexes, and thus in the reduction in ion intensities in the ESI mass spectra used for quantitive measurements. Therefore, results differed from those obtained using potentiometry.

As previously mentioned, the major quantitative applications of ESI-MS to metal-ligand systems involve the estimation of the complex formation constant. For a given complexation reaction between a metal, M, and a ligand, L, leading to the formation of the metal-ligand complex ML (Equation 1.4), various methods for the determination of the formation constant (K) using ESI-MS have been proposed. These methods have been reviewed by Daniel et al.[77]

For the reaction $M + L \rightleftarrows ML$ $\qquad K = \dfrac{[ML]}{[M][L]}$ Equation 1.4

One method of estimating the formation constant involves measuring the peak intensities (*I*) of the free ligand (L) and of the complex (ML).[78, 79] The ratios of the peak intensities of the ions related to ML and to L are then estimated, and related to the concentration ratio using Equation 1.5. In this method, it is assumed that the response factors of both ligand and complex are the same. This method is applicable to the determination of formation constants of complexes having multiple stoichiometric ratios.

$$\frac{I(\mathrm{ML})}{I(\mathrm{L})} = \frac{[\mathrm{ML}]}{[\mathrm{L}]} \qquad \text{Equation 1.5}$$

Another method of estimating formation constants involves titrating a solution of the ligand with metal ion, where the concentration of unbound ligand (L) is indirectly estimated. This method requires creating a calibration curve by plotting ion intensity vs. ligand concentration. The formation constant is estimated from the Scatchard plot of the resulting titration data. The Scatchard plot is made by plotting the ratios of the concentrations of ML to L against the ML concentration, i.e. $\frac{[ML]}{[L]}$ vs. [ML].

As suggested by Di Marco et al.[38] in their review, ESI-MS is a powerful tool when it comes to determining complex stoichiometries and characterizing gas-phase species. ESI-MS gives a complete description of solution equilibria when used in conjunction with other established techniques. However, its application to quantitative studies of metal-ligand systems is not recommended, as there are other techniques that can give more reliable results. For example, potentiometry is a preferred technique for accurate determination of complex formation constants.

1.4.5.3 Ternary systems

All the studies that have been discussed so far are binary systems, where the metal-and-ligand-containing solutions investigated consist of only one metal and one ligand. A ternary system on the other hand, consists of either two metals and a ligand, or two ligands and a metal. In most cases, the aim of creating a ternary system is to determine the binding selectivity of metal ions toward a given ligand, or vice versa. The first form of a ternary study using ESI-MS was reported in 1995 by Bond et al.,[80] who investigated the competition between Cd^{2+} and Hg^{2+} for phosphine ligands. Bonnigton et al.[81] in a related study

determined the binding affinities of a series of triphenylphosphine ligands (PPh_3, $AsPh_3$, $SbPh_3$ and $BiPh_3$ (Ph = phenyl)) towards two metal ions, Ag^+ and Cu^+. They observed that the selectivity of the ligand towards both Ag^+ and Cu^+ followed the order $PPh_3 > AsPh_3 > SbPh_3$, while $BiPh_3$ was unstable during the analysis.

The most common reason for the use of ternary systems in ESI-MS is to investigate the competition between two metals for a ligand, or two ligands for a metal, or the displacement of one metal or ligand by another. Keith-Roach et al.[82] employed this technique to investigate the competition between two siderophores, ferrichrome and desferrioxamine B, for iron and thorium binding, and also to investigate the competition between iron and thorium for each siderophore. Meda et al.,[83] in a similar study, reported the displacement of Cd^{2+} from its 2-deoxymugineic acid complex upon the addition of either of Fe^{3+} or Zn^{2+}, while Rellan-Alvarez et al.[53] illustrated the effect of citrate addition on iron-nitriloacetic acid complexes. In each of these studies, data interpretation is usually based on the relative ion intensities of the complexes.

Apart from determining the relative binding affinities between metals and ligands, ESI-MS techniques used to study ternary systems allow the identification of mixed ligands formed in solution, such as $[Th(EDTA)(NTA)]^{3-}$ in a thorium, ethylenediaminetetraacetic acid (EDTA), and nitriloacetic acid (NTA) ternary system,[54] or $[Eu(L)_3(phen)_2(H_2O)]^+$ in a europium, nicotinic acid (L), and phenanthroline (phen) ternary system.[84] Mixed complexes often have different chemical behaviors compared to complexes containing only one type of ligand (or metal). For this reason, the use of ESI-MS to identify and characterize ternary complexes is very important in obtaining a complete description of metal-ligand solution

equilibria, especially, when the ternary complexes cannot be identified by other techniques, such as potentiometry, UV-Visible spectroscopy, NMR, infrared spectroscopy, or Raman spectroscopy.

1.5 Conclusion

In conclusion, the advantages and disadvantages of ESI-MS, compared to other techniques such as potentiometry, UV-Visible spectroscopy, NMR, infrared, and Raman spectroscopies etc., in studying metal-ligand interactions have been presented. It is obvious that ESI-MS is a very powerful tool for obtaining qualitative information about metal-ligand systems. This information can include the numbers of metal-ligand complexes formed and the stoichiometric ratios of those complexes. In most cases, qualitative data obtained from this technique can be used to corroborate data from other established techniques. Thus, when used in conjunction with techniques such as potentiometry, UV-Visible spectroscopy, infrared spectroscopy, Raman spectroscopy, and NMR, ESI-MS completes the description of metal-ligand solution equilibria. However, the application of ESI-MS as a quantitative tool has not really been accepted due to the high sensitivity of ion intensities to instrumental parameters, although some successes have been reported in this area.

1.6 Research Objectives

In this dissertation, I have two major aims. The first aim is to show how silver and copper ions can be used to improve the ESI-MS detection of poorly ionized organophosphorus pesticides. The second major aim is to investigate the gas-phase

interactions of uranyl(VI), iron(III), and vanadium(V) with amidoxime ligands. I have used ESI-MS as two different types of tool to achieve these two aims:

1. ESI-MS used as an analytical tool. ESI-MS was used to investigate the analytical importance of metal-ligand interactions in a system containing organophosphorus pesticides and transition metals.
2. ESI-MS used as a characterization tool for metal-ligand complexes. ESI-MS was used to characterize the gas-phase complexes formed as a results of metal-ligand interaction in systems containing uranyl(VI), iron(III) and vanadium and amidoxime ligands.

The dissertation general plan is summarized in the flowchart shown in Figure 1.2. The specific objectives of the research include the following:

1. To investigate the effect of silver and copper ions on analytical detection of fenitrothion, parathion, malathion and diazinon pesticides. This involves examining the effect of each metal on the sensitivity and detection limit of the pesticide-metal complexes detected using ESI-MS.
2. To investigate the effect of silver and copper ions on the fragmentation patterns of fenitrothion, parathion, malathion and diazinon.
3. To characterize the gas-phase complexes of uranyl(VI) with DHIP, DHPD and DHED, and understand how the speciation will be affected by changes in the metal:ligand mole ratio and ligand structure.

4. To characterize the gas-phase complexes of iron(III) and vanadium(V) with DHIP and DHPD, and investigate how the uranyl(VI)-DHIP gas-phase complexes will be affected by the presence of iron(III) or vanadium(V).

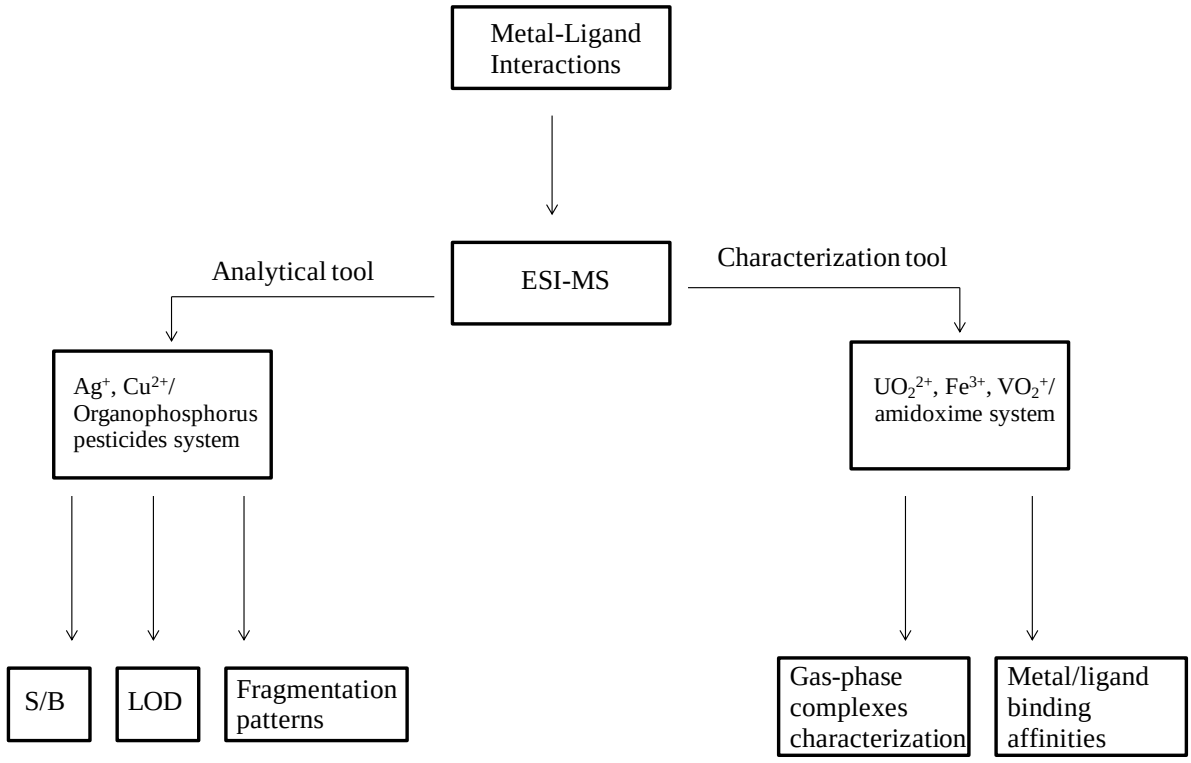

Figure 1.2 Flowchart illustrating the general research plan of this dissertation. S/B = signal-to-background ratio, LOD = limits of detection.

References

1. Gu, Y. Y.; Yeung, A. T.; Tsang, D. C. W.; Fu, R. B. Applications of citric acid industrial wastewater and phosphonates for soil remediation: effects on temporal change of cadmium distribution. *Soil Sediment Contam.* **2013,** *22*, 876-889.
2. Francis, A. J.; Dodge, C. J. Remediation of soils and wastes contaminated with uranium and toxic metals. *Environ. Sci. Technol.* **1998,** *32*, 3993-3998.
3. Ullmann, A.; Brauner, N.; Vazana, S.; Katz, Z.; Goikhman, R.; Seemann, B.; Marom, H.; Gozin, M. New biodegradable organic-soluble chelating agents for simultaneous removal of heavy metals and organic pollutants from contaminated media. *J. Hazard. Mater.* **2013,** *260*, 676-688.
4. Andreini, C.; Bertini, I.; Cavallaro, G.; Holliday, G. L.; Thornton, J. M. Metal ions in biological catalysis: From enzyme databases to general principles. *J. Biol. Inorg. Chem.* **2008,** *13*, 1205-1218.
5. Frausto Da Silva, J. J. R.; Williams, R. J. P. The biological chemistry of the elements: The inorganic chemistry of life. *Oxford University Press: Oxford, England, UK; New York, New York, USA.* **1991**, pg 561.
6. Martin, B. L. Evidence for a structure-function relationship in the activation of calcineurin by metal ions. *Bioorg. Chemi.* **2000,** *28*, 17-27.
7. Klein, D. J.; Moore, P. B.; Steitz, T. A. The contribution of metal ions to the structural stability of the large ribosomal subunit. *RNA* **2004,** *10*, 1366-1379.
8. Marques, M. P. M.; Gianolio, D.; Cibin, G.; Tomkinson, J.; Parker, S. F.; Valero, R.; Lopes, R. P.; Batista de Carvalho, L. A. E. A molecular view of cisplatin's mode of action: Interplay with DNA bases and acquired resistance. *Phys. Chem. Chem. Phys.* **2015,** *17*, 5155-5171.
9. Dasari, S.; Tchounwou, P. B. Cisplatin in cancer therapy: Molecular mechanisms of action. *Euro. J. Pharmacol.* **2014,** *740*, 364-378.
10. Gans, P.; Sabatini, A.; Vacca, A. Investigation of equilibria in solution. Determination of equilibrium constants with the HYPERQUAD suite of programs. *Talanta* **1996,** *43*, 1739-1753.

11. Sabatini, A.; Vacca, A.; Gans, P. MINIQUAD - General computer-program for computation of formation constants from potentiometric data. *Talanta* **1974,** *21*, 53-77.
12. Zekany, L.; Nagypal, I. PSEQUAD: A comprehensive program for the evaluation of potentiometric and/or spectrophotometric equilibrium data using analytical derivatives. In *Computational methods for the determination of formation constants*, Leggett, D. J., Ed. Plenum Press: New York, **1985**; pp 291-354.
13. Motekaitis, R. J.; Martell, A. E. BEST - A new program for rigorous calculation of equilibrium parameters of complex multicomponent systems. *Can. J. Chem.* **1982,** *60*, 2403-2409.
14. Martell, A. E.; Motekaitis, R. J. *Determination and use of stability constants*. Second ed.; VCH Publishers: New York, **1992**.
15. Pistolis, G.; Malliaris, A. Limitations on the determination of the stoichiometry and equilibrium constants of weak complexes by computer fitting methods: experimental verification. *Chem. Phys. Lett.* **1999,** *310*, 501-507.
16. Pistolis, G.; Malliaris, A. On the determination of the stoichiometry and equilibrium constants of weak complexations. *Chemi. Phys. Lett.* **1999,** *303*, 334-340.
17. Hartley, F. R.; Burgess, G.; Alcock, R. M. *Solution equilibria*. Ellis Horwood Limited: Chichester, **1980**.
18. Connors, K. A. *Binding constants: The measurement of molecular complex stability*. John Wiley & Sons: New York, **1987**.
19. Popov, A. I. Equilibria studies in solutions. In *Modern NMR techniques and their application in chemistry*, Popov, A. I.; Hallenga, K., Eds. Marcel Dekker, Inc.: New York, **1991**; pp 485-520.
20. Dole, M.; Mack, L. L.; Hines, R. L. Molecular beams of macroions. *J. Chem. Phys.* **1968,** *49*, 2240.
21. Yamashita, M.; Fenn, J. B. Electrospray ion-source - Another variation on the free-jet theme. *J. Phys. Chem.* **1984,** *88*, 4451-4459.
22. Yamashita, M.; Fenn, J. B. Negative-ion production with the electrospray ion-source. *J. Phys. Chem.* **1984,** *88*, 4671-4675.

23. Han, L.; Kitova, E. N.; Li, J.; Nikjah, S.; Lin, H.; Pluvinage, B.; Boraston, A. B.; Klassen, J. S. Protein-glycolipid interactions studied in vitro using ESI-MS and nanodiscs: Insights into the mechanisms and energetics of binding. *Anal. Chem.* **2015,** *87*, 4888-4896.

24. Yang, Y.; Boysen, R. I.; Chowdhury, J.; Alam, A.; Hearn, M. T. W. Analysis of peptides and protein digests by reversed phase high performance liquid chromatography-electrospray ionisation mass spectrometry using neutral pH elution conditions. *Anal. Chim. Acta* **2015,** *872*, 84-94.

25. Chary, V. N.; Reddy, B. S.; Kumar, C. D.; Srinivas, R.; Prabhakar, S. Characterization of N,N-dimethyl amino acids by electrospray ionization-tandem mass spectrometry. *J. Mass Spectrom.* **2015,** *50*, 771-781.

26. Kebarle, P.; Verkerk, U. H. Electrospray: From ions in solution to ions in the gas phase, what we know now. *Mass Spectrom. Rev.* **2009,** *28*, 898-917.

27. Kebarle, P.; Tang, L. From ions in solution to ions in the gas-phase - The mechanism of electrospray mass-spectrometry. *Anal. Chem.* **1993,** *65*, A972-A986.

28. Iribarne, J. V.; Thomson, B. A., Evaporation of small ions from charged droplets. *J. Chem. Phys.* **1976,** *64*, 2287-2294.

29. Cech, N.B.; Enke, C. G. Practical implications of some recent studies in electrospray ionization fundamentals. *Mass Spectrom. Rev.* **2001,** *20* 362-387.

30. Van Berkel, G. J.; Kertesz, V. Using the electrochemistry of the electrospray ion source. *Anal. Chem.* **2007,** *79*, 5510-5520.

31. Pozniak, B. P.; Cole, R. B. Perspective on electrospray ionization and its relation to electrochemistry. *J. Am. Soc. Mass Spectrom.* **2015,** *26*, 369-385.

32. Prudent, M.; Mendez, M. A.; Roussel, C.; Su, B.; Lion, N.; Rossier, J. S.; Girault, H. H. About the electrospray ionization source in mass spectrometry: Electrochemistry and on-chip reactions. *Chimia* **2009,** *63*, 283-287.

33. Cole, R. B. Some tenets pertaining to electrospray ionization mass spectrometry. *J. Mass Spectrom.* **2000,** *35*, 763-772.

34. Van Berkel, G. J.; Zhou, F. M. Characterization of an electrospray ion-source as a controlled-current electrolytic cell. *Anal. Chem.* **1995,** *67*, 2916-2923.

35. Van Berkel, G. J. The electronic nature of electrospray. In *Electrospray ionization mass spectrometry: Fundamentals, instrumentation and applications*, Cole, R. B., Ed. Wiley: New York, **1997**; pp 65-105.

36. Blades, A. T.; Ikonomou, M. G.; Kebarle, P. Mechanism of electrospray mass-spectrometry - electrospray as an electrolysis cell. *Anal. Chem.* **1991,** *63*, 2109-2114.

37. Van Berkel, G. J.; Zhou, F. M.; Aronson, J. T. Changes in bulk solution pH caused by the inherent controlled-current electrolytic process of an electrospray ion source. *Int. J. Mass Spectrom.* **1997,** *162*, 55-67.

38. Di Marco, V. B.; Bombi, G. G. Electrospray mass spectrometry (ESI-MS) in the study of metal-ligand solution equilibria. *Mass Spectrom. Rev.* **2006,** *25*, 347-379.

39. Keith-Roach, M. J. A review of recent trends in electrospray ionisation-mass spectrometry for the analysis of metal-organic ligand complexes. *Anal. Chim. Acta* **2010,** *678*, 140-148.

40. Hao, C. Y.; March, R. E. Electrospray ionization tandem mass spectrometric study of salt cluster ions: Part 2 - Salts of polyatomic acid groups and of multivalent metals. *J. Mass Spectrom.* **2001,** *36*, 509-521.

41. Wang, H. J.; Agnes, G. R. Evaluation of electrospray mass spectrometry as a technique for quantitative analysis of kinetically labile solution species. *Anal. Chem.* **1999,** *71*, 3785-3792.

42. Wang, H. J.; Agnes, G. R. Kinetically labile equilibrium shifts induced by the electrospray process. *Anal. Chem.* **1999,** *71*, 4166-4172.

43. Constantopoulos, T. L.; Jackson, G. S.; Enke, C. G. Effects of salt concentration on analyte response using electrospray ionization mass spectrometry. *J. Am. Soc. Mass Spectrom.* **1999,** *10*, 625-634.

44. Di Marco, V. B.; Bombi, G. G.; Zambon, S.; Traidi, P. Metal-ligand solution equilibria studied by electrospray ionization mass spectrometry: Effect of instrumental parameters. *J. Mass Spectrom.* **2009,** *44*, 120-127.

45. Di Marco, V. B.; Raveane, L.; Dean, A.; Traldi, P. Perturbations produced by electrospray ionization mass spectrometry in the speciation of aluminium(III)/1,6-dimethy1-4-hydroxy-3-pyridinecarboxylate aqueous solutions. *Rapid Commun. Mass Spectrom.* **2010,** *24*, 868-874.

46. Schmidt, A.; Karas, M.; Dulcks, T. Effect of different solution flow rates on analyte ion signals in nano-ESI MS, or: When does ESI turn into nano-ESI? *J. Am. Soc. Mass Spectrom.* **2003,** *14*, 492-500.

47. Benkestock, K.; Sundqvist, G.; Edlund, P. O.; Roeraade, J. Influence of droplet size, capillary-cone distance and selected instrumental parameters for the analysis of noncovalent protein-ligand complexes by nano-electrospray ionization mass spectrometry. *J. Mass Spectrom.* **2004,** *39*, 1059-1067.

48. Sherman, C. L.; Brodbelt, J. S. An equilibrium partitioning model for predicting response to host-guest complexation in electrospray ionization mass spectrometry. *Anal. Chem.* **2003,** *75*, 1828-1836.

49. Miao, X. S.; Metcalfe, C. D.; Hao, C. Y.; March, R. E. Electrospray ionization mass spectrometry of ginsenosides. *J. Mass Spectrom.* **2002,** *37*, 495-506.

50. Katta, V.; Chowdhury, S. K.; Chait, B. T. Electrospray ionization - A new tool for the analysis of ionic transition-metal complexes. *J. Am. Soc. Mass Spectrom.* **1990,** *112*, 5348-5349.

51. Cheng, Z. L.; Siu, K. W. M.; Guevremont, R.; Berman, S. S. Electrospray mass-spectrometry - A study on some aqueous-solutions of metal-salts. *J. Am. Soc. Mass Spectrom.* **1992,** *3*, 281-288.

52. Jaison, P. G.; Kumar, P.; Telmore, V. M.; Aggarwal, S. K. Electrospray ionization mass spectrometric studies on uranyl(VI) complex with alpha-hydroxyisobutyric acid in water-methanol medium. *Rapid Commun. Mass Spectrom.* **2013,** *27*, 1105-1118.

53. Rellan-Alvarez, R.; Abadia, J.; Alvarez-Fernandez, A. Formation of metal-nicotianamine complexes as affected by pH, ligand exchange with citrate and metal exchange. A study by electrospray ionization time-of-flight mass spectrometry. *Rapid Commun. Mass Spectrom.* **2008,** *22*, 1553-1562.

54. Cartwright, A. J.; May, C. C.; Worsfold, P. J.; Keith-Roach, M. J. Characterisation of thorium-ethylenediaminetetraacetic acid and thorium-nitrilotriacetic acid species by electrospray ionisation-mass spectrometry. *Anal. Chim. Acta* **2007,** *590*, 125-131.

55. Couto, N.; Duarte, M. F.; Fernandez, M. T.; Rodrigues, P.; Barros, M. T.; Costa, M. L.; Cabral, B. J. C. Complexation of transition metals by 3-azidopropionitrile. An

electrospray ionization mass spectrometry study. *J. Am. Soc. Mass Spectrom.* **2007,** *18*, 453-465.

56. Yu, Q.; Yu, B.; Yang, H.; Li, X.; Liu, S. Silver (I)-assisted enantiomeric analysis of ginsenosides using electrospray ionization tandem mass spectrometry. *J. Mass Spectrom.* **2012,** *47*, 1313-1321.
57. Chai, Y.; Shen, S.; Weng, G.; Pan, Y. Gas-phase synthesis and reactivity of Cu^{+}-benzyne complexes. *Chem. Commun.* **2014,** *50*, 11668-11671.
58. Banu, L.; Blagojevic, V.; Bohme, D. K. Dissociations of gas-phase complexes of deprotonated glutathione with Co^{2+}, Ni^{2+}, Cu^{2+} and Zn^{2+}: The importance of metal ion reduction. *Int. J.Mass Spectrom.* **2013,** *345*, 142-152.
59. Tsybizova, A.; Rulisek, L.; Schroder, D.; Rokob, T. A. Coordination and bond activation in complexes of regioisomeric phenylpyridines with the nickel(II) chloride cation in the gas phase. *J. Phys. Chem. A* **2013,** *117*, 1171-1180.
60. Wu, L. M.; Zhou, L.; Liu, D. Q.; Vogt, F. G.; Kord, A. S. LC-MS/MS and density functional theory study of copper(II) and nickel(II) chelating complexes of elesclomol (a novel anticancer agent). *J. Pharmaceut. Biomed.* **2011,** *54*, 331-336.
61. Lodyga-Chruscinska, E.; Szebesczyk, A.; Sanna, D.; Hegetschweiler, K.; Micera, G.; Garribba, E. Formation in aqueous solution of a non-oxido V-IV complex with VN6 coordination. Potentiometric, ESI-MS, spectroscopic and computational characterization. *Dalton Trans.* **2013,** *42*, 13404-13416.
62. Enyedy, E. A.; Nagy, N. V.; Zsigo, E.; Kowol, C. R.; Arion, V. B.; Keppler, B. K.; Kiss, T. Comparative solution equilibrium study of the interactions of copper(II), iron(II) and zinc(II) with triapine (3-aminopyridine-2-carbaldehyde thiosemicarbazone) and related ligands. *Eur. J. Inorg. Chem.* **2010,** *11*, 1717-1728.
63. Caudle, M. T.; Stevens, R. D.; Crumbliss, A. L. Electrospray mass-spectrometry study of 1/1 ferric dihydroxamates. *Inorg. Chem.* **1994,** *33*, 843-844.
64. Caudle, M. T.; Stevens, R. D.; Crumbliss, A. L. A monomer-to-dimer shift in a series of 1/1-ferric dihydroxamates probed by electrospray mass-spectrometry. *Inorg. Chem.* **1994,** *33*, 6111-6115.
65. Damante, C. A.; Osz, K.; Nagy, Z.; Papalardo, G.; Grasso, G.; Impellizzeri, G.; Rizzarelli, E.; Sovago, I. The metal loading ability of beta-amyloid n-terminus: A

combined potentiometric and spectroscopic study of copper(II) complexes with beta-amyloid(1-16), its short or mutated peptide fragments, and its polyethylene glycol (peg)-ylated analogue. *Inorg. Chem.* **2008,** *47* (20), 9669-9683.

66. Djurdjevic, P.; Joksovic, L.; Jelic, R.; Djurdjevic, A.; Stankov, M. J. Solution equilibria between aluminum(III) ion and some fluoroquinolone family members. Spectroscopic and potentiometric study. *Chem. Pharm. Bull.* **2007,** *55*, 1689-1699.
67. Di Marco, V. B.; Karoly-Lakatos, A.; Venzo, A.; Bertani, R.; Seraglia, R.; Kiss, T. The aluminium(III)-sialic acid interaction: A potential role in aluminium-induced cellular membrane degeneration. *Inorg. Chim. Acta* **2006,** *359*, 4227-4234.
68. Matsumoto, A.; Fukumoto, T.; Adachi, H.; Watarai, H. Electrospray ionization mass spectrometry of metal complexes. Gas phase formation of a binuclear copper(II)-5-Br-PADAP complex. *Anal. Chim. Acta* **1999,** *390*, 193-199.
69. Murner, H.; von Zelewsky, A.; Hopfgartner, G. Dinuclear metal complexes of Cd(II), Zn(II) and Fe(II) with triple-helical structure and predetermined chirality. *Inorg. Chim. Acta* **1998,** *271*, 36-39.
70. Jezowska-Bojczuk, M.; Lesniak, W.; Szczepanik, W.; Gatner, K.; Jezierski, A.; Smoluch, M.; Bal, W. Copper(II)-lincomycin: Complexation pattern and oxidative activity. *J. Inorg. Biochem.* **2001,** *84*, 189-200.
71. Murariu, M.; Dragan, E. S.; Drochioiu, G. Model peptide-based system used for the investigation of metal ions binding to histidine-containing polypeptides. *Biopolymers* **2010,** *93*, 497-508.
72. Groenewold, G. S.; Van Stipdonk, M. J.; Gresham, G. L.; Chien, W.; Bulleigh, K.; Howard, A. Collision-induced dissociation tandem mass spectrometry of desferrioxamine siderophore complexes from electrospray ionization of UO_2^{2+}, Fe^{3+} and Ca^{2+} solutions. *J. Mass Spectrom.* **2004,** *39*, 752-761.
73. McDonald, L. W.; Campbell, J. A.; Clark, S. B. Failure of ESI spectra to represent metal-complex solution composition: A study of lanthanide-carboxylate complexes. *Anal. Chem.* **2014,** *86*, 1023-1029.
74. Di Marco, V. B.; Bombi, G. G.; Ranaldo, M.; Traldi, P. Metal-ligand solution equilibria studied by electrospray ionization mass spectrometry: Correlation between

ion intensity and acid-base equilibria in solution. *Rapid Commun. Mass Spectrom.* **2007,** *21*, 3825-3832.

75. Di Marco, V. B.; Bombi, G. G.; Tubaro, M.; Traldi, P. Electrospray ionization mass spectrometry in studies of aluminium(III)-ligand solution equilibria. *Rapid Commun. Mass Spectrom.* **2003,** *17*, 2039-2046.
76. Di Marco, V. B.; Yokel, R. A.; Ferlin, M. G.; Tapparo, A.; Bombi, G. G. Evaluation of 3,4-hydroxypyridinecarboxylic acids as possible bidentate chelating agents for aluminium(III): Synthesis and metal-ligand solution chemistry. *Eur. J. Inorg. Chem.* **2002,** *10*, 2648-2655.
77. Daniel, J. M.; Friess, S. D.; Rajagopalan, S.; Wendt, S.; Zenobi, R. Quantitative determination of noncovalent binding interactions using soft ionization mass spectrometry. *Int. J. Mass Spectrom.* **2002,** *216*, 1-27.
78. Gabelica, V.; Galic, N.; Rosu, F.; Houssier, C.; De Pauw, E. Influence of response factors on determining equilibrium association constants of non-covalent complexes by electrospray ionization mass spectrometry. *J. Mass Spectrom.* **2003,** *38*, 491-501.
79. Chen, Z.; Weber, S. G. Determination of binding constants by affinity capillary electrophoresis, electrospray ionization mass spectrometry and phase-distribution methods. *Trac-Trends Anal. Chem.* **2008,** *27*, 738-748.
80. Bond, A. M.; Colton, R.; Traeger, J. C.; Harvey, J. Phosphine derivatives of mercury and cadmium dithiolates - An electrospray mass-spectrometric study. *Inorg. Chim. Acta* **1995,** *228*, 193-197.
81. Bonnington, L. S.; Coll, R. K.; Gray, E. J.; Flett, J. I.; Henderson, W. Electrospray mass spectrometric investigation of the relative ligand properties of EPh_3 ligands (E = P, As, Sb or Bi) towards Ag^+ and Cu^+. *Inorg. Chim. Acta* **1999,** *290*, 213-221.
82. Keith-Roach, M. J.; Buratti, M. V.; Worsfold, P. J. Thorium complexation by hydroxamate siderophores in perturbed multicomponent systems using flow injection electrospray ionization mass spectrometry. *Anal. Chem.* **2005,** *77*, 7335-7341.
83. Meda, A. R.; Scheuermann, E. B.; Prechsl, U. E.; Erenoglu, B.; Schaaf, G.; Hayen, H.; Weber, G.; von Wiren, N. Iron acquisition by phytosiderophores contributes to cadmium tolerance. *Plant Physiol.* **2007,** *143*, 1761-1773.

84. Zheng, X. J.; Jin, L. P.; Mei, Y. H.; Zhu, L. G. Photochromism and electrospray mass spectrum of the ternary europium system with nicotinic acid and 1,10-phenanthroline. *J. Solution Chem.* **2001,** *30* (11), 985-994.

Chapter 2

Gas-Phase Copper and Silver Complexes with Phosphorothioate and Phosphorodithioate Pesticides Investigated using Electrospray Ionization Mass Spectrometry*

Abstract

Efforts to improve agricultural productivity have led to a growing dependency on organophosphorus pesticides. Phosphorothioate and phosphorodithioate pesticides are organophosphorus pesticide subclasses with widespread application for the control of insects feeding on vegetables and fruits. However, even low doses of these pesticides can cause neurological problems in humans; thus, their determination and monitoring in agricultural foodstuffs is important for human health. Phosphorothioate and phosphorodithioate pesticides may be poorly ionized during electrospray, adversely affecting limits of detection. These pesticides can form complexes with Cu^{2+} and Ag^{+}, however, potentially improving ionization. In the present work we used electrospray ionization mass spectrometry (ESI-MS) to study fenitrothion, parathion, diazinon, and malathion coordination complexes with silver and copper ions. Stable 1:1 and 1:2 metal/pesticide complexes were detected. Mass spectra acquired from pesticide solutions containing Ag^{+} or Cu^{2+} showed a significant increase in signal-to-background ratio over those acquired from solutions containing only the pesticides,

---

*Chapter published in *J. Mass Spectrom.* **2015**, 50, 145−152. Reproduced with permission from John Wiley and Sons. See Appendix B for letter of permission to republish this material.

with Ag^+ improving detection more effectively than Cu^{2+}. Addition of Ag^+ to a pesticide solution improved the limit of detection by ten times. The relative affinity of each pesticide for Ag^+ was related to complex stability, following the order diazinon > malathion > fenitrothion > parathion. The formation of Ag^+-pesticide complexes can significantly improve the detection of phosphorothioate and phosphorodithioate pesticides using ESI-MS. The technique could potentially be used in reactive desorption electrospray ionization/mass spectrometry to detect phosphorothioate and phosphorodithioate pesticides on fruit and vegetable skins.

2.1 Introduction

The increasing global demand for food has led to a growing dependency on the use of pesticides to improve agricultural productivity. Organophosphorus pesticides (OPs), which have widespread application for the control of insect pests that feed on fresh vegetables and fruits,[1, 2] comprise ~35% of the pesticides used in the United States.[3] OPs may be divided into eight subclasses based on structural characteristics,[4] but the general structure can be represented as in Figure 2.1a. R_1 and R_2 may be alkoxy, aryl, alkylthio, or alkylamino groups, while L is an easily hydrolysable leaving group that is displaced during the phosphorylation of acetylcholinesterase, an enzyme responsible for catalyzing the hydrolysis of the neurotransmitter acetylcholine. Because OPs or their metabolites act to inhibit acetylcholinesterase, they have toxic effects on humans and other mammals.[5] Exposure to these pesticides is a major health problem, with thousands of accidental poisonings occurring each year across the globe.[6] Even low-dose chronic exposure to OPs can cause a variety of neurological problems.[7] Thus, there is great interest in the

determination and monitoring of OPs in agricultural products, food products, and the environment.

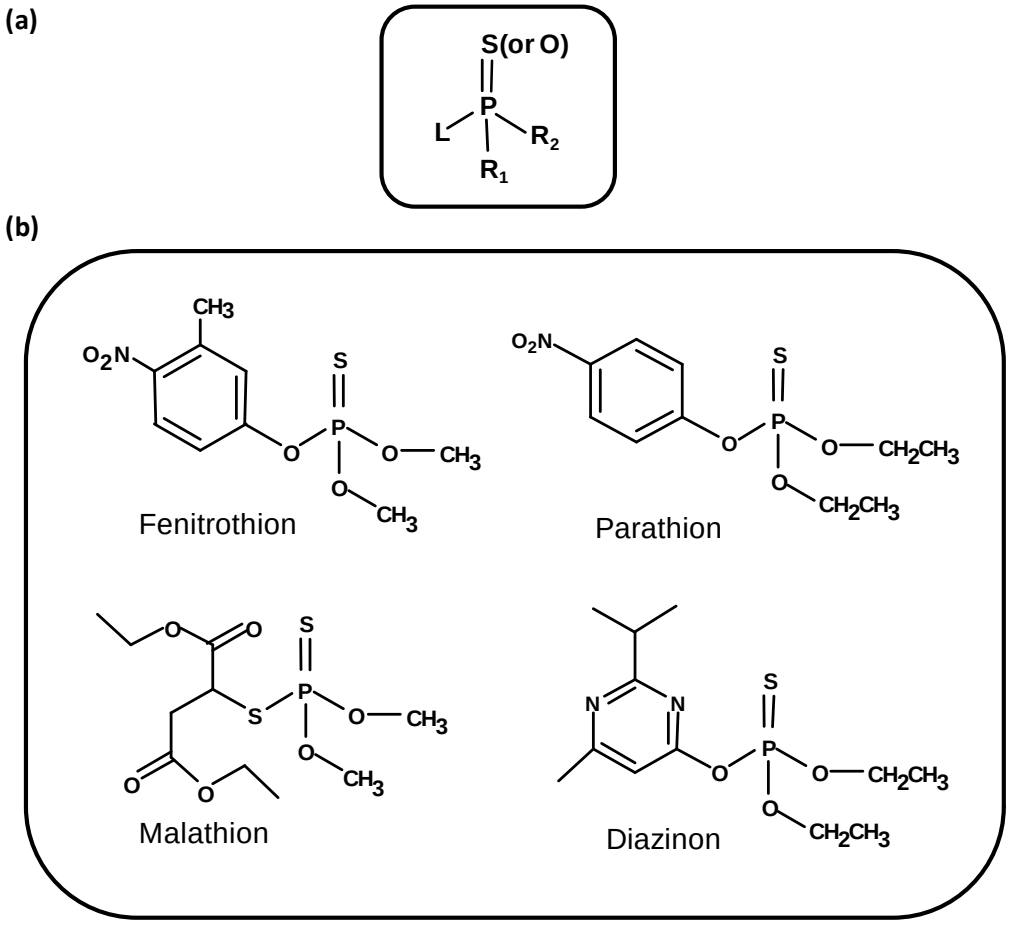

Figure 2.1 (a) General structure of an organophosphorus pesticide. (b) Structures of the organophosphorus pesticides used in this study.

Organophosphorus pesticides are known to form solution complexes with transition metal ions.[8-11] In one investigation using both nuclear magnetic resonance (NMR) and electrospray ionization mass spectrometry (ESI-MS), Koo et al.[8] showed that Cu^{2+} binds to the thiophosphoryl sulfur atom in fenitrothion (FN) to form a coordination complex. A

similar observation was also recorded for complexes of Hg^{2+} and FN.[11] The formation of OP-transition metal complexes is important to understand because certain transition metals may catalyze pesticide hydrolysis in the environment.[12-15] Cu^{2+} and Hg^{2+}, in particular, can promote the hydrolysis of certain OPs.[12, 14, 15] The rate at which hydrolysis proceeds depends on pesticide structure.[15] A recent study showed that the OP-metal complex can be investigated using ESI-MS before the onset of degradation.[16] In that study, ESI-MS was used to characterize Ag^{+}, Cu^{2+}, and Hg^{2+} complexes with the OP quinalphos in order to gain insight into the solution complexes formed between quinalphos and these transition metal ions. The 1:1 metal-quinalphos complexes were observed for Ag^{+} and Cu^{2+}, while a 2:3 complex was observed for Hg^{2+}.

Over the years, the major analytical methods that have been employed in analysis of OPs and their metabolites are gas chromatography (GC), gas chromatography/mass spectrometry (GC-MS), and liquid chromatography/mass spectrometry (LC-MS),[2, 17-19] although electrochemical[20] and enzyme-based methods[21] have also been reported. Alder et al.[22] compared the scope and sensitivities of GC-MS and LC-MS methods for the analysis of different classes of pesticides. Their results show that LC-MS provides greater sensitivity than GC-MS for most OPs studied when ESI is used as ionization method. However, OPs having groups that are only weakly basic or weakly acidic may be poorly ionized during electrospray, affecting the sensitivity of the analysis. The formation of charged OP-metal complexes suggests that it is possible to improve the ionization of OPs in ESI-MS using transition metals, and that the ionization efficiency relates to the stability of the OP-metal complex.

Improved ionization of weak proton acceptors in ESI-MS is commonly achieved using either derivatization techniques or metal adduct formation. In a recent review, Iwasaki et al.[23] discussed the various chemical derivatization strategies useful for ionization enhancement in ESI-MS. The addition of alkali or transition metal ions to solutions of poorly ionizable compounds that can form metal coordination complexes is a relatively common way of improving the detection of these types of compounds in ESI-MS. Kohler and Leary[24] showed that introducing solutions containing LiCl, NaC1, KCl, RbCl, CsCl, and $CoC1_2$ during electrospray enhanced detection sensitivity for carbohydrate compounds, while Rogatsky et al.[25] reported that high sensitivities could be obtained in LC-MS when Cs^+ was added to the mobile phase during the separation of carbohydrates from human plasma. Sodium adducts generated through electrospray allowed improved detection of thiol compounds containing carboxylic acid and carboxylic acid amides for selected-ion-monitoring experiments,[26] as well as of certain steroids.[27] Transition metals, especially Ag^+, have also been used to enhance ionization in ESI-MS. Rentel et al.[28] used Ag^+ to enhance ionization of carotenoids and tocopherols, and Bayer et al.[29] were able to successfully analyze unsaturated compounds such as steroids, polystyrenes, carotinoids, terpenes, and unsaturated fatty acid esters by introducing reagent solutions containing Ag^+ or Pd^{2+} during electrospray. Charged π or π-allyl metal coordination complexes were formed, significantly improving sensitivity. Ag^+ coordination has also been successfully used to ionize lipid peroxides for detection by ESI-MS.[30]

In the study reported here, we investigate the formation of Ag^+ and Cu^{2+} coordination complexes during ESI-MS with four commonly used OPs: fenitrothion (FN), parathion (PT), malathion (MT), and diazinon (DZ) (Figure 2.1b). FN, PT, and DZ are

phosphorothioate pesticides, while MT is a phosphorodithioate pesticide. The phosphorothioate and phosphorodithioate pesticides are OP subclasses having widespread application for the control of insects feeding on vegetables and fruits. FN-metal complexes have been well documented,[8, 11] while PT, MT, and DZ were chosen to investigate the effect of both ring substituents and alkyl chain length on the formation of the metal/pesticide complex. We also demonstrate that complex formation can serve to improve ESI-MS detection of these pesticides, with complex stability playing a role in detection.

2.2 Experimental

2.2.1 Materials

Silver(I) nitrate (ReagentPlus®, ≥99.0 %) was purchased from Sigma-Aldrich (St. Louis, MO). Copper(II) nitrate trihydrate (puriss. p.a., 99.0–104%) was purchased from Fluka (St. Louis, MO). FN, PT, MT, and DZ analytical standards (PESTANAL®) were purchased from Sigma-Aldrich (St. Louis, MO) and stored at 2 °C. All chemicals were used as received. High purity (99%) Omnisolv grade methanol was purchased from EMD Chemicals (Gibbstown, NJ). Water was purified using a Milli-Q UV system (Millipore Corporation).

2.2.2 Sample preparation

10 mM stock solutions of FN, PT, MT, and DZ were prepared by dissolving the appropriate amount of pesticide in methanol. 10 mM solutions of each metal salt ($Cu(NO_3)_2 \cdot 3H_2O$ or $AgNO_3$) were also prepared by dissolving the appropriate amount of salt

in a 50:50 (v/v) methanol:water solution. The 10 mM metal and pesticide stock solutions were combined and diluted with a 50:50 (v/v) methanol:water solution to give a final metal and pesticide concentration of 0.1 mM each. Stock solutions and samples were prepared on the day of use.

2.2.3 Instrumentation

Electrospray ionization mass spectra were collected using a Finnigan LCQ Deca XP plus ion trap mass spectrometer (ThermoFinnigan Corporation, San Jose, CA). The sample solutions were infused at a flow rate of 3 µl/min. The spray needle voltage was maintained at +4.00 kV, while the nitrogen sheath gas flow rate was set to 35 (arbitrary units). A capillary voltage of 15 V was applied. The capillary temperature was maintained at 275 $^{\circ}$C. The ion trap mass analyzer was operated at a pressure of 1.5 x 10^{-5} Torr. The instrument was set to detect ion species in the *m/z* range of 100 – 1000. Spectra were acquired in positive ion mode and processed using Xcalibur software (Thermo Electron, San Jose, CA).

2.3 Results and Discussion

2.3.1 Effect of Ag^{+} and Cu^{2+} on ESI-MS detection of phosphorothioate and phosphorodithioate pesticides

We have used ESI-MS to investigate the complexes formed between the OPs FN, PT, MT, and DZ, and the transition metals Ag^{+} and Cu^{2+} to determine whether pesticide structure plays a role in the stabilities of the metal complexes and overall signal-to-background ratios (S/B) of the metal-pesticide complexes. The S/B is defined by

Sparkman[31] as "the ratio of the signal strength produced by a sample to that of the background for a measurement." The background signal must be measured as closely as possible to the sample signal. In this study, S/B was measured by dividing the signal intensity of the most intense peak in the mass spectrum by the average signal intensity of the baseline region closest to that peak. The spectra used to calculate S/B for one pesticide (FN) are shown in Figure 2.2, along with additional explanation of the method. Calculated S/B values for the various systems studied are averages and were determined using the results of at least three separate experiments.

A solution containing only 0.1 mM FN in 50:50 (v/v) methanol:water gives rise to a mass spectrum with a S/B of ~60 (Figure 2.3a). A peak at *m/z* 278 was assigned to protonated FN ($[FN+H]^+$), while the ammonium adduct, $[FN+NH_4]^+$, was observed at *m/z* 295. Peaks at *m/z* 436, 574, 637, and 654 can be assigned to singly- and doubly-charged FN-containing ions, including sodium, potassium, and ammonium adducts. Peak assignments are given in Table 2.1. Mass spectra acquired from solutions containing 0.1 mM FN and 0.1 mM of either Ag^+ or Cu^{2+} are shown in Figures 2.3b and 2.3c, respectively. *m/z* values given for metal-pesticide complexes here and elsewhere are for the ^{107}Ag- and ^{63}Cu-containing ions. The addition of either Ag^+ or Cu^{2+} to the FN solution increased the S/B, with a much greater increase observed for the Ag^+-containing solution. The mass spectrum acquired from the FN solution containing Ag^+ had a S/B of ~1500, approximately 25 times higher than that determined from the mass spectrum acquired from the FN solution in the absence of Ag^+. The S/B determined from the mass spectrum acquired using a solution containing Cu^{2+} was ~300, an approximately fivefold increase over that determined from the mass spectrum acquired from the FN solution alone. Ion identifications and peak assignments for the

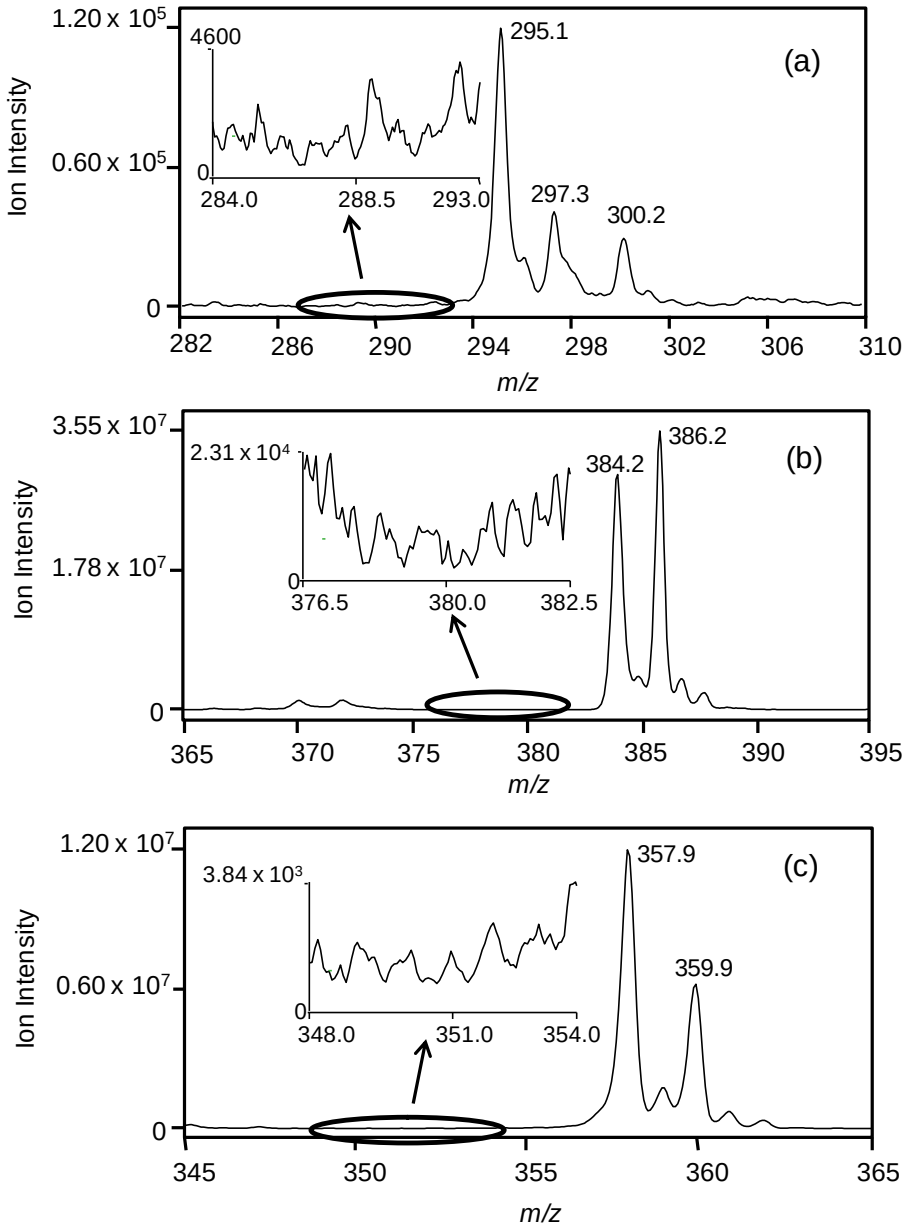

Figure 2.2 Positive-ion mass spectra acquired from solutions containing a) 0.1mM fenitrothion, b) 0.1 mM fenitrothion and 0.1 mM Ag^{+}, and c) 0.1 mM fenitrothion and 0.1 mM Cu^{2+} showing peaks assigned to fenitrothion-containing ions. Each mass spectrum shows the signal intensity of the major peak as well as that of a portion of the baseline region (insert). The circled region of the baseline was used to determine the signal intensity of the baseline. The ratio of the signal intensity of *m/z* 295.1 ($[FN+H]^{+}$) to the average signal intensity of the baseline region was used in calculating the signal-to-background ratio (S/B) for spectrum (a), the ratio of the signal intensity of *m/z* 384.2 ($[FN+^{107}Ag]^{+}$) to the average signal intensity of the baseline region was used in calculating the S/B for spectrum (b), and the ratio of the signal intensity of *m/z* 357.9 ($[FN+^{63}Cu]^{+}$) to the average signal intensity of the baseline region was used in calculating the S/B for spectrum (c).

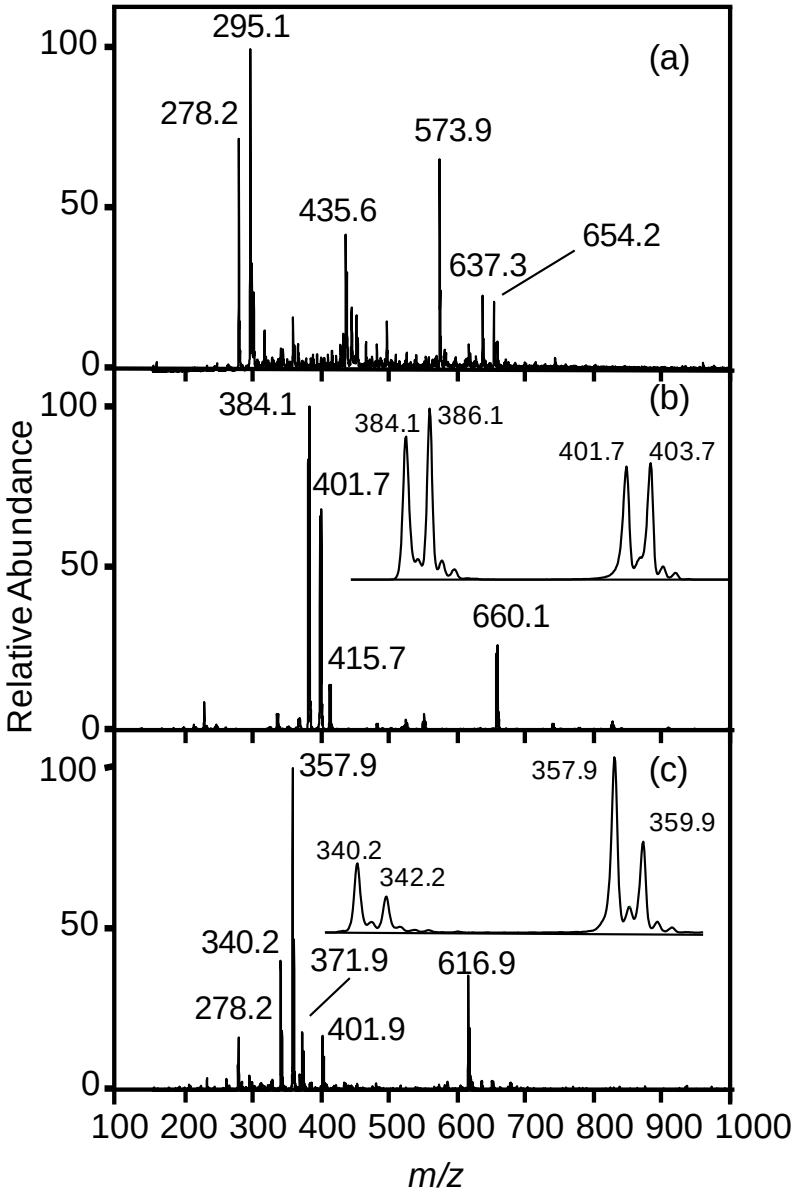

Figure 2.3 Positive-ion mass spectra obtained from solutions containing a) 0.1 mM fenitrothion, b) 0.1 mM fenitrothion and 0.1 mM Ag^{+}, and c) 0.1 mM fenitrothion and 0.1 mM Cu^{2+}. The solutions were prepared using 50:50 (v/v) methanol:water. The inset in (b) and (c) shows the isotopic distributions of selected Ag-fenitrothion and Cu-fenitrothion complexes. *m/z* values given for metal-pesticide complexes are for the ^{107}Ag- and ^{63}Cu-containing ions.

spectra shown in Figures 2.3b and c are given in Table 2.1. With a few exceptions, the oxidation state of copper in the detected ions is +1, and no doubly-charged Cu(II)-containing ions were observed in the mass spectra. The reduction of Cu^{2+} to Cu^{+} during electrospray is a well-known phenomenon.[32]

The effect of Ag^{+} and Cu^{2+} on S/B calculated from mass spectra acquired using solutions containing PT, MT, and DZ was also examined. The mass spectra are shown in Figures 2.4, 2.5, and 2.6, respectively. Peak assignments are given in Table 2.1. Figure 2.7 summarizes the effect of Ag^{+} and Cu^{2+} addition to the pesticide-containing solutions on S/B for each pesticide. The data used to construct Figure 2.7 are given in Table 2.2. In what seems to be a common trend for all the pesticides studied, S/B was always greater in mass spectra acquired from Ag^{+}-containing solutions than in those acquired from Cu^{2+}-containing solutions, suggesting that Ag^{+} forms a complex more readily with the pesticide than does Cu^{2+}. In addition, a peak resulting from a protonated pesticide ion was visible in mass spectra acquired from pesticide solutions containing Cu^{2+}, but not from those containing Ag^{+}. An example of this can be seen in Figure 2.3, where a peak due to protonated FN ($[FN+H]^{+}$, *m/z* 278) appears in mass spectra acquired from solutions containing FN and Cu^{2+} (Figure 2.3c), but not in mass spectra acquired from solutions containing FN and Ag^{+} (Figure 2.3b). The increase in S/B observed in positive ion mode upon addition of either Cu^{2+} or Ag^{+} to the pesticide solution is likely because formation of the pesticide-metal complex is more likely to occur than H^{+} adduction. Both Cu^{2+} and Ag^{+} have been reported to form stable complexes with phosphorothioate pesticides.[8, 16]

Table 2.1 Pesticide-containing ions detected using ESI-MS.

Solution species	**Ion**	**Observed *m/z****	**Theoretical *m/z****
FN ($C_9H_{12}NO_5PS$)			
	$[FN+H]^+$	278.2	278.0
	$[FN+NH_4]^+$	295.1	295.0
	$[3(FN)+NH_4+Na)]^{2+}$	435.6	436.0
	Unassigned	495.9	-------
	$[4(FN)+K+H]^{2+}$	573.9	574.0
	$[2(FN)+H_2O+2(CH_3OH)+H]^+$	637.3	637.1
	$[2(FN)+H_2O+2(CH_3OH)+NH_4]^+$	654.2	654.1
$FN+Ag^+$			
	$[FN+Ag]^+$	384.1	383.9
	$[FN+H_2O+Ag]^+$	401.7	401.9
	$[FN+CH_3OH+Ag]^+$	415.7	415.9
	$[2(FN)+Ag]^+$	660.7	660.9
$FN+Cu^{2+}$			
	$[FN+Cu]^+$	340.2	339.9
	$[FN+H_2O+Cu]^+$	357.9	357.9
	$[FN+CH_3OH+Cu]^+$	371.9	372.0
	$[FN+NO_3+Cu]^+$	401.7	401.9
	$[2(FN)+Cu]^+$	616.9	617.0
PT ($C_{10}H_{14}NO_5PS$)	$[PT+H]^+$	292.0	292.0
	Unassigned	501.8	-------
	$[4(PT)+K+H]^{2+}$	601.9	602.0
	Unassigned	654.1	-------
$PT+Ag^+$			
	$[PT+Ag]^+$	398.0	397.9
	$[PT+H_2O+Ag]^+$	415.6	415.9
	$[PT+CH_3OH+Ag]^+$	429.7	430.0
	$[2(PT)+Ag]^+$	688.8	689.0
	$[2(PT)+NO_3+2Ag]^+$	857.6	857.9
$PT+Cu^{2+}$			
	$[PT+H_2O+Cu]^+$	371.7	372.0
	$[PT+CH_3OH+Cu]^+$	385.7	386.0
	$[PT+NO_3+Cu]^+$	415.8	416.0
	$[2(PT)+Cu]^+$	644.9	645.0
	$[2(PT)+NO_3+Cu]^+$	706.7	707.0

* Observed *m/z* values for Ag and Cu-containing ions are those for the ^{107}Ag and ^{63}Cu isotopes. Theoretical *m/z* values for complexes were calculated based on ^{107}Ag and ^{63}Cu isotopes.

Table 2.1 continued. Pesticide-containing ions detected using ESI-MS

Solution species	**Ions**	**Observed *m/z***	**Theoretical *m/z***
MT ($C_{10}H_{19}O_6PS_2$)			
	$[MT+H]^+$	330.9	331.0
	$[MT+NH_4]^+$	347.9	348.1
	$[MT+Na]^+$	353.1	353.0
	$[2(MT)+Na]^+$	682.7	683.1
$MT+Ag^+$			
	$[MT+Ag]^+$	437.1	436.9
	$[2(MT)+Ag]^+$	766.7	767.0
$MT+Cu^{2+}$			
	$[MT+Cu]^+$	392.9	393.0
	$[MT+NO_3+Cu]^+$	454.8	455.0
	$[2(MT)+Cu]^+$	722.7	723.0
DZ ($C_{12}H_{21}N_2O_3PS$)	$[DZ+H]^+$	305.1	305.1
	$[DZ+Na]^+$	327.1	327.1
	$[2(DZ)+Na]^+$	630.8	631.2
$DZ+Ag^+$			
	$[C_8H_{12}N_2O+Ag]^+$	259.1	259.0
	$[C_8H_{12}N_2O+H_2O+Ag]^+$	276.8	277.0
	$[DZ-C_2H_4+Ag]^+$	382.9	383.0
	$[DZ+Ag]^+$	410.9	411.0
	$[2(DZ)+Ag]^+$	714.8	715.1
$DZ+Cu^{2+}$			
	$[C_8H_{12}N_2O+H_2O+Cu]^+$	232.9	233.0
	$[DZ+Cu]^+$	367.0	367.0
	$[DZ+NO_3+Cu]^+$	428.9	429.0
	$[2(DZ)+Cu]^+$	670.8	671.1
Mixed ligand complexes			
	$[Ag+FN+PT]^+$	674.8	675.0
	$[Ag+FN+DZ]^+$	687.7	688.0
	$[Ag+PT+MT]^+$	727.7	728.0
	$[Ag+MT+DZ]^+$	740.7	741.0
	$[Ag+MT+FN]^+$	713.8	714.0

* Observed *m/z* values for Ag and Cu-containing ions are those for the ^{107}Ag and ^{63}Cu isotopes. Theoretical *m/z* values for complexes were calculated based on ^{107}Ag and ^{63}Cu isotopes.

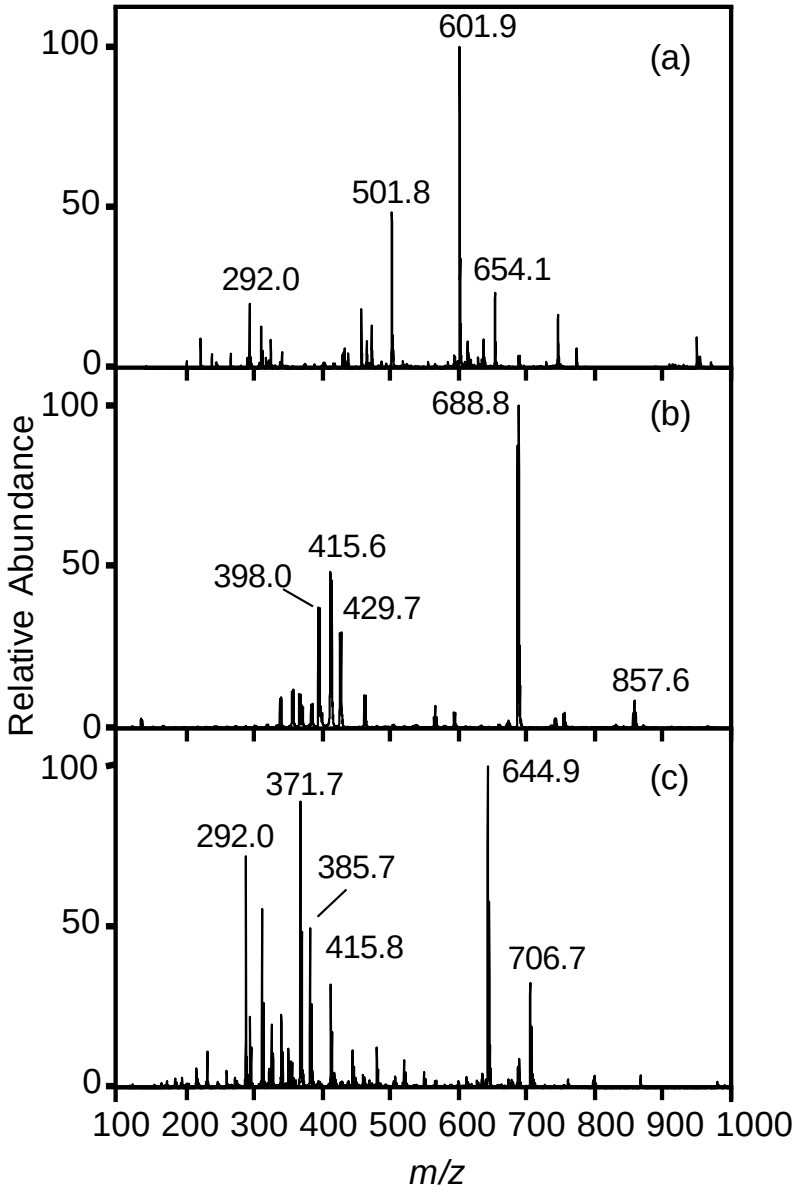

Figure 2.4 Positive-ion mass spectra obtained from solutions containing a) 0.1 mM parathion, b) 0.1 mM parathion and 0.1 mM Ag^{+}, and c) 0.1 mM parathion and 0.1 mM Cu^{2+}. All samples in 50:50 (v/v) methanol:water. *m/z* values given for metal-pesticide complexes are for the ^{107}Ag- and ^{63}Cu-containing ions.

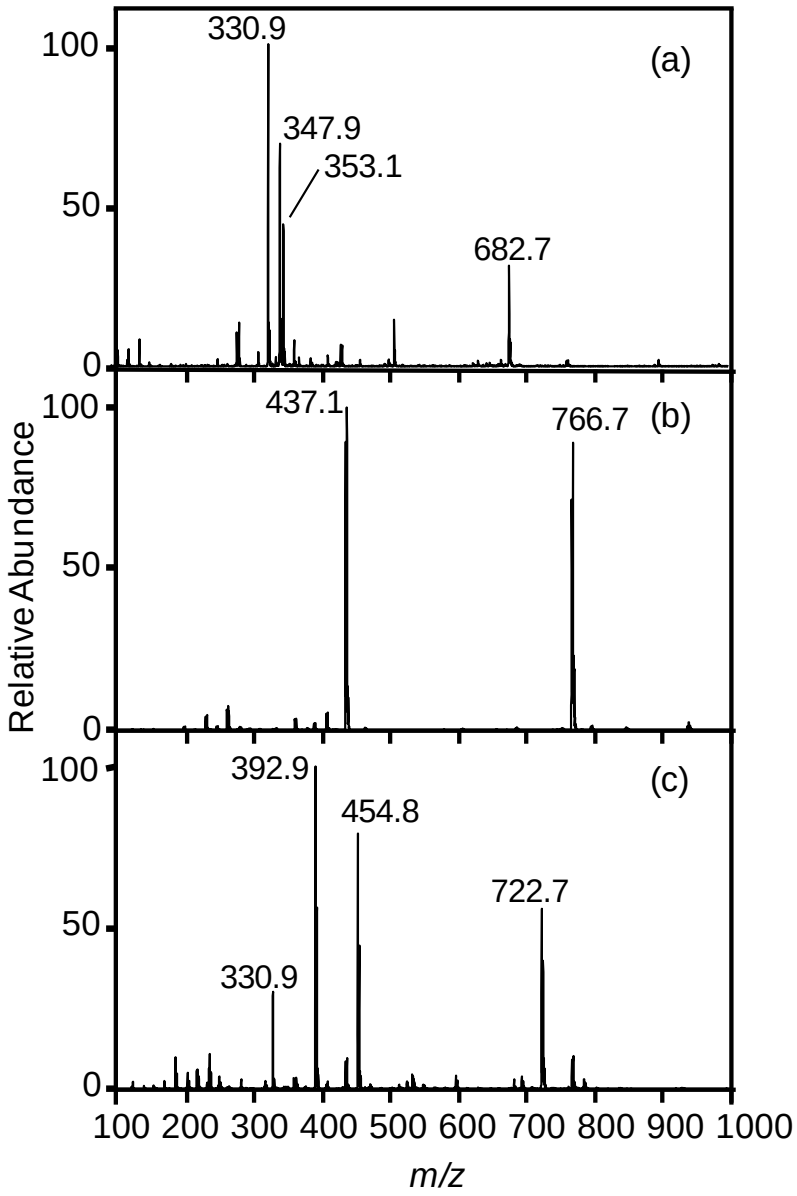

Figure 2.5 Positive-ion mass spectra obtained from solutions containing a) 0.1 mM malathion, b) 0.1 mM malathion and 0.1 mM Ag^{+}, and c) 0.1 mM malathion and 0.1 mM Cu^{2+}. All samples in 50:50 (v/v) methanol:water. *m/z* values given for metal-pesticide complexes are for the ^{107}Ag- and ^{63}Cu-containing ions.

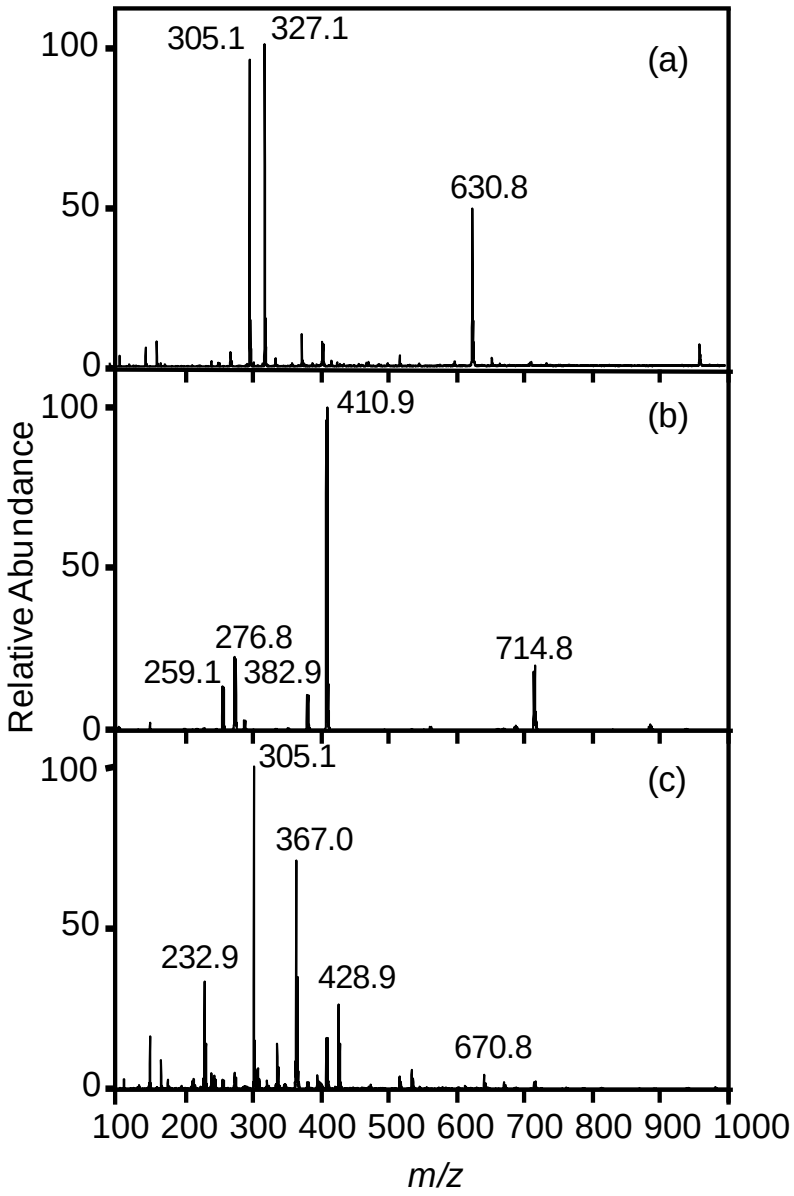

Figure 2.6 Positive-ion mass spectra obtained from solutions containing a) 0.1 mM diazinon, b) 0.1 mM diazinon and 0.1 mM Ag^{+}, and c) 0.1 mM diazinon and 0.1 mM Cu^{2+}. All samples in 50:50 (v/v) methanol:water. *m/z* values given for metal-pesticide complexes are for the ^{107}Ag- and ^{63}Cu-containing ions.

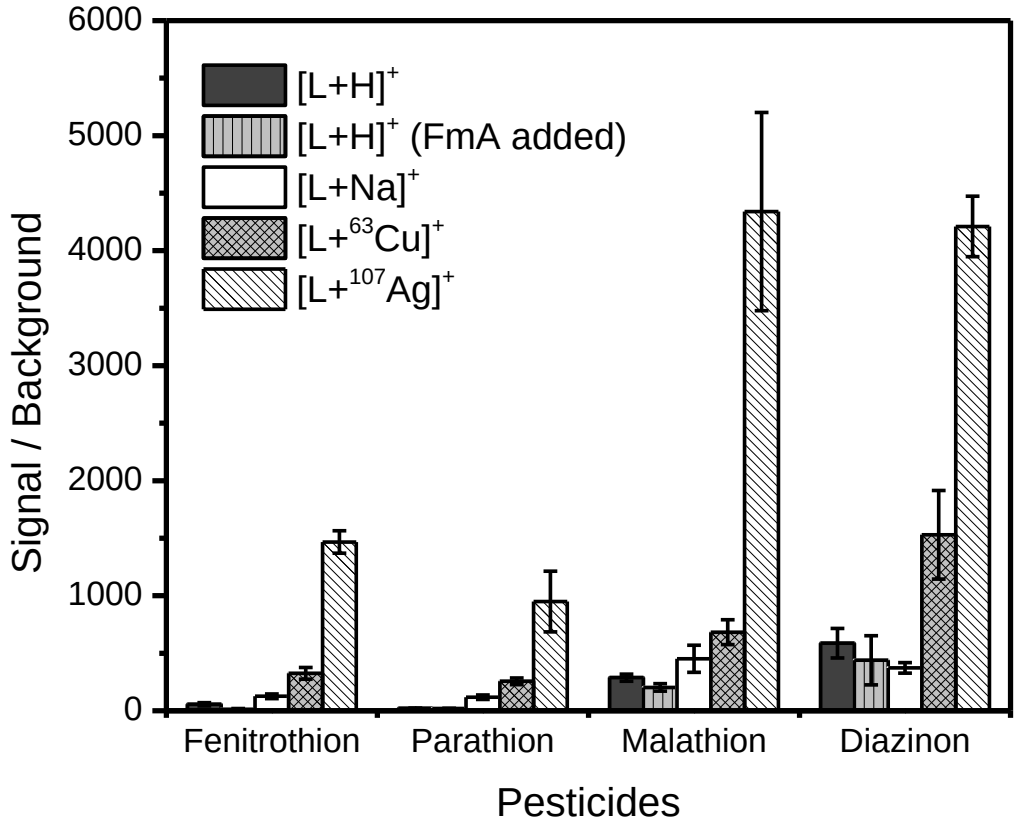

Figure 2.7 Signal-to-background ratios calculated using mass spectra acquired from 0.1 mM solutions of fenitrothion, parathion, malathion, and diazinon in the presence and absence of formic acid (FmA), Na^+, Cu^{2+}, and Ag^+. L indicates the pesticide. Na^+, Cu^{2+}, and Ag^+ concentrations were 0.1 mM each, while formic acid was used to adjust the pH of the pesticide solutions to pH ~4. The solutions were prepared in 50:50 (v/v) methanol:water. The error bars were obtained by averaging the S/B values obtained from spectra of three separate experiments.

Table 2.2 Signal-to-background ratios calculated using mass spectra acquired from 0.1 mM solutions of fenitrothion, parathion, malathion, and diazinon in the presence and absence of formic acid, Na^+, Cu^{2+}, and Ag^+. L indicates the pesticide. Na^+, Cu^{2+}, and Ag^+ concentrations were 0.1 mM each, while formic acid was used to adjust the pH of the pesticide solutions to pH ~4. The solutions were prepared in 50:50 (v/v) methanol:water. The standard deviation values were obtained by averaging the S/B values obtained from spectra of three separate experiments.

	Signal-to-background ratio			
	Fenitrothion	Parathion	Malathion	Diazinon
$[L+H]^+$ (no formic acid)	56 ± 14	20.7 ± 0.2	288 ± 31	587 ± 130
$[L+H]^+$ (formic acid added)	13 ± 6	20 ± 2	203 ± 32	439 ± 210
$[L+^{107}Ag]^+$	1467 ± 98	949 ± 260	4340 ± 860	4210 ± 260
$[L+^{63}Cu]^+$	325 ± 51	256 ± 29	683 ± 110	1530 ± 380
$[L+Na]^+$	126 ± 20	117 ± 20	452 ± 120	370 ± 46

The formation of a metal-pesticide complex generally depends on the favorable interaction between the metal and an active site on the pesticide molecule. The active site for the phosphorothioate pesticides has been established to be the 'soft' thiophosphoryl S-atom (Figure 2.1b).[8, 9] According to the Pearson hard-soft acid-base (HSAB) principle,[33] the interaction with the soft atom center will be favorable if the metal ion is also a soft atom. An atom with a relatively large atomic size is considered soft. Because Ag^+, with an ionic radius of 0.067 nm, is a softer atom than Cu^{2+}, which has an ionic radius of 0.057 nm, the formation of a Ag^+ complex in solution is expected to be favored over the formation of a Cu^{2+} complex for the pesticides studied. This explains the greater signal enhancement observed for mass spectra acquired from FN, PT, MT, and DZ solutions containing Ag^+ compared to those containing Cu^{2+}.

In the absence of Cu^{2+} or Ag^+, S/B values calculated from mass spectra acquired from solutions of MT and DZ were higher in general than those acquired from solutions of

FN and PT. However, S/B values calculated using mass spectra acquired from MT-containing and DZ-containing solutions were significantly increased when Ag^{+} or Cu^{2+} was added to the solutions containing these pesticides, and were three or more times higher than S/B for FN and PT (Figure 2.7). This observation is consistent with the structural differences between the pesticides. Both MT and DZ contain atoms other than the soft thiophosphoryl S-atom having accessible electron lone pairs that can interact with the metal. These are the carbonyl oxygen in MT and the ring nitrogen in DZ (Figure 2.1b). Thus, it is possible for MT and DZ to act as bidentate ligands. Mortland and Raman[15] suggested in their study involving Cu^{2+} and DZ that the metal ion can coordinate to the pesticide through both the thiophosphoryl S-atom and a pyrimidine ring nitrogen. This ability to form bidentate complexes improves the pesticide-metal interaction, and is thought to be responsible for the higher S/B observed for mass spectra acquired from Ag^{+}-spiked MT and DZ solutions.

Formic acid or Na^{+} may also be added to a solution to facilitate ionization in ESI-MS. However, neither addition of formic acid nor addition of Na^{+} to our solutions significantly increased the S/B of mass spectra acquired from the pesticide solutions (Figure 2.7). This suggests that complex formation between Ag^{+} or Cu^{2+} and the pesticide is key to the improvement in S/B. Co^{2+}, Ni^{2+}, Zn^{2+}, Pb^{2+}, Fe^{3+}, and Au^{3+} coordination complexes with fenitriothion were studied, but offered little or no improvement in S/B compared to Ag^{+} and Cu^{2+}. In addition, Co^{2+}, Ni^{2+}, and Fe^{3+} coordination complexes with PT, MT, and DZ were investigated, again with little to no improvement in S/B. Hg^{2+} complexes were not investigated because of the toxicity of mercury and its compounds.

Ions such as Ca^{2+}, Mg^{2+}, and Fe^{3+} are commonly found in foods and could potentially suppress complex formation between the pesticides and Ag^{+} or Cu^{2+} if not removed prior to analysis. We investigated the effects of potential interferents by adding Ca^{2+}, Mg^{2+}, or Fe^{3+} to solutions containing 0.1mM DZ and 0.1mM Ag^{+}. In the absence of Ag^{+}, the mass spectrum acquired from the 0.1mM DZ solution showed only a peak arising from $[DZ+H]^{+}$ (*m/z* 305). No Ca^{2+}-, Mg^{2+}-, or Fe^{3+}-DZ complexes were observed. When Ag^{+} was present in solution, peaks arising from the ions $[DZ+H]^{+}$, $[DZ+Ag]^{+}$ (*m/z* 411), and $[2DZ+Ag]^{+}$ (*m/z* 715) were observed, and the expected improvement in S/B occurred. The concentration of either Ca^{2+}, Mg^{2+}, or Fe^{3+}, was then increased incrementally from 0 to 1 mM and the effect on $[DZ+Ag]^{+}$ peak intensity and S/B was monitored. The results are shown in Figure 2.8. The presence of Ca^{2+} or Mg^{2+} in solution had little effect on $[DZ+Ag]^{+}$ peak intensity, but because the baseline noise increased, a significant decrease in S/B for $[DZ+Ag]^{+}$ was seen as the concentration of these alkaline earth metal ions increased. Fe^{3+} appeared to suppress formation of $[DZ+Ag]^{+}$, as its peak intensity decreased and the peak intensity of $[DZ+H]^{+}$ increased with Fe^{3+} concentration (data not shown). Increasing the Ag^{+} concentration in solutions containing Ca^{2+} or Fe^{3+} increased the S/B of $[DZ+Ag]^{+}$. However, the S/B never reached its pre-interferent level even when the solution concentration of Ag^{+} was significantly greater than that of either Ca^{2+} or Fe^{3+} (Figure 2.9). Thus, the presence of interfering metal cations can have a significant effect on the detection of the silver-pesticide complex, and an appropriate sample pretreatment method should be used to reduce the concentrations of potentially interfering metals.

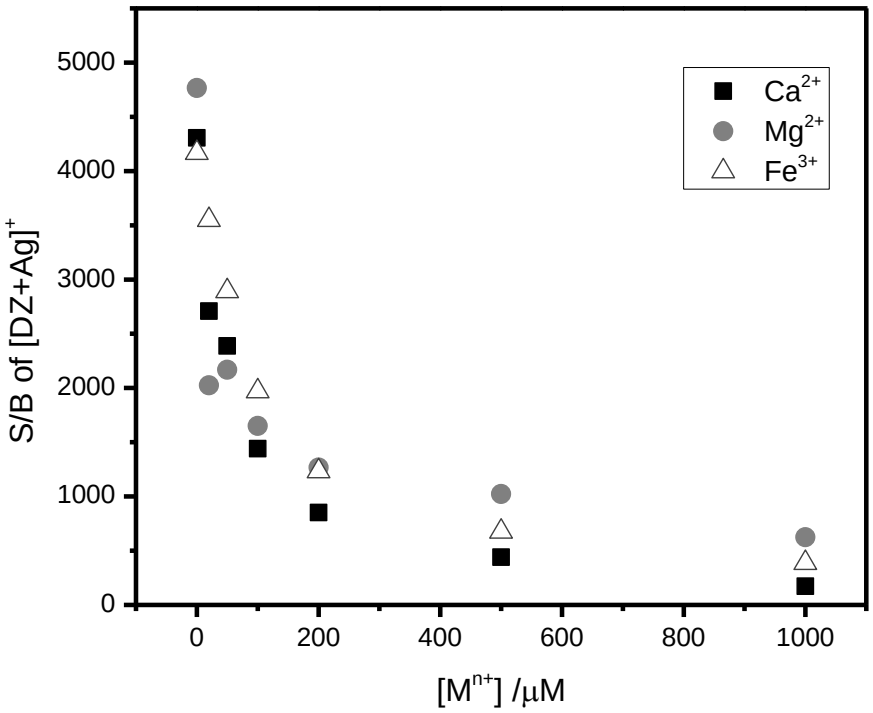

Figure 2.8 Effect of increasing Ca^{2+}, Mg^{2+}, and Fe^{3+} concentrations on $[DZ+^{107}Ag]^+$ signal-to-background ratio (S/B). The concentrations of Ca^{2+}, Mg^{2+}, and Fe^{3+} were varied from 10 to 1000 μM, while the concentrations of Ag^+ and diazinon were kept constant at 100 μM. M indicates either Ca, Mg, or Fe and n is the charge on the ion. Each data point was obtained by averaging the result of two separate experiments.

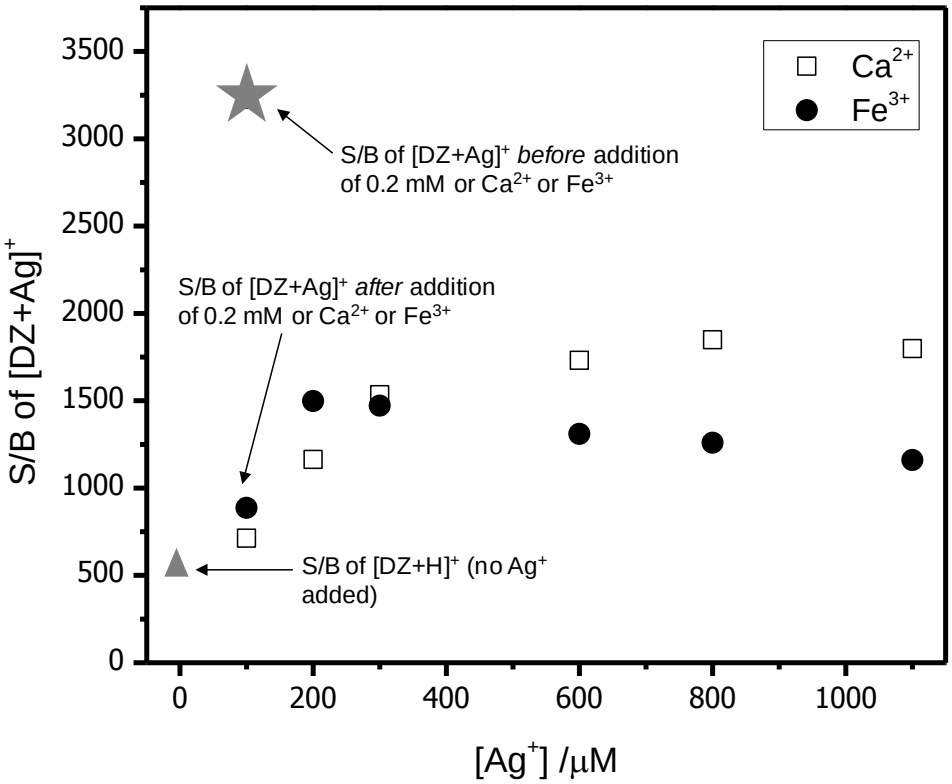

Figure 2.9 Effect of increasing Ag^+ concentrations on $[DZ+^{107}Ag]^+$ signal-to-backgound ratio (S/B) when 200 μM Ca^{2+} or Fe^{3+} is present in the solution. The concentration of diazinon was kept constant at 100 μM, while the concentration of Ag^+ was varied from 100 to 1100 μM. The S/B of $[DZ+H]^+$ in the absence of Ag^+, Ca^{2+}, or Fe^{3+} was ~520. Each data point was obtained by averaging the results of two separate experiments.

2.3.2 Competition for Ag^+ binding

A competitive binding study was carried out to determine the relative affinity of each pesticide for Ag^+. Ag^+ was chosen instead of Cu^{2+} because it provides greater signal enhancement and improved S/B. The mass spectra acquired from Ag^+-containing solutions are also relatively simple and clear. Experiments were carried out using solutions containing

0.1 mM Ag^+ and one of the following pesticide pairs (0.2 mM each): FN and PT, FN and MT, FN and DZ, PT and MT, PT and DZ, and MT and DZ.

A mass spectrum acquired from a solution containing Ag^+, FN, and PT is shown in Figure 2.10a. Ion assignments are given in Table 2.1, with assignments for mixed-ligand species given at the bottom of the table. Peaks that can be assigned to ions containing FN predominate, indicating that Ag^+ has a greater affinity for FN than for PT. Ions containing FN but not PT include $[FN+Ag]^+$ (*m/z* 384), $[FN+H_2O+Ag]^+$ (*m/z* 402), $[FN+CH_3OH+Ag]^+$ (*m/z* 416), and $[2(FN)+Ag]^+$ (*m/z* 661). A peak assigned to $[2(PT)+Ag]^+$ was observed at *m/z* 689, and a peak assigned to the mixed pesticide complex $[FN+PT+Ag]^+$ was observed at *m/z* 675. $[2(FN)+Ag]^+$ occurred in the greatest abundance and gave rise to the most prominent peak in the spectrum. In general, ~80% of the ions formed in the Ag^+/FN/PT system resulted from Ag^+-FN complexes, while <5% of the ions were due to Ag^+-PT complexes. As can be seen in Figure 2.1b, the major differences in the structure of FN and PT are alkoxy group chain length and the fact that FN has an alkyl substituent on the aromatic ring. The effect of these groups on the interaction of the pesticides with the metal ion is not yet understood but it is clear that Ag^+-FN complexes are favored over Ag^+-PT complexes.

A similar experiment was conducted using a solution containing Ag^+, FN, and MT. The resulting mass spectrum is shown in Figure 2.10b. Ion assignments are given in Table 2.1. Ions containing MT ($[MT+Ag]^+$ (*m/z* 437) and $[2(MT)+Ag]^+$ (*m/z* 767)) occur in the greatest abundance and only one FN-containing ion was observed: $[2(FN)+Ag]^+$ (*m/z* 661). In the Ag^+/FN/MT system, ~90% of the ions in the spectrum could be assigned to Ag^+-MT

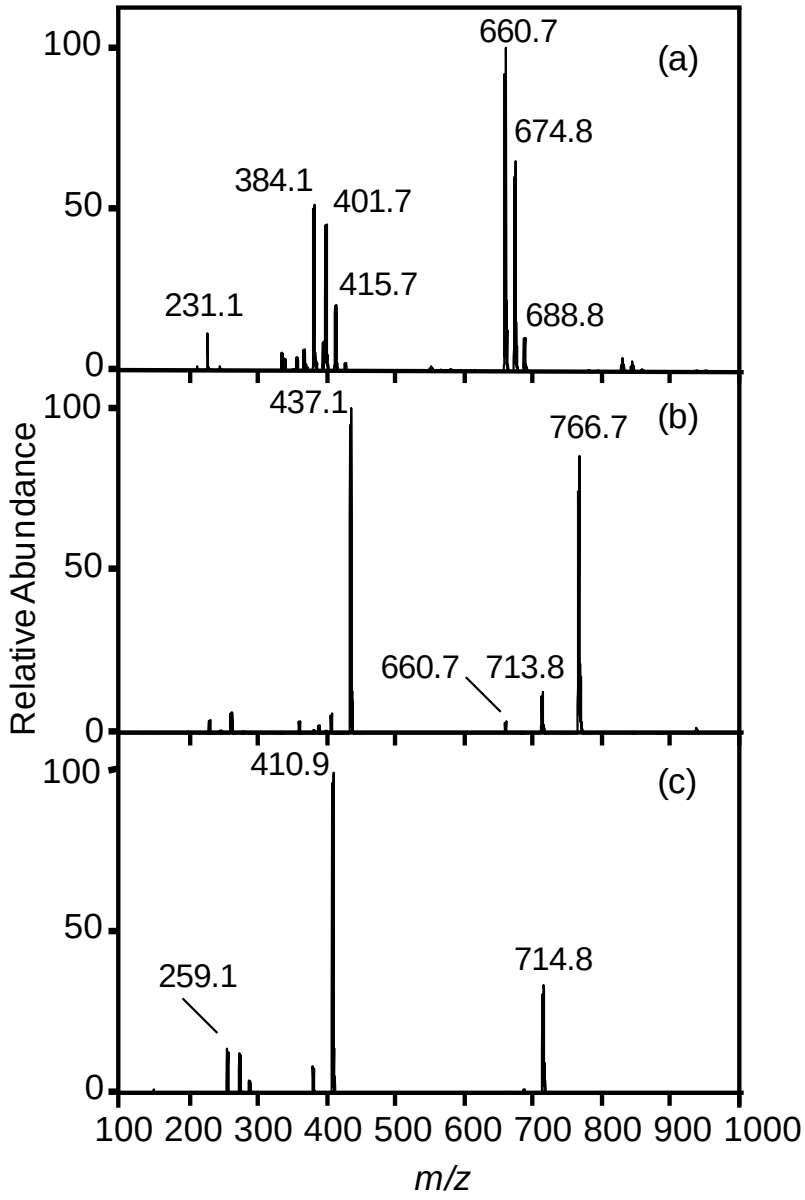

Figure 2.10 Positive-ion mass spectra obtained from solutions containing fenitrothion, Ag^+, and either a) parathion, b) malathion, or c) diazinon in a 2:1:2 molar ratio (0.2 mM fenitrothion, 0.1 mM Ag^+, and 0.2 mM parathion, malathion, or diazinon). The solvent was 50:50 (v/v) methanol:water. *m/z* values given for metal-pesticide complexes are for the ^{107}Ag- and ^{63}Cu-containing ions.

species, while Ag^+-FN species account for <5% of the total ion in the spectrum. This suggests that MT has a stronger affinity for Ag^+ than does FN. The major difference in the structures of FN and MT (Figure 2.1b) lies in the moieties linked to each thiophosphoryl group. In MT, a bulky ester group is connected through a sulfide linkage to the thiophosphoryl phosphorus, while in FN an aromatic group is linked to the thiophosphoryl phosphorus. According to Mortland and Raman,[15] bidentate interactions are possible whenever a pesticide has two possible coordination sites; thus, it is possible that MT binds Ag^+ in a bidentate fashion through both the thiophosphoryl sulfur and the carbonyl oxygen on the ester group, making the Ag^+-MT complex more stable than the Ag^+-FN complex.

A mass spectrum acquired from a solution containing Ag^+, FN, and DZ shows that DZ binds Ag^+ more effectively than FN (Figure 2.10c). The predominant ions in the mass spectrum include both $[DZ+Ag]^+$ (*m/z* 411) and $[2(DZ)+Ag]^+$ (*m/z* 715). Ion assignments are given in Table 2.1. Approximately 99% of the peaks observed in the mass spectrum resulted from Ag^+-DZ species. Ag^+-DZ complexes are much more likely to form than are Ag^+-FN complexes because of the presence of two possible coordinating sites on DZ (the thiophosphoryl sulfur and the pyrimidine ring nitrogen). Mortland and Raman[15] suggested that these sites allow DZ to interact with Cu^{2+} as a bidentate ligand to form a more stable complex. This is also likely true of the Ag^+-DZ complex. FN can only form a monodentate complex because it has only one coordinating center.

The PT/MT and PT/DZ pesticide sets were also compared. The spectra for these two systems are given in Figure 2.11a and b. Ion assignments are given in Table 2.1. In the Ag^+/PT/MT system Ag^+-MT species $[MT+Ag]^+$ (*m/z* 437) and $[2(MT)+Ag]^+$ (*m/z* 767) dominate the spectrum, while the ion abundance of the mixed-ligand complex

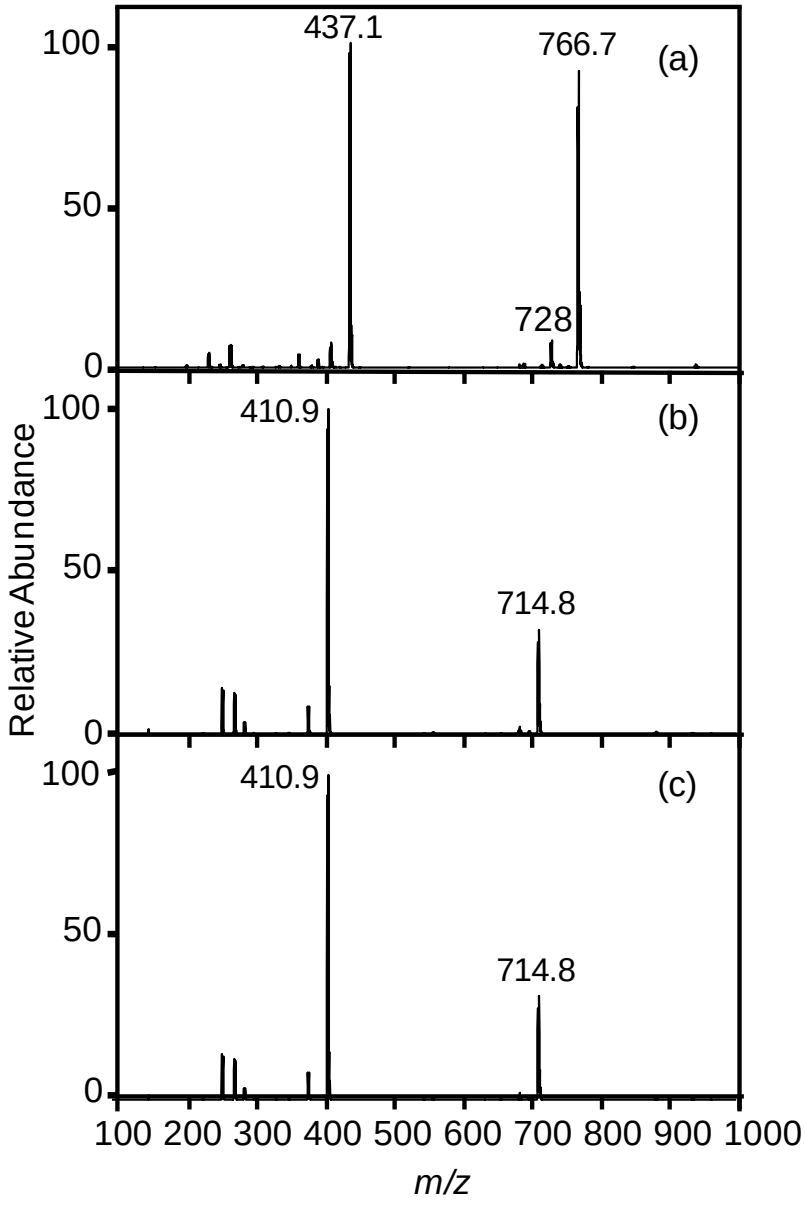

Figure 2.11 Positive-ion mass spectra obtained from solutions containing Ag^+ with a) parathion and malathion, b) parathion and malathion, and c) malathion and diazinon in a 2:1:2 molar ratio (0.2 mM fenitrothion, 0.1 mM Ag^+, and 0.2 mM parathion, malathion, or diazinon.). The solvent was 50:50 (v/v) methanol:water. *m/z* values given for metal-pesticide complexes are for the ^{107}Ag- and ^{63}Cu-containing ions.

$[MT+PT+Ag]^+$ (*m/z* 728) is <5% of the total. Ag^+-MT complexes are formed more readily than Ag^+–PT complexes. As discussed earlier, MT is capable of behaving as a bidentate ligand, enhancing its ability to bind to Ag^+. In the Ag^+-PT complexes, binding to Ag^+ can occur only via the thiophosphoryl sulfur.

Because PT can coordinate Ag^+ only through monodentate binding, while DZ can act as a bidentate ligand, PT should be a less effective ligand than diazinon. As predicted, the formation of Ag^+-DZ complexes is favored over the formation of Ag^+-PT complexes (Figure 2.11b). The Ag^+-DZ ions $[DZ+Ag]^+$ (*m/z* 411) and $[2(DZ)+Ag]^+$ (*m/z* 715) were observed, but not Ag^+-PT or mixed ligand complexes.

The Ag^+/MT/DZ system was the final system investigated. Both $[DZ+Ag]^+$ (*m/z* 411) and $[2(DZ)+Ag]^+$ (*m/z* 715) dominate the mass spectrum, indicating that Ag^+-DZ complexes formed more readily than Ag^+-MT complexes (Figure 2.11c). Ion assignments are given in Table 2.1. Even though both DZ and MT can potentially form bidentate complexes with Ag^+, the mass spectrum suggests that complex formation is more favorable in the Ag^+-DZ system than in the Ag^+-MT system. The pyrimidine nitrogen (in DZ) can interact more readily with the metal ion than can the carbonyl oxygen (in MT).

Figure 2.12, which summarizes the information discussed above, shows the relative abundance of each pesticide-Ag^+ complex formed when two pesticides' affinity for Ag^+ was compared. The relative abundances were calculated as follows: the ion abundances of all related ions (for example, ions containing both FN and Ag^+) in a mass spectrum were summed, and then this number was divided by the sum of the ion abundances of all ions in the mass spectrum. Using Figure 2.12, the relative affinity of each pesticide for Ag^+ can be

determined based on the relative abundances of the $^{107}Ag^{+}$-pesticide species formed. DZ is much more effective in complexing Ag^{+} than either FN, PT, or MT. MT is a more effective ligand for Ag^{+} than either FN or PT. FN complexes Ag^{+} more effectively than PT, and PT is the least effective ligand. Pesticide affinity for Ag^{+} then follows the order DZ > MT > FN > PT. This order corroborates the data shown in Figure 2.7, where S/B values for DZ and MT increased more significantly through metal ion coordination than S/B values for FN and PT. The presence of a second coordination site on a pesticide has an obvious effect on the degree of signal enhancement.

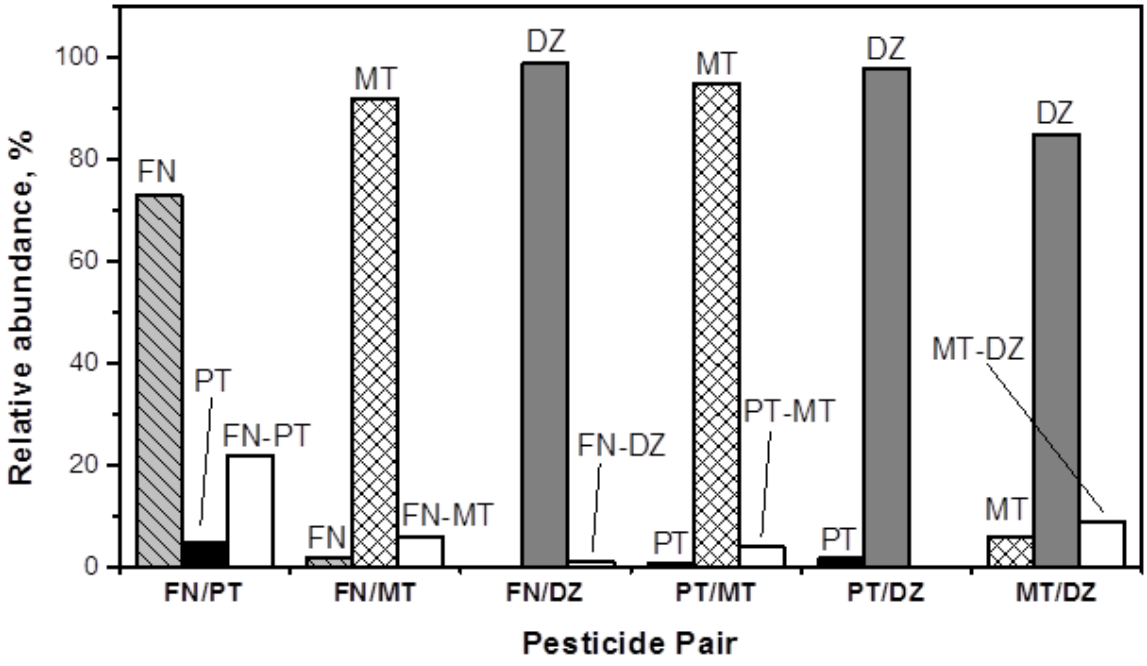

Figure 2.12 Relative abundances of $^{107}Ag^{+}$-pesticide complexes. The pesticides are fenitrothion (FN), parathion (PT), malathion (MT), and diazinon (DZ). Mixed pesticide complexes are indicated by two pesticide names joined using a hyphen.

2.3.3 Effect of metal on pesticide limit of detection

It was of interest to us to see how the addition of Ag^+ affects the limit of detection (LOD) of the four OPs. If the formation of a metal-pesticide complex acts to increase the S/B of the mass spectra, it should also improve the LOD of that pesticide. We defined the LOD for each pesticide as the lowest concentration of pesticide giving an Ag-pesticide peak in the mass spectrum having a S/B of ~3. The LOD for each of the pesticides was determined using the dual syringe pump system shown in Figure 2.13.

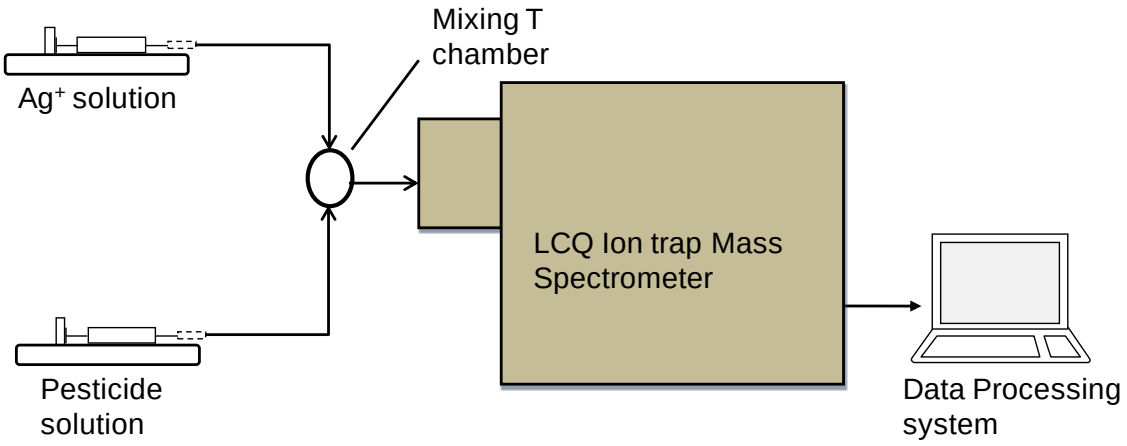

Figure 2.13 Schematic of the setup used in determining limits of detection.

One syringe was filled with a 10 μM solution of Ag^+, while the second syringe was filled with a pesticide solution. Pesticide solution concentrations ranged from 0.001 μM to 10 μM. The pesticide solution and the metal ion solution, both flowing at 3 μL/min, underwent mixing in the mixing T, and then were introduced to the electrospray needle. To determine the pesticide LOD in the absence of Ag^+, one syringe was filled with only the solvent mixture, which the other was filled with the pesticide solution. The results of this study are shown in Table 2.3. Addition of Ag^+ improves pesticide LOD by at least ten times

for all the pesticides investigated. Consistent with our results indicating that DZ and MT more readily interact with the metal ion than do FN and PT, LOD for DZ is three orders of magnitude lower than LOD for either FN or PT both with and without Ag^+, while LOD for MT is two orders of magnitude lower.

Table 2.3 Limits of detection determined from ESI-MS measurements made in the presence and absence of Ag^+.

Pesticides	Detection limit, μM	
	No Ag^+ added	Ag^+ added
Fenitrothion	1	0.1
Parathion	1	0.1
Malathion	0.01	0.001
Diazinon	0.001	0.0001

The study described above shows that the metal-containing solution can be introduced into a pesticide solution via a flow-through arrangement. We envision that this technique could be used to introduce Ag^+ or Cu^{2+}-containing solutions to a pesticide exiting a HPLC column. The setup envisioned is similar to that shown in Figure 2.13, but with the syringe containing the pesticides replaced by the HPLC column.

2.4 Conclusions

In this study we investigated the formation of Ag^+ and Cu^{2+}-coordination complexes with FN, PT, MT, and DZ during ESI-MS. Stable 1:1 and 1:2 metal/pesticide complexes were detected. Our results also show that the S/B measured by dividing the signal intensity of the most intense peak in the spectrum by the average signal intensity of the background increased significantly when Ag^+ or Cu^{2+} was added to a pesticide-containing solution. The

increase was metal dependent, with mass spectra acquired from Ag^+-containing pesticide solutions having S/B from three to six times greater than those acquired from solutions containing Cu^{2+}, depending on the pesticide. S/B of mass spectra acquired from solutions containing MT and DZ to which Ag^+ or Cu^{2+} had been added were two to five times greater than S/B of mass spectra acquired from solutions containing FN and PT supplemented with Ag^+ or Cu^{2+}. This may be because MT and DZ can bind the metal in a more stable bidentate configuration, while FN and PT can only engage in monodentate binding. The relative affinities of each pesticide for Ag^+ in a solution containing a mixture of pesticides were also investigated. The pesticide affinity for Ag^+ follows the order DZ > MT > FN > PT. In addition, the LOD for each of the pesticides investigated was lowered by an order of magnitude when Ag^+ was added to the pesticide solution. A drawback to this method is that cations such as Mg^{2+}, Ca^{2+}, and Fe^{3+} cause significant signal suppression. Thus, metal cations which may interfere must be removed before analysis. We hope in future to use this technique to detect phosphorothioate and phosphorodithioate pesticides on fruit and vegetable skins with reactive desorption electrospray ionization mass spectrometry.

References

1. Fenik, J.; Tankiewicz, M.; Biziuk, M. Properties and determination of pesticides in fruits and vegetables. *TrAC, Trends Anal. Chem.* **2011**, *30*, 814.
2. Sharma, D.; Nagpal, A.; Pakade, Y. B.; Katnoria, J. K. Analytical methods for estimation of organophosphorus pesticide residues in fruits and vegetables: A review. *Talanta* **2010**, *82*, 1077.
3. Gube, A.; Donaldson, D.; Kiely, T.; Wu, L. *Pesticides industry sales and usage 2006 and 2007: Market estimates*; EPA 733-R-11-001; U. S. environmental Protection Agency, Office of Chemical Safety and Pollution Prevention, Washington DC, **2011**.
4. Chambers, H. W.; Meek, E. C.; Chambers, J. E. Chemistry of organophosphorus insecticides. in *Hayes' handbook of pesticide toxicology*, 3rd ed. (Ed: R. Krieger) Elsevier Inc., New York, **2010**, Vol. 1.
5. Sultatos, L. G. Mammalian toxicology of organophosphorus pesticides. *J. Toxicol. Environ. Health* **1994**, *43*, 271.
6. Eddleston, M.; Karalliedde, L.; Buckley, N.; Fernando, R.; Hutchinson, G.; Isbister, G.; Konradsen, F.; Murray, D.; Piola, J. C.; Senanyake, N.; Sheriff, R.; Singh, S.; Siwach, S. B.; Smit, L. Pesticide poisoning in the developing world - A minimum pesticides list. *Lancet* **2002**, *360*, 1163.
7. Androutsopoulos, V. P.; Hernandez, A. F.; Liesivuori, J.; Tasatsakis, A. M. A mechanistic overview of health associated effects of low levels of organochlorine and organophosphorous pesticides. *Toxicology* **2013**, *307*, 89.
8. Choi, H.; Yang, K.; Park, J. K.; Koo, I. S. P-31 NMR and ESI-MS study of fenitrothion-copper ion complex: Experimental and theoretical study. *Bull. Korean Chem. Soc.* **2010**, *31*, 1339.
9. Koo, I. S.; Ali, D.; Yang, K.; Park, Y.; Wardlaw, D. M.; Buncel, E. Theoretical study of P-31 NMR chemical shifts for organophosphorus esters, their anions and *O,O*-dimethylthiophosphorate anion with metal complexes. *Bull. Korean Chem. Soc.* **2008**, *29*, 2252.

10. Koo, I. S.; Ali, D.; Yang, K.; Park, Y.; Esbata, A.; van Loon, G. W.; Buncel, E. P-31 NMR and ESI-MS studies of metal ion-phosphorus pesticide residue complexes. *Can. J. Chem.* **2009**, *87*, 433.
11. Koo, I. S.; Ali, D.; Yang, K.; van Loon, G. W.; Buncel, E. Theoretical and experimental P-31 NMR and ESI-MS study of Hg^{2+} binding to fenitrothion. *Bull. Korean Chem. Soc.* **2009**, *30*, 1257.
12. Zeinali, M.; Torrents, A. Mercury-promoted hydrolysis of parathion-methyl: Effect of chloride and hydrated species. *Environ. Sci. Technol.* **1998**, *32*, 2338.
13. Sarkouhi, M.; Shamsipur, M.; Hassan, J. P-31-NMR evaluation of organophosphorus pesticides degradation through metal ion promoted hydrolysis. *Environ. Monit. Assess.* **2012**, *184*, 7383.
14. Smolen, J. M.; Stone, A. T. Divalent metal ion-catalyzed hydrolysis of phosphorothionate ester pesticides and their corresponding oxonates. *Environ. Sci. Technol.* **1997**, *31*, 1664.
15. Mortland, M. M.; Raman, K. V. Catalytic hydrolysis of some organic phosphate pesticides by copper(II). *J. Agric. Food. Chem.* **1967**, *15*, 163.
16. Keller, B. O.; Esbata, A. A.; Buncel, E.; van Loon, G. W. Rapidly formed quinalphos complexes with transition metal ions characterized by electrospray ionization mass spectrometry. *Rapid Commun. Mass Spectrom.* **2013**, *27*, 1319.
17. Tankiewicz, M.; Fenik, J.; Biziuk, M. Determination of organophosphorus and organonitrogen pesticides in water samples. *TrAC, Trends Anal. Chem.* **2010**, *29*, 1050.
18. Jin, B.; Xie, L.; Guo, Y.; Pang, G. Multi-residue detection of pesticides in juice and fruit wine: A review of extraction and detection methods. *Food Res. Int.* **2012**, *46*, 399.
19. Andreu, V.; Picó, Y. Determination of currently used pesticides in biota. *Anal. Bioanal. Chem.* **2012**, *404*, 2659.
20. Llorent-Martinez, E. J.; Ortega-Barrales, P.; Fernandez de Cordova, M. L.; Ruiz-Medina, A. Trends in flow-based analytical methods applied to pesticide detection: A review. *Anal. Chim. Acta* **2011**, *684*, 30.

21. Pundir, C. S.; Chauhan, N. Acetylcholinesterase inhibition-based biosensors for pesticide determination: A review. *Anal. Biochem.* **2012**, *429*, 19.

22. Alder, L.; Greulich, K.; Kempe, G.; Vieth, B. Residue analysis of 500 high priority pesticides: Better by GC-MS or LC-MS/MS? *Mass Spectrom. Rev.* **2006**, *25*, 838.

23. Iwasaki, Y.; Nakano, Y.; Mochizuki, K.; Nomoto, M.; Takahashi, Y.; Ito, R.; Saito, K.; Nakazawa, H. A new strategy for ionization enhancement by derivatization for mass spectrometry. *J. Chromatogr. B* **2011**, *879*, 1159.

24. Kohler, M.; Leary, J. A. LC/MS/MS of carbohydrates with postcolumn addition of metal chlorides using a triaxial electrospray probe. *Anal. Chem.* **1995**, *67*, 3501.

25. Rogatsky, E.; Jayatillake, H.; Goswami, G.; Tomuta, V.; Stein, D. Sensitive LC MS quantitative analysis of carbohydrates by Cs^+ attachment. *J. Am. Soc. Mass. Spectrom.* **2005**, *16*, 1805.

26. Jemal, M.; Almond, R. B.; Teitz, D. S. Quantitative bioanalysis utilizing high-performance liquid chromatography electrospray mass spectrometry via selected-ion monitoring of the sodium ion adduct $[M+Na]^+$. *Rapid Commun. Mass Spectrom.* **1997**, *11*, 1083.

27. Ma, Y. C.; Kim, H. Y. Determination of steroids by liquid chromatography mass spectrometry. *J. Am. Soc. Mass. Spectrom.* **1997**, *8*, 1010.

28. Rentel, C.; Strohschein, S.; Albert, K.; Bayer, E. Silver-plated vitamins: A method of detecting tocopherols and carotenoids in LC/ESI-MS coupling. *Anal. Chem.* **1998**, *70*, 4394.

29. Bayer, E.; Gfrorer, P.; Rentel, C. Coordination-ionspray-MS (CIS-MS), a universal detection and characterization method for direct coupling with separation techniques. *Angew. Chem. Int. Ed.* **1999**, *38*, 992.

30. Yin, H.; Porter, N. A. Identification of intact lipid peroxides by Ag^+ coordination ion-spray mass spectrometry (CIS-MS). In *Methods in enzymology*, (Ed: H. A. Brown), Elsevier Inc., **2007**, Volume 433, pp 193-211.

31. Sparkman, O. D. *Mass spec desk reference*, 2nd ed. Global View Publishing, Pittsburgh, **2006**.

32. Gianelli, L.; Amendola, V.; Fabbrizzi, L.; Pallavicini, P.; Mellerio, G. G. Investigation of reduction of Cu(II) complexes in positive-ion mode electrospray mass spectrometry. *Rapid Commun. Mass Spectrom.* **2001**, *15*, 2347.

33. Pearson, R. G. Hard and soft acids and bases. *J. Am. Chem. Soc.* **1963**, *85*, 3533.

Chapter 3

Collision-Induced Dissociation of Phosphorothioate and Phosphorodithioate Ions Containing Silver and Copper

Abstract

Organophosphorus pesticides have been used for control of pests in fruits and vegetables for many years, and there is a need to understand their fragmentation patterns in order to improve their accurate detection during analysis of their residues in foods and other substances. Phosphorothioate and phosphorodithioate pesticides are two organophosphorus pesticide subclasses. Recent work has shown that the detection of phosphorothioate and phosphorodithioate pesticides using electrospray ionization mass spectrometry can be improved through formation of gas-phase complexes with silver or copper. In the study described in this chapter, I used multistage collision-induced dissociation with electrospray ionization mass spectrometry to investigate the effect of silver and copper ions on the fragmentation patterns of four phosphorothioate pesticides (fenitrothion (FN), parathion (PT), and diazinon (DZ)) and one phosphorothioate pesticide (malathion (MT)). The fragmentation patterns of $[FN+H]^+$, $[PT+H]^+$, $[MT+H]^+$, and $[DZ+H]^+$ are consistent with previously reported results. The fragmentation patterns of $[FN+M]^+$, $[PT+M]^+$, $[MT+M]^+$, and $[DZ+M]^+$ (M = Ag or Cu) were similar to those observed for $[FN+H]^+$, $[PT+H]^+$, $[MT+H]^+$, and $[DZ+H]^+$, respectively. Changing the metal from Ag to Cu did not appreciably change the fragmentation pattern of an ion, which differed only in the relative

abundances of fragment ions produced. Fragment ions arising from ions in which M = Ag were usually observed in high relative abundance compared to those in which M = Cu suggesting that silver stabilized the fragment ions more effectively than copper. Silver or copper complexes of FN, PT, or DZ did not undergo a thiono-thiolo rearrangement, which is known to occur in the protonated analogues of these ions.

3.1 Introduction

The importance of organophosphorus pesticides (OPs) to agriculture and the need for analytical methods for their detection and analysis have been discussed extensively in Chapter 2. Liquid chromatography mass spectrometry with an electrospray ionization interface (liquid chromatography electrospray ionization mass spectrometry, abbreviated as LC-ESI-MS) is the preferred analytical technique for the detection and quantification of these pesticides in food samples.[1, 2] Pesticide residue analysis using LC-ESI-MS sometimes employs tandem mass spectrometry methods in order to confirm the structural identity of the pesticides being quantified.

Since the introduction of electrospray ionization mass spectrometry (ESI-MS), there has been an increased interest in the application of the technique to the investigation of the fragmentation patterns of different types of pesticides.[3-6] ESI is a commonly used ionization technique for the mass spectral analysis of analytes in solutions. ESI has the advantage of being a soft ionization technique where analyte species experience little or no fragmentation.[7] However, fragmentation can be induced using collision-induced dissociation (CID) in order to investigate the structural features of an analyte. ESI-MS analysis of pesticides sometimes demands the use of CID in order to understand the structural features

and fragmentation patterns of the pesticides in the gas phase. The fragmentation pattern of a compound is a fingerprint that is unique to that particular compound. Knowing the fragmentation patterns of any particular compound will aid in its identification.

Tandem mass spectrometry is a common method for investigating structural detail and fragmentation of a compound.[8] In tandem mass spectrometry, the structural detail and fragmentation pathways of compounds are studied by isolating the compound parent ion (called the precursor ion) and subjecting it to CID in a collision cell. CID is achieved by accelerating the precursor ions in the collision cell, which is filled with neutral gas molecules. The acceleration of the precursor ions results in an increase in their kinetic energies. The precursor ions collide with the neutral gas molecules. During these inelastic collisions, the kinetic energies of the ions are converted to internal energy. The increased internal energy thus induces the fragmentation of the precursor ions into product ions of smaller *m/z*.[8, 9] Tandem mass spectrometry can be carried out in one of two ways: tandem-in-space or tandem-in-time. In the tandem-in-space method, two mass analyzers are placed in series, with a collision cell in between them. Isolation of the precursor ion occurs in the first mass analyzer, after which the ion is passed into a collision cell where it undergoes CID. The product ions formed in the collision cell are then passed into the second mass analyzer, where they are separated based on *m/z*. Common mass analyzer combinations for tandem-in-space MS include the triple-quadrupole (QqQ), the quadrupole-time of flight (Q-TOF) and the magnetic/electric field sector (BEEB) mass analyzer.

In tandem-in-time MS, precursor ion isolation, fragmentation, and mass analysis of product ions take place within a single mass analyzer, but at different times. The mass

analyzer is programmed to perform each of these three steps at different times.[8] Unlike in tandem-in-space MS, where the process of ion isolation and fragmentation (i.e. MS/MS) is limited to two or three stages, tandem-in-time MS/MS can be performed in up to nine stages. Common examples of mass analyzers that can be used for tandem-in-time mass analysis are the linear quadruople ion trap, the orbitrap, and the Fourier transform ion cyclotron mass analyzer.

The application of tandem mass spectrometry for the investigation of fragmentation patterns of some OPs has been reported.[10-15] Kuivalainen et al.[10, 11] studied the fragmentation patterns of dimethyl- and diethyl-*O*-aryl phosphorothionates. They observed that, upon CID, the protonated dimethyl-*O*-aryl phosphorothionates fragment to form product ions via the loss of methanol, while protonated diethyl-*O*-aryl phosphorothionates instead yield fragment ions via the loss of ethene. Major fragment ions observed in both sets of spectra include $(CH_3O)_2PS^+$ (*m/z* 125) and $(CH_3O)_2PO^+$ (*m/z* 109). $(CH_3O)_2PS^+$ results from a thiono-thiolo isomerization reaction. Both $(CH_3O)_2PS^+$ and $(CH_3O)_2PO^+$ are diagnostic ions for phosphorothioate compounds.

The thiono-thiolo isomerization reaction is a rearrangement reaction that is usually observed in phosphorothioate compounds, and can be used to confirm the presence of phosphorothioate pesticides.[16] Thiono-thiolo isomerization reactions in phosphorothioate compounds typically occur when an alkyl (or aryl) group migrates from the oxygen atom to the sulfur atom, as shown in Figure 3.1.[16] These rearrangements can occur as a result of exposure to UV radiation or heat. Alkyl (or aryl) group migration has also been known to

occur during mass spectrometry, possibly as a result of protonation in the ion source, or during collisional activation.[10, 17]

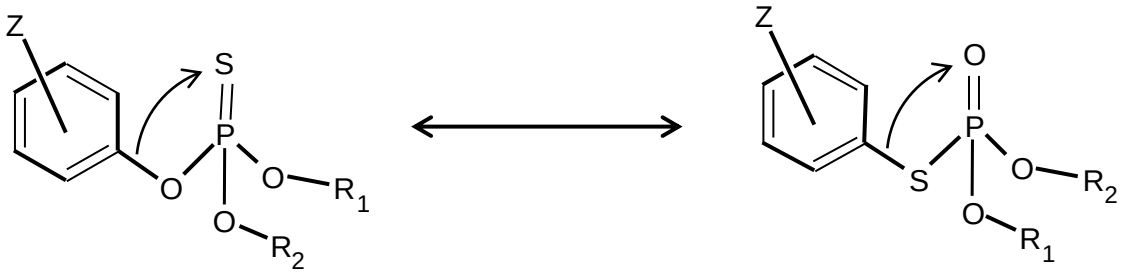

Figure 3.1 Illustration of the thiono-thiolo rearrangement in phosphorothioate pesticides. R_1 and R_2 may be an either alkyl or an aryl group.

The presence of major fragment ions such as $(CH_3O)_2PO^+$ and $[ZPhS]^+$ (Z = substituent on the benzene ring; Ph = C_6H_4) in CID spectra of dimethyl-*O*-aryl phosphorothionates, and $[ZPhOH_2]^+$, $[ZPhSH_2]^+$ and $[ZPhS]^+$ in CID spectra of diethyl-*O*-aryl phosphorothionates suggests that a thiono-thiolo rearrangement takes place.[10, 11]

Barr et. al.[13] investigated the fragmentation and gas phase reactions of diazinon (Figure 2.1b) using ESI-MS/MS. They observed that diazinon, when subjected to CID, fragments by losing an ethene group to form the fragment ion $[DZ-C_2H_4+H]^+$ (*m/z* 277, DZ = diazinon), which subsequently loses another ethene group to form $[DZ-2(C_2H_4)+H]^+$ (*m/z* 249). Other fragment ions observed are $[HOC_8H_{12}N_2]^+$ (*m/z* 153) and $[HSC_8H_{12}N_2]^+$ (*m/z* 169). The fragment ion $[HOC_8H_{12}N_2]^+$ (*m/z* 153) is formed by loss of PO_2SH from $[DZ-2(C_2H_4)+H]^+$ (*m/z* 249), while the thiono-thiolo rearrangement in protonated diazinon results in a loss of PO_3H instead, resulting in the fragment ion $[HSC_8H_{12}N_2]^+$ (*m/z* 169).

While there have been many reported studies[10, 11, 13, 14, 18] on fragmentation of protonated phosphorothioate compounds, no single study, to the best of our knowledge, has been reported on the fragmentation and gas phase reactions of metal-phosphorothioate or metal-phosphorodithioate complexes. In Chapter 2, we discussed the complexation of some selected organophosphorus pesticides with silver and copper ions and showed how the formation of charged metal complexes can improve the signal-to-background ratio and detection limit of phosphorothioate or phosphorodithioate pesticides. We then proposed the use of these metal ions in LC-ESI-MS analysis of residual OPs in foods, where the resulting metal-pesticide ions formed will enhance their detection. It is therefore of interest to us to see how silver and copper ions affect the fragmentation patterns of the pesticides. Understanding the differences (or similarities) in the fragmentation patterns of protonated pesticides and metal-pesticide complexes will aid in the identification of the pesticides during the LC-ESI-MS analysis. In the study described in this chapter, we used ESI-MS/MS to investigate the effect of silver and copper ions on the fragmentation patterns of four phosphorothioate and phosphoroditioate pesticides: fenitrothion (FN), parathion (PT), malathion (MT), and diazinon (DZ). The reasons behind the choice of these metals and pesticides have been explained in Chapter 2.

3.2 Experimental

3.2.1 Materials

Materials and samples used for this study are the same as those described in Chapter 2, Section 2.2.1.

3.2.2 Sample preparation

10 mM stock solutions of fenitrothion, parathion, malathion, and diazinon were prepared by dissolving the appropriate amount of pesticide in methanol. 10 mM solutions of each metal salt ($Cu(NO_3)_2 \cdot 3H_2O$ or $AgNO_3$) were also prepared by dissolving the appropriate amount of salt in a 50:50 (v/v) methanol:water solution. The metal complexes of the pesticides were prepared by mixing the stock solutions of the metals and pesticides, and diluting these with a 50:50 (v/v) methanol:water solution to give a solution containing 0.1 mM each of the metal and pesticide. Solutions containing pesticides only were prepared by diluting the 10 mM stock solutions of the respective pesticides to 0.1 mM using 50:50 methanol:water. Stock solutions and samples were prepared on the day of use.

3.2.3 Instrumentation

The instrument and operating parameters have been described in Chapter 2, Section 2.3.3. Helium gas was used as the buffer gas, and CID was achieved by isolating the appropriate precursor ion in the ion trap and subjecting it to collision with the buffer gas at 20 – 30% collision energy. For the metal-containing complexes, ^{63}Cu- and ^{107}Ag-containing ions were isolated for fragmentation. The instrument was set to detect ion species in the *m/z* range of 100 – 1000. Spectra were acquired in positive ion mode and processed using Xcalibur software (Thermo Electron, San Jose, CA), as in Chapter 2.

3.3 Results and Discussion

3.3.1 CID of fenitrothion and fenitrothion-metal complexes

Fragmentation pathways and mechanisms for $[FN+H]^+$ (*m/z* 278) have been previously described in some detail.[10, 11, 19] Product ion spectra I obtained for $[FN+H]^+$ are similar to those already published, differing mainly in the relative abundances of the product ions. Product ion spectra are shown in Figure 3.2a, and ion assignments are given in Table 3.1 Fragmentation of $[FN+H]^+$ (*m/z* 278) leads to a neutral loss of CH_3OH to give the product ion $[FN-CH_3OH+H]^+$ at *m/z* 246. The loss of methanol is consistent with the dissociation pathways of organophosphorus compounds. Schwarzenberg et al.[15] proposed that during CID of any organophosphorus compound, bond cleavage will occur at the P-O bond if both R_1 and R_2 are methyl groups (see Figure 2.1a), and that the high proton affinity of the resulting methoxide will lead to formation of methanol. The source of the proton abstracted by the methoxide group during fragmentation of $[FN+H]^+$ is yet unclear, but Schwarzenberg et al. suggested it is lost from the aryl group.[10] The appearance of $[FN-CH_3OH+H_2O+H]^+$ (*m/z* 264) is consistent with the observation of Bell et al.[20] that for every methanol loss from protonated fenitrothion, there will be a water addition to the resulting fragment ions. Losses of NO and NO_2 from the aryl group lead to the formation of $[FN-NO+H]^+$ (*m/z* 248) and $[FN-NO_2+H]^+$ (*m/z* 232). The peak at *m/z* 261 is thought to result from the conversion of fenitrothion ($C_9H_{12}O_5NPS$, *m/z* 277) to fenitrooxon ($C_9H_{12}O_5NPO$, *m/z* 261), which we here designate as FO. As shown in Figure 3.3, this results from a simple replacement of the thiolphosphoryl sulfur atom with oxygen. The mechanism for this conversion is not yet understood. The fenitrooxon ion (*m/z* 261)

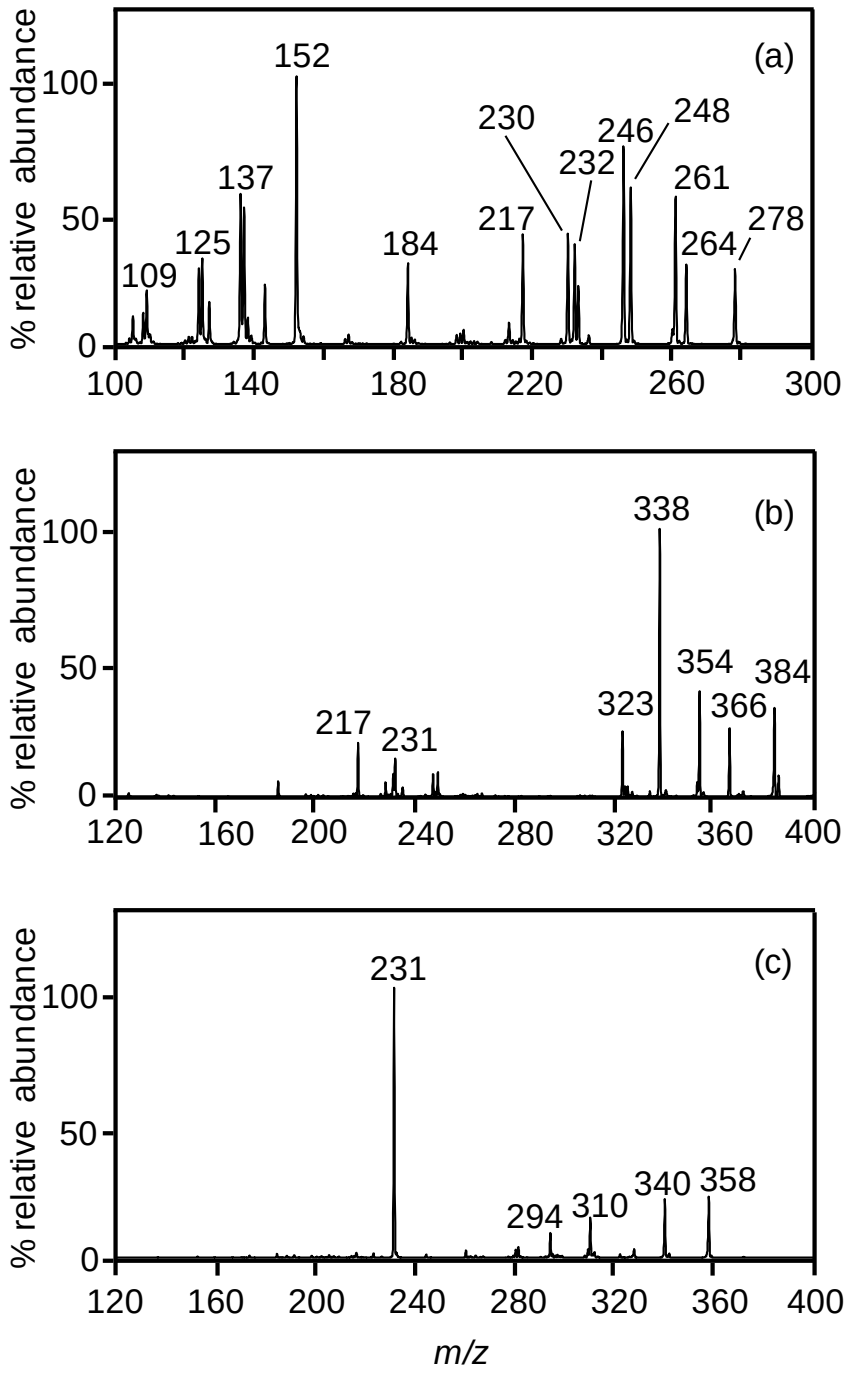

Figure 3.2 Product ion spectra of (a) $[FN+H]^+$ (*m/z* 278), (b) $[FN+^{107}Ag]^+$ (*m/z* 384), and (c) $[FN+^{63}Cu]^+$ (*m/z* 340). FN = fenitrothion.

Table 3.1 Ions formed during CID of protonated fenitrothion and fenitrothion-metal complexes.

Solution species	**Fragment Ions**	**Observed *m/z***	**Theoretical *m/z****
FN ($C_9H_{12}O_5NPS$)			
	$[FN+H]^+$	278.1	278.0
	$[FN-CH_3OH+H_2O+H]^+$	264.1	264.0
	$[FO]^{+\,\xi}$	261.0	261.0
	$[FN-NO+H]^+$	248.1	248.0
	$[FN-CH_3OH+H]^+$	246.0	246.0
	$[FN-NO_2+H]^+$	232.0	232.0
	$[FO-CH_3O]^{+\,\xi}$	230.1	230.0
	$[FO-2(CH_3O)+H_2O]^{+\,\xi}$	217.1	217.0
	$[NO_2CH_3PhOP]^+$ *	184.1	184.0
	$[NO_2CH_3PhO]^+$ *	152.1	152.0
	$[NO_2CH_3Ph]^+$ *	137.1	137.0
	$[(CH_3O)_2PS]^+$	125.1	125.0
	$[(CH_3O)_2PO]^+$	109.1	109.0
$FN+Ag^+$			
	$[FN+^{107}Ag]^+$	384.0	383.9
	Unassigned	366.0	-------
	$[FN-NO+^{107}Ag]^+$	354.0	353.9
	$[FN-NO_2+^{107}Ag]^+$	338.0	337.9
	$[FN-NO_2-CH_3+^{107}Ag]^+$	323.1	322.9
	$[FN-NO_2]^+$	231.1	231.0
	$[FN-NO_2-CH_3+H]^+$	217.0	217.0
$FN+Cu^{2+}$			
	$[FN+^{63}Cu]^+$	340.0	339.9
	$[FN+H_2O+^{63}Cu]^+$	357.7	357.9
	$[FN-NO+^{63}Cu]^+$	310.0	309.9
	$[FN-NO_2+^{63}Cu]^+$	294.0	294.0
	$[FN-NO_2]^+$	231.0	231.0

*Ph = C_4H_6.

$^{\xi}$FO (fenitrooxon, $C_9H_{12}O_5NPO$) is formed by simple replacement of phosphoryl sulfur atom in fenitrothion by oxygen atom.

undergoes a methoxide loss and water addition upon fragmentation to form fragment ions $[FO-CH_3O]^+$ (*m/z* 230) and $[FO-2(CH_3O)+H_2O]^+$ (*m/z* 217). Other fragment ions observed in the spectrum include $[NO_2CH_3PhOP]^+$ (*m/z* 184), $[NO_2CH_3PhO]^+$ (*m/z* 152), and $[NO_2CH_3Ph]^+$ (*m/z* 137). These ions are formed by the loss of $(S(OCH_3)_2$, $PS(OCH_3)_2$, and $OPS(OCH_3)_2$, respectively, from protonated fenitrothion $[FN+H]^+$ (*m/z* 278). The thiono-thiolo rearrangement is apparent from the $[FN+H]^+$ fragmentation pattern, as the loss of the *O*-aryl group from the pesticide leads to the formation of $[(CH_3O)_2PS]^+$ (*m/z* 125). The loss of the *O*-aryl group from the product of the thiono-thiolo rearrangement, however, produces $[(CH_3O)_2PO]^+$ (*m/z* 109).[10]

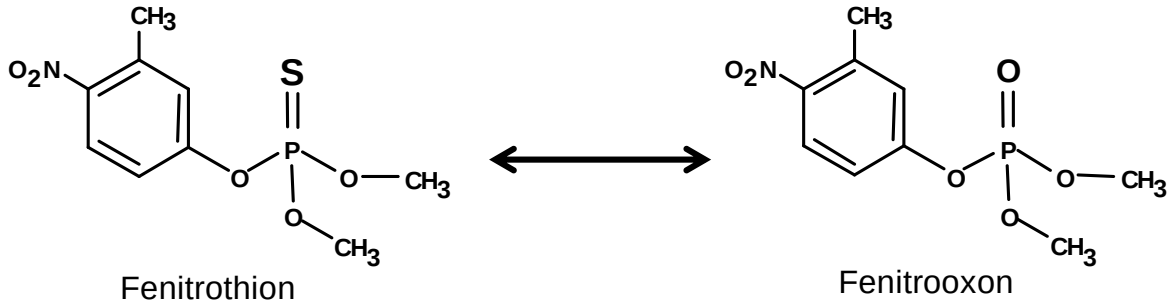

Figure 3.3 Conversion of fenitrothion (FN) to fenitrooxon (FO) by simple replacement of phosphoryl sulfur atom with oxygen.

The presence of silver or copper ion does appear to affect the fenitrothion fragmentation pattern. Unlike during the fragmentation of $[FN+H]^+$ where methanol loss followed by water addition was observed, fragmentation of $[FN+^{107}Ag]^+$or $[FN+^{63}Cu]^+$ led to neither methanol loss nor water addition. However, the loss of NO and NO_2 were observed in the fragmentation patterns of both protonated FN and metal-FN complexes.

Also, fragmentation patterns were similar for $[FN+^{107}Ag]^+$ and $[FN+^{63}Cu]^+$, mainly differing in the relative abundances of the various fragment ions.

CID of $[FN+^{107}Ag]^+$ (*m/z* 384) produced fragment ions such as $[FN-NO+^{107}Ag]^+$ (*m/z* 354), $[FN-NO_2+^{107}Ag]^+$ (*m/z* 338) and $[FN-NO_2]^+$ (*m/z* 231), as shown in Figure 3.2b. The fragment ion observed at *m/z* 366 could not be assigned. The peak at *m/z* 323 is believed to arise from an ion formed via loss of both CH_3 and NO_2 from the $[FN+^{107}Ag]^+$ complex, while the loss of $^{107}Ag^+$ from the fragment ion $[FN-NO_2-CH_3+^{107}Ag]^+$ (*m/z* 323) resulted in the peak at *m/z* 217 (Figure 3.2b, Table 3.1).

Analogue fragment ions were observed upon CID of the $[FN+^{63}Cu]^+$ complex (*m/z* 340). As shown in Figure 3.2c, these fragment ions include $[FN-NO+^{63}Cu]^+$ (*m/z* 310), $[FN-NO_2+^{63}Cu]^+$ (*m/z* 294), and $[FN-NO_2]^+$ (*m/z* 231). While fragmentation of $[FN+^{107}Ag]^+$ gave $[FN-NO_2+^{107}Ag]^+$ (*m/z* 338) as the most abundant ion, fragmentation of $[FN+^{63}Cu]^+$ resulted in $[FN-NO_2]^+$ (*m/z* 231) as the most abundant ion, suggesting that the interaction between fenitrothion and copper is not as strong as the interaction between fenitrothion and silver. This observation is consistent with the HSAB principle discussed in Chapter 2, Section 2.3.1.[21]

As stated above, the presence of $[(CH_3O)_2PO]^+$ (*m/z* 109) in the $[FN+H]^+$ fragmentation pattern indicates that fenitrothion undergoes a thiono-thiolo rearrangement.[10] This fragment ion was absent in product ion spectra of $[FN+^{107}Ag]^+$ and $[FN+^{63}Cu]^+$ (Figure 3.2b and c). This observation suggests that the presence of a metal ion inhibits the thiono-thiolo rearrangement.

3.3.2 CID of parathion and parathion-metal complexes

Parathion and fenitrothion are structurally the most similar of the four OP investigated, differing only in the R_1 and R_2 groups, and in the presence or absence of a methyl group on the benzene ring (Figure 2.1a and b). For fenitrothion, $R_1 = R_2 = CH_3$, while for parathion $R_1 = R_2 = CH_2CH_3$. Fragmentation pathways and mechanisms for $[PT+H]^+$ have also been previously described, and our results are similar to those reported.[10, 11, 19]

The major ions observed upon fragmentation of $[PT+H]^+$ (*m/z* 292) result from a neutral loss of first one, and then a second ethene moiety, forming ions at *m/z* 264 and *m/z* 236, respectively. The loss of an alkene group is usually favored when the alkyl group (R_1 or R_2) chain length is greater than one (Figure 2.1a and b).[15] Figure 3.4a shows the product ion spectrum resulting from the isolation and fragmentation of the fragment ion $[PT-2(C_2H_4)+H]^+$ (*m/z* 236). Upon fragmentation, $[PT-2(C_2H_4)+H]^+$ (*m/z* 236) loses H_2O to form the fragment ion $[PT-2(C_2H_4)-H_2O+H]^+$ (*m/z* 218), and NO_2 to form the fragment ion $[PT-2(C_2H_4)-NO_2+H]^+$ (*m/z* 190). The loss of the thiophosphoryl group results in the fragment ion $[NO_2PhOH+H]^+$ (*m/z* 140, Ph = C_6H_4). However, the most abundant ion in the product ion spectrum is the sulfur analogue of $[NO_2PhOH+H]^+$, $[NO_2PhSH+H]^+$ (*m/z* 156, Ph = C_6H_4). The presence of this ion suggests that parathion also undergoes a thiono-thiolo rearrangement.[11]

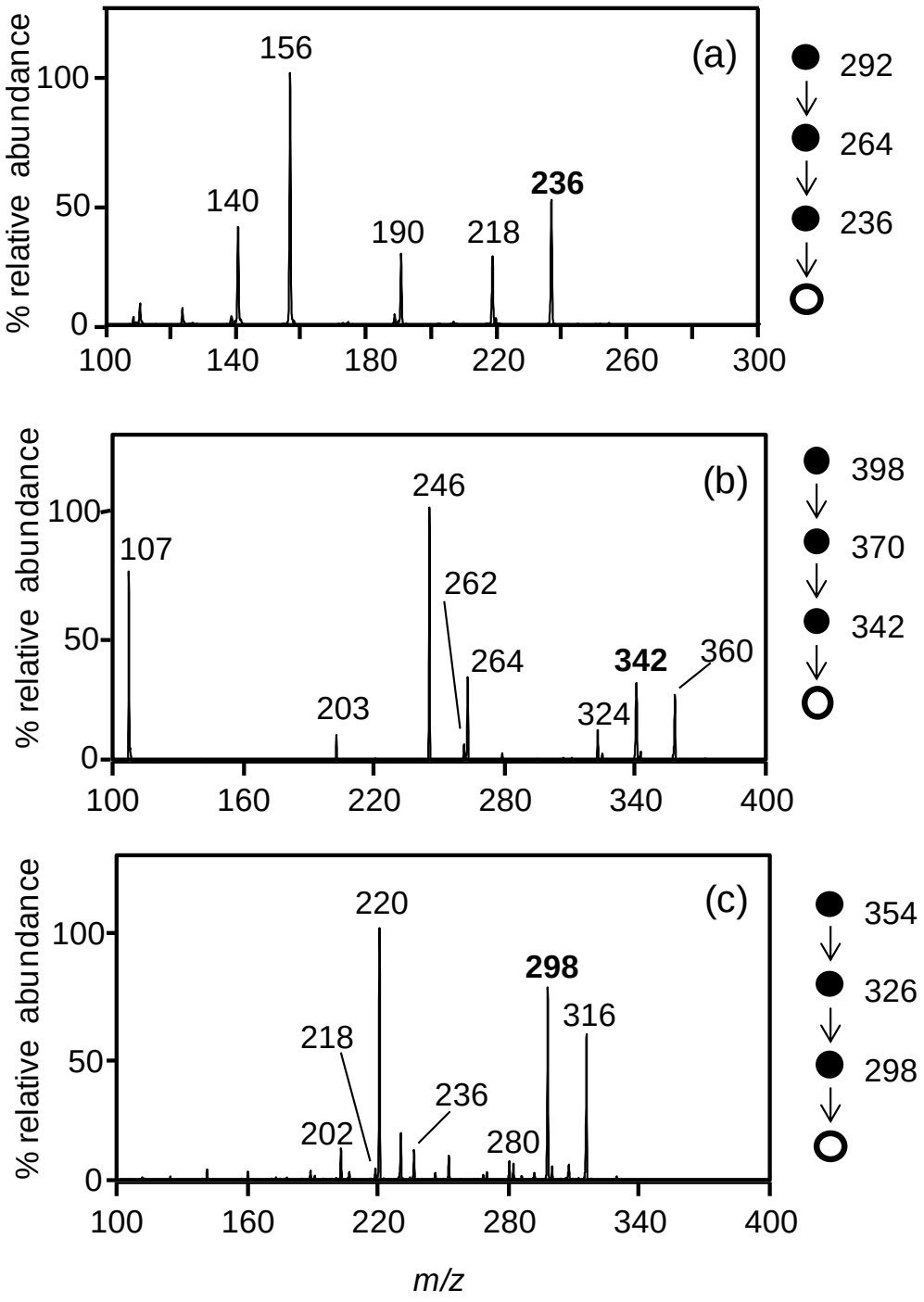

Figure 3.4 Product ion spectra of (a) $[PT-2(C_2H_4)+H]^+$ (*m/z* 236), (b) $[PT-2(C_2H_4)+^{107}Ag]^+$ (*m/z* 342), and (c) $[PT-2(C_2H_4)+^{63}Cu]^+$ (*m/z* 298). PT = parathion.

Table 3.2 Ions formed during CID of protonated parathion and parathion-metal complexes.

Solution species	**Fragment Ions**	**Observed *m/z***	**Theoretical *m/z****
PT			
($C_{10}H_{14}O_5NPS$)	$[PT+H]^+$	292.0	292.0
	$[PT-C_2H_4+H]^+$	264.0	264.0
	$[PT-2(C_2H_4)+H]^+$	236.1	236.0
	$[PT-2(C_2H_4)-H_2O+H]^+$	218.1	218.0
	$[PT-2(C_2H_4)-NO_2+H]^+$	190.0	190.0
	$[NO_2PhSH+H]^+$*	156.1	156.0
	$[NO_2PhOH+H]^+$*	140.2	140.0
$PT+Ag^+$			
	$[PT+^{107}Ag]^+$	397.9	397.9
	$[PT-C_2H_4+^{107}Ag]^+$	369.9	369.9
	$[PT-2(C_2H_4)+H_2O+^{107}Ag]^+$	359.5	359.9
	$[PT-2(C_2H_4)+^{107}Ag]^+$	341.7	341.9
	$[PT-2(C_2H_4)-H_2O+^{107}Ag]^+$	323.9	323.9
	$[NO_2PhOH+H_2O+^{107}Ag]^+$ *	263.7	263.9
	$[NO_2PhSH+^{107}Ag]^+$ *	262.0	261.9
	$[NO_2PhOH+^{107}Ag]^+$ *	246.1	245.9
	$[PSO_2H+^{107}Ag]^+$	203.0	202.8
	$^{107}Ag^+$	107.0	106.9
$PT+Cu^{2+}$			
	$[PT+^{63}Cu]^+$	353.9	354.0
	$[PT-C_2H_4+H_2O+^{63}Cu]^+$	343.7	343.9
	$[PT-C_2H_4+^{63}Cu]^+$	325.9	325.9
	$[PT-2(C_2H_4)+H_2O+^{63}Cu]^+$	315.8	315.9
	$[PT-2(C_2H_4)+^{63}Cu]^+$	297.8	297.9
	$[PT-2(C_2H_4)-H_2O+^{63}Cu]^+$	280.1	279.9
	$[NO_2PhSH+H_2O+^{63}Cu]^+$ *	235.9	235.9
	$[NO_2PhOH+H_2O+^{63}Cu]^+$ *	219.9	220.0
	$[NO_2PhSH+^{63}Cu]^+$ *	218.0	217.9
	$[NO_2PhOH+^{63}Cu]^+$ *	202.1	202.0
	$[PSO_2H+^{63}Cu]^+$	159.0	158.9

*Ph = C_4H_6.

The fragmentation pattern of $[PT+M]^+$ (M = ^{107}Ag or ^{63}Cu) is similar to that of $[PT+H]^+$, as sequential losses of ethene were observed in both cases. CID of $[PT+^{107}Ag]^+$ (*m/z* 398) led to formation of $[PT-C_2H_4+^{107}Ag]^+$ (*m/z* 370) and $[PT-2(C_2H_4)+^{107}Ag]^+$ (*m/z* 342) fragment ions, while CID of $[PT+^{63}Cu]^+$ (*m/z* 354) resulted in fragment ions $[PT-C_2H_4+^{63}Cu]^+$ (*m/z* 326) and $[PT-2(C_2H_4)+^{63}Cu]^+$ (*m/z* 298), along with their water adducts (spectra not shown). Figure 3.4b and c show the product ion spectra resulting from isolation and subsequent fragmentation of $[PT-2(C_2H_4)+M]^+$ (*m/z* 342 for M = ^{107}Ag and *m/z* 298 for M = ^{63}Cu). In each case, fragmentation of $[PT-2(C_2H_4)+M]^+$ led to loss of H_2O to form the fragment ion $[PT-2(C_2H_4)-H_2O+M]^+$ (*m/z* 324 for M = ^{107}Ag and *m/z* 280 for M = ^{63}Cu) and loss of thiophosphoryl group to form the fragment ion $[NO_2PhOH+M]^+$ (*m/z* 246 for M = ^{107}Ag and *m/z* 202 for M = ^{63}Cu; Ph = C_6H_4). Water addition to $[NO_2PhOH+M]^+$ gives rise to fragment ion $[NO_2PhOH+H_2O+^{107}Ag]^+$ (*m/z* 264) in Figure 3.4b and fragment ion $[NO_2PhOH+H_2O+^{63}Cu]^+$ (*m/z* 220) in Figure 3.4c. The peaks at *m/z* 360 (in Figure 3.4b) and *m/z* 316 (in Figure 3.4c) are due to water addition to $[PT-2(C_2H_4)+M]^+$.

The fragment ion $[NO_2PhOH+M]^+$ (*m/z* 246 for M = ^{107}Ag and *m/z* 202 for M = ^{63}Cu; Ph = C_6H_4) is the metal analogue of $[NO_2PhOH+H]^+$ (*m/z* 140), formed during fragmentation of $[PT-2(C_2H_4)+H]^+$ (Figure 3.4a, Table 3.2). The fragment ion $[NO_2PhSH+H]^+$ (*m/z* 156) in Figure 3.4a is formed from the phosphorothioate isomer as a result of the thiono-thiolo rearrangement of protonated parathion. However, $[NO_2PhSH+^{107}Ag]^+$ (*m/z* 262) and $[NO_2PhSH+^{63}Cu]^+$ (*m/z* 218), the metal analogues of $[NO_2PhSH+H]^+$ (*m/z* 156), were observed only in very low abundance. This observation is in agreement with our earlier observation that the thiono-thiolo rearrangement is inhibited

by the presence of the metal ion. The fragment ion $[NO_2PhOH+^{107}Ag]^+$ (*m/z* 246, Ph = C_6H_4) forms in the highest abundance during fragmentation of $[PT-2(C_2H_4)+^{107}Ag]^+$ (*m/z* 342), while the water adduct ion $[NO_2PhOH+^{63}Cu+H_2O]^+$ (*m/z* 220, Ph = C_6H_4) forms in the highest abundance during fragmentation of $[PT-2(C_2H_4)+^{63}Cu]^+$ (Figure 3.4b and c).

Kuivalainen et al.[11] suggested that parathion can be protonated at either of three different sites: the thiophosphoryl sulfur atom, an ethoxy group oxygen, or a phenoxy group oxygen. However, protonation at the thiophosphoryl S atom is thermodynamically preferred compared to protonation at an ethoxy group or phenoxy group oxygen.[11] The presence of peaks that can be assigned to the fragment ions $[PSO_2H+^{107}Ag]^+$ (*m/z* 203) and $[NO_2PhOH+^{107}Ag]^+$ (*m/z* 246, Ph = C_6H_4) in the product ion spectrum of $[PT-2(C_2H_4)+^{107}Ag]^+$ (*m/z* 342) (Figure 3.4b) suggests that Ag^+ can bind either to the thiophosphoryl sulfur atom or the phenoxy oxygen atom (Figure 2.1b). Based on the higher ion abundance of $[NO_2PhOH+^{107}Ag]^+$ (*m/z* 246, Ph = C_6H_4) compared to $[PSO_2H+^{107}Ag]^+$ (*m/z* 203), it can be inferred that the coordination of Ag^+ to parathion via the phenoxy oxygen atom is more stable, and thus preferred. Similar results were also observed in the product ion spectrum of $[PT-2(C_2H_4)+^{63}Cu]^+$ (*m/z* 298, Figure 3.4c).

3.3.3 CID of malathion and malathion-metal complexes

Unlike fenitrothion and parathion, malathion belongs to the phosphorodithioate class of OPs. In the phosphorodithioate pesticides, a second sulfur atom, in addition to the thiophosphoryl sulfur atom, forms a single bond with the central phosphorus atom (Figure 2.1b). We investigated the fragmentation patterns of malathion in the absence and presence of silver and copper ion, and determined how the fragmentation patterns differ from those of

fenitrothion and parathion. Our results show that the protonated malathion ion, $[MT+H]^+$ (*m/z* 331), fragments with a loss of C_2H_5OH, forming $[MT-C_2H_5OH+H]^+$ (*m/z* 285) (Figure 3.5a). Isolation and subsequent fragmentation of $[MT-C_2H_5OH+H]^+$ (*m/z* 285) results in loss of the dithiophosphate group, forming $[C_6H_7O_3]^+$ (*m/z* 127). Further fragmentation of $[C_6H_7O_3]^+$ (*m/z* 127) leads to loss of C_2H_4 with the formation of the fragment ion $[C_4H_3O_3]^+$ (*m/z* 99). The fragmentation pathway described above is summarized in Figure 3.6. Ion assignments are given in Table 3.3. These results are consistent with those of Garcia-Reyes et al.[12] who examined the fragmentation pathways of malathion using TOF/MS and in-source CID fragmentation.

The substitution of silver or copper ion for the proton led to a change in fragmentation pathways. CID of $[MT+^{107}Ag]^+$ (*m/z* 437) led to separate losses of ethene, ethanol, and the di-ester group ($C_8H_{12}O_4$), giving fragment ions $[MT-C_2H_4+^{107}Ag]^+$ (*m/z* 409), $[MT-C_2H_5OH+^{107}Ag]^+$ (*m/z* 391), $[MT-C_2H_5OH-C_2H_4+^{107}Ag]^+$ (*m/z* 363), and $[C_2H_7O_2PS_2+^{107}Ag]^+$ (*m/z* 265), respectively (Figure 3.5b, Table 3.3). The fragment ion $[C_2H_7O_2PS+^{107}Ag]^+$ (*m/z* 233) arises from $[C_2H_7O_2PS_2+^{107}Ag]^+$ (*m/z* 265) via loss of a sulfur atom. Fragmentation of $[C_2H_7O_2PS+Ag]^+$ (*m/z* 233) lead to loss of $C_2H_7O_2PS$ to give Ag^+ (*m/z* 107). Isolation and subsequent fragmentation of $[MT-C_2H_5OH-C_2H_4+^{107}Ag]^+$ (*m/z* 363) led to formation of $[MT-C_2H_5OH-2(C_2H_4)+^{107}Ag]^+$ (*m/z* 335) and two unassigned ions at *m/z* 195 and 249. The fragmentation pathways described here are illustrated in Figure 3.7.

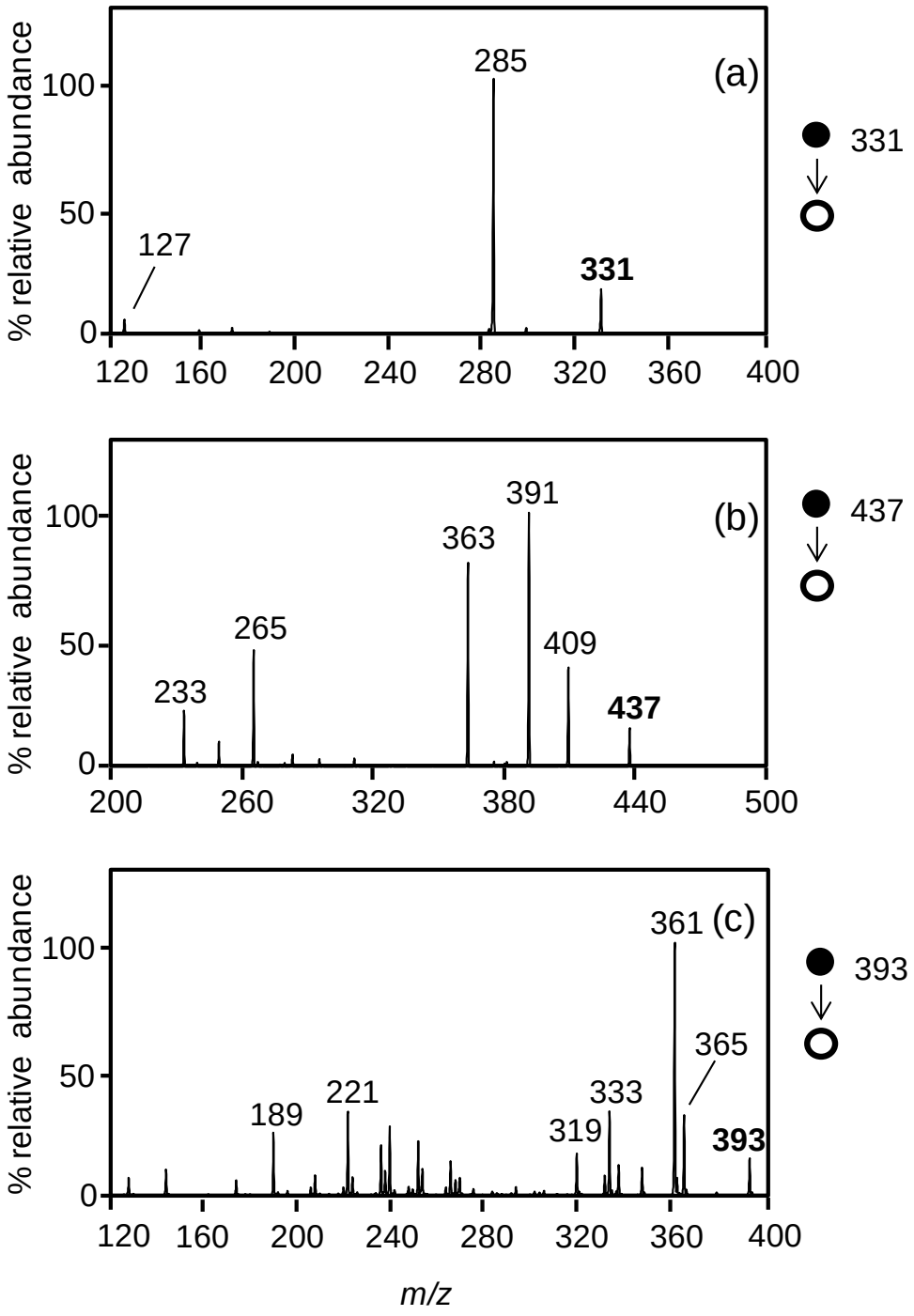

Figure 3.5 Product ion spectra of (a) $[MT+H]^+$ (*m/z* 331), (b) $[MT+^{107}Ag]^+$ (*m/z* 437), and (c) $[MT+^{63}Cu]^+$ (*m/z* 393). MT = malathion.

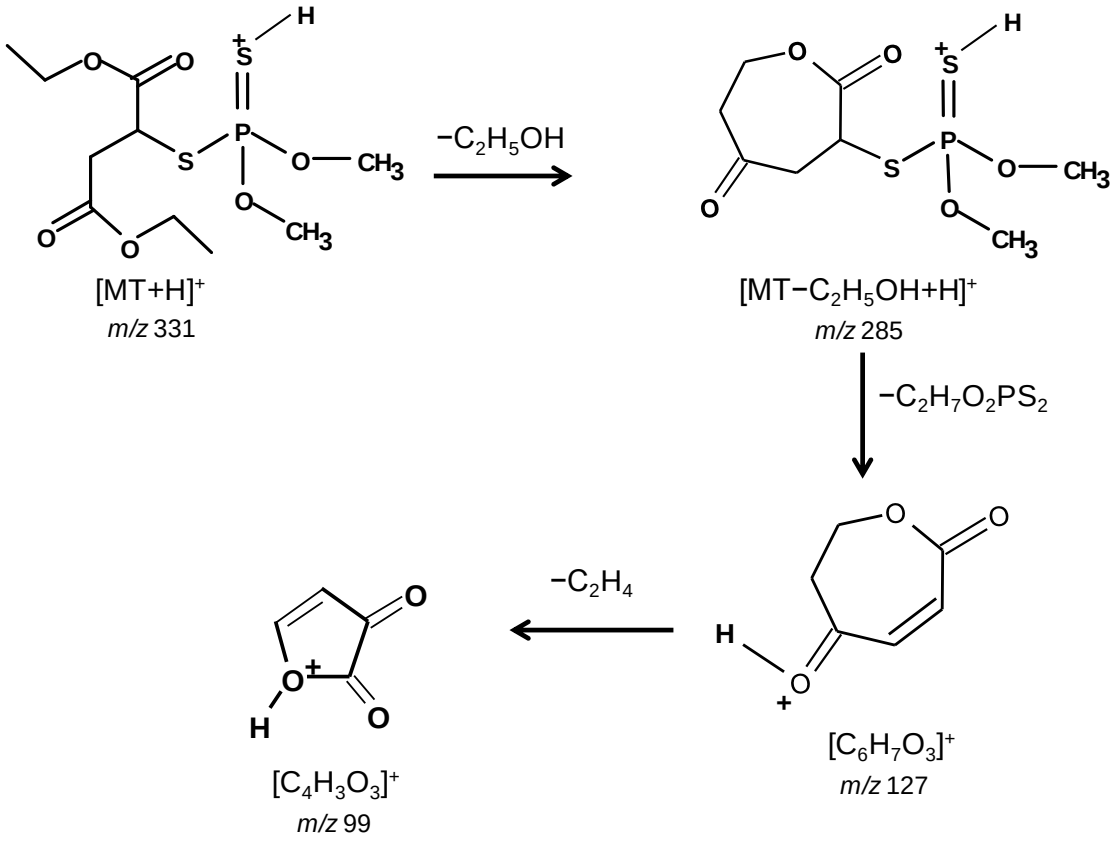

Figure 3.6 Fragmentation pathway of protonated malathion. Figure adapted from Reference 12.

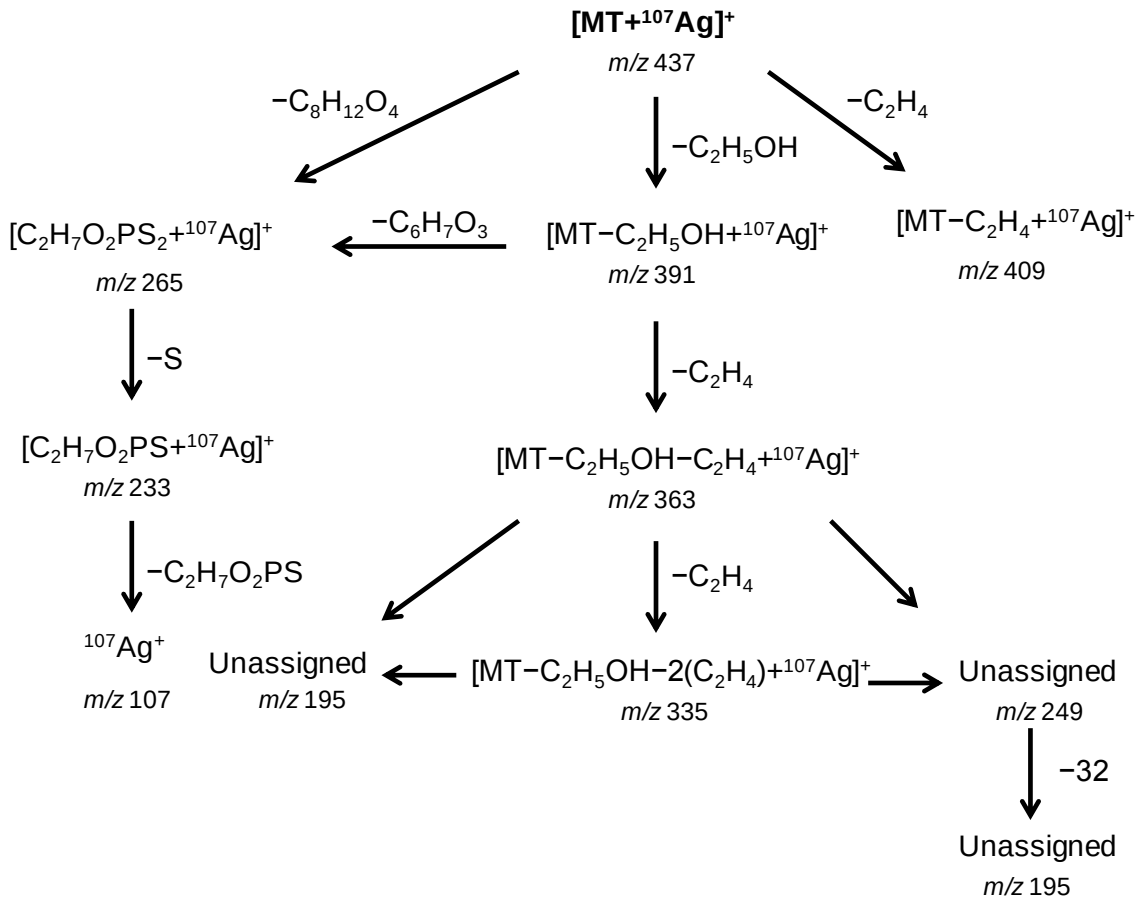

Figure 3.7 Fragmentation pathways of $[MT+^{107}Ag]^+$. MT = malathion.

Table 3.3 Ions formed during CID of protonated malathion and malathion-metal complexes.

Solution species	**Fragment Ions**	**Observed *m/z***	**Theoretical *m/z****
MT			
($C_{10}H_{19}O_6PS_2$)	$[M+H]^+$	330.9	331.0
	$[MT-C_2H_5OH+H]^+$	284.9	285.0
	$[C_6H_7O_3]^+$	127.0	127.0
	$[C_4H_3O_3]^+$	99.1	99.0
$MT+Ag^+$			
	$[MT+^{107}Ag]^+$	436.9	436.9
	$[MT-C_2H_4+^{107}Ag]^+$	408.9	408.9
	$[MT-C_2H_5OH+^{107}Ag]^+$	390.9	390.9
	$[MT-C_2H_5OH-C_2H_4+^{107}Ag]^+$	362.9	362.9
	$[MT-C_2H_5OH-2(C_2H_4)+^{107}Ag]^+$	335.0	334.8
	$[C_2H_7O_2PS_2+^{107}Ag]^+$	264.9	264.9
	Unassigned	249.0	-------
	$[C_2H_7O_2PS+^{107}Ag]^+$	233.0	232.9
	Unassigned	195.1	-------
	$^{107}Ag^+$	107.0	106.9
$MT+Cu^{2+}$			
	$[MT+^{63}Cu]^+$	392.9	393.0
	$[MT-C_2H_4+^{63}Cu]^+$	364.9	364.9
	$[MT-CH_3OH+^{63}Cu]^+$	360.9	360.9
	$[MT-CH_3OH-C_2H_4+^{63}Cu]^+$	332.9	332.9
	$[MT-C_2H_5OH-C_2H_4+^{63}Cu]^+$	318.9	318.9
	$[C_2H_7O_2PS_2+^{63}Cu]^+$	220.9	220.9
	$[C_2H_7O_2PS+^{63}Cu]^+$	189.0	188.9

The fragmentation pattern for $[MT+^{63}Cu]^+$ (*m/z* 393) appear to follow a trend similar to that observed for $[MT+^{107}Ag]^+$. As shown in Figure 3.5c, CID of $[MT+^{63}Cu]^+$ (*m/z* 393) resulted in a loss of ethene to form the fragment ion $[MT-C_2H_4+^{63}Cu]^+$ (*m/z* 365), and a loss of methanol to form the fragment ion $[MT-CH_3OH+^{63}Cu]^+$ (*m/z* 361). Other fragment ions observed included $[MT-CH_3OH-C_2H_4+^{63}Cu]^+$ (*m/z* 333), $[MT-C_2H_5OH-C_2H_4+^{63}Cu]^+$ (*m/z* 319), $[C_2H_7O_2PS_2+^{63}Cu]^+$ (*m/z* 221) and $[C_2H_7O_2PS+^{63}Cu]^+$ (*m/z* 189). Except for the methanol loss observed here, all the other losses are similar to those observed during CID of $[MT+^{107}Ag]^+$. The fragmentation spectra of $[MT+^{107}Ag]^+$ and $[MT+^{63}Cu]^+$ differ only in which fragment ion gives rise to the dominant peak in each product ion spectra. The fragment ion $[MT-C_2H_5OH+^{107}Ag]^+$ (*m/z* 391) gives rise to the most intense peak in the product ion spectrum of $[MT+^{107}Ag]^+$ (Figure 3.5b), while $[MT-CH_3OH+^{63}Cu]^+$ (*m/z* 361) is the most abundant ion formed by fragmentation of $[MT+^{63}Cu]^+$ (Figure 3.5c). The reason for this difference is not yet understood, but is believed to relate to stabilization of a particular fragment ion by silver or copper. The loss of OCH_2CH_3 from the malathion ester group appears to be preferred over the loss of OCH_3 from the dithiophosphoryl group. This loss of OCH_2CH_3 is a commonly observed fragmentation pattern for malathion (Figure 3.6).[12]

3.3.4 CID of diazinon and diazinon-metal complexes

The fragmentation pathways of diazinon have been well characterized.[13, 14, 22] Protonated diazinon, $[DZ+H]^+$ (*m/z* 305), can undergo an intramolecular thiono-thiolo rearrangement to form a second isomeric ion at *m/z* 305.[13] Each of these isomers can undergo sequential losses of first one, then a second, ethene from ethoxy groups, giving ions

at *m/z* 277 and *m/z* 249. Figure 3.8a shows the product ion spectrum of $[DZ-C_2H_4+H]^+$ (*m/z* 277), where peaks were observed at *m/z* 249, 169 and 153. The peak at *m/z* 249 is due to a loss of a second ethene moiety to form fragment ion $[DZ-2(C_2H_4)+H]^+$. Fragmentation of the $[DZ-2(C_2H_4)+H]^+$ isomers (both at *m/z* 249) led on the one hand to a loss of PO_2SH, giving rise to a protonated pyrimadol ion, $[C_8H_{12}N_2O+H]^+$ (*m/z* 153), and on the other hand to a loss of PO_3H to give a protonated pyrimidinethiol ion, $[C_8H_{12}N_2S+H]^+$ (*m/z* 169). Isolation and fragmentation of either $[C_8H_{12}N_2O+H]^+$ (*m/z* 153) or $[C_8H_{12}N_2S+H]^+$ (*m/z* 169) led to the formation of fragment ion $[C_8H_{10}N_2+H]^+$ (*m/z* 135) via the loss of either H_2O or H_2S (spectrum not shown). Fragmentation patterns discussed here are summarized in Figure 3.9.

Fragmentation of the diazinon-metal complexes appears to follow the pattern described above, as metal analogues of the $[DZ+H]^+$ fragment ions were observed during CID of $[DZ+M]^+$. Fragmentation of $[DZ+^{107}Ag]^+$ (*m/z* 411), for example, gives rise to $[DZ-C_2H_4+^{107}Ag]^+$ (*m/z* 383) through loss of one ethene moiety from an ethoxy group. The product ion spectrum of $[DZ-C_2H_4+^{107}Ag]^+$ (*m/z* 383) shows the formation of fragment ions at *m/z* 355, 277, 259, 153 (Figure 3.8b). The loss of a second ethene group gives rise to $[DZ-2(C_2H_4)+^{107}Ag]^+$ (*m/z* 355). CID of $[DZ-2(C_2H_4)+^{107}Ag]^+$ (*m/z* 355) led to a loss of PO_2SH, giving the silver-pyrimadol ion $[C_8H_{12}N_2O+^{107}Ag]^+$ (*m/z* 259), which in turn fragments with loss of the metal to give a protonated pyrimadol ion at *m/z* 153. The peak observed at *m/z* 277 is the water adduct of the silver-pyrimadol ion. Ion assignments are given in Table 3.4.

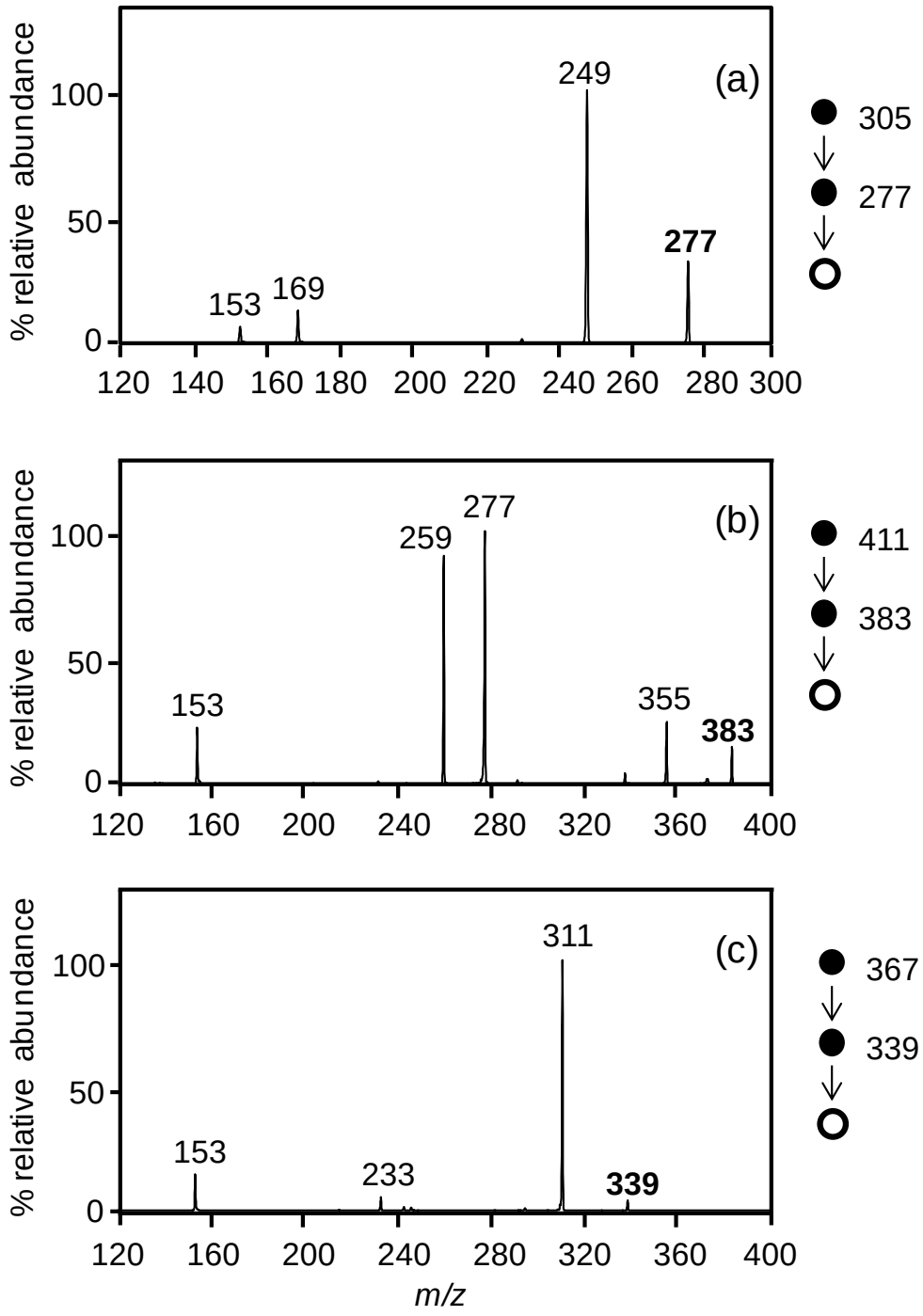

Figure 3.8 Product ion spectra of (a) $[DZ-(C_2H_4)+H]^+$ (*m/z* 277), (b) $[DZ-(C_2H_4)+^{107}Ag]^+$ (*m/z* 383), and (c) $[DZ-(C_2H_4)+^{63}Cu]^+$ (*m/z* 339). DZ = diazinon.

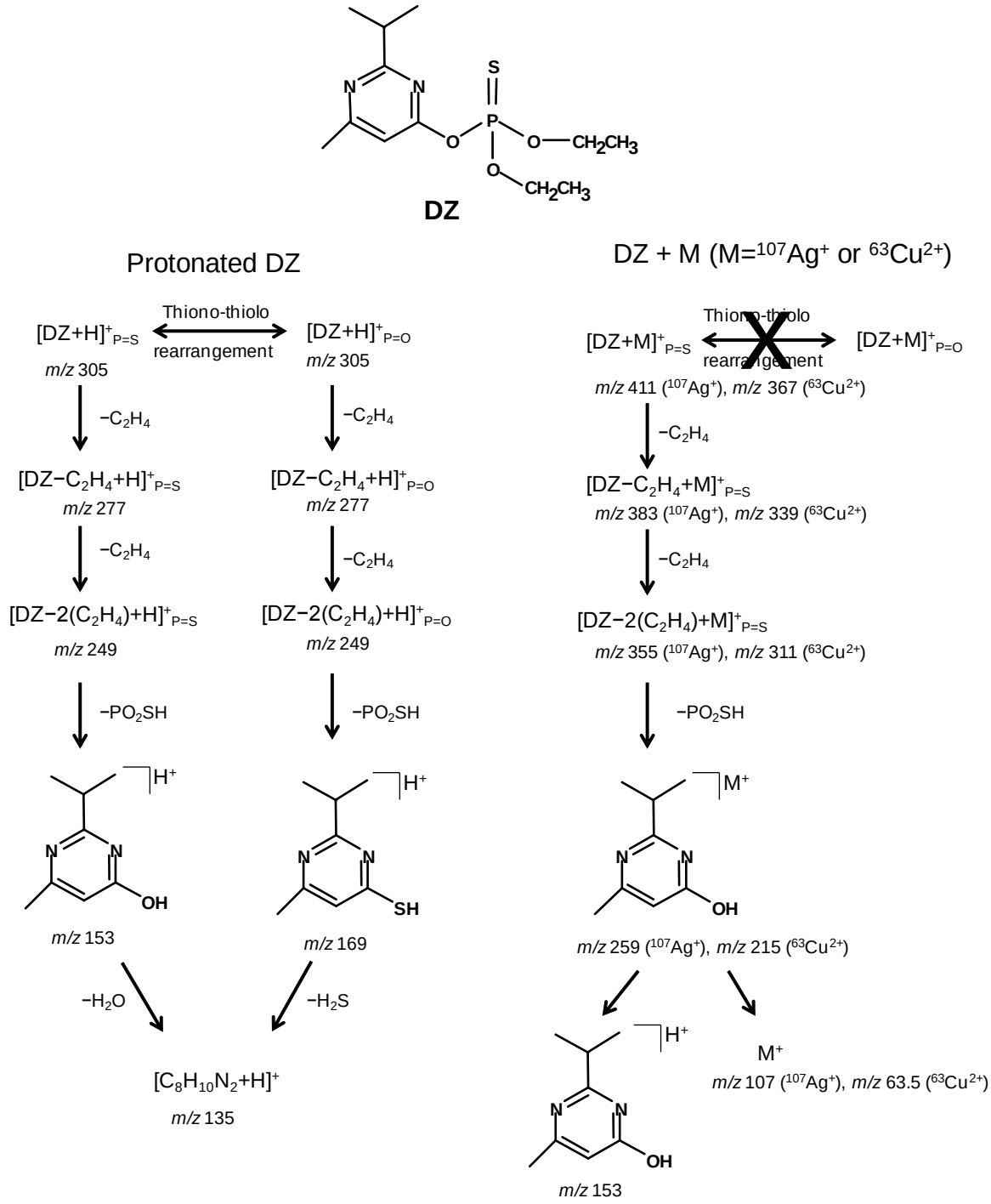

Figure 3.9 Fragmentation pathways of $[DZ+H]^+$ and $[DZ+M]^+$. M = ^{107}Ag or ^{63}Cu.

Table 3.4 Ions formed during CID of protonated diazinon and diazinon-metal complexes.

Solution species	**Fragment Ions**	**Observed *m/z***	**Theoretical *m/z****
DZ			
	$[DZ+H]^+$	305.1	305.1
	$[DZ-C_2H_4+H]^+$	277.1	277.1
	$[DZ-2(C_2H_4)+H]^+$	249.1	249.0
	$[DZ-2(C_2H_4)-H_2O+H]^+$	231.2	231.0
	$[C_8H_{12}N_2S+H]^+$	169.2	169.1
	$[C_8H_{12}N_2O+H]^+$	153.2	153.1
	$[C_8H_{10}N_2+H]^+$	135.1	135.1
$DZ+Ag^+$			
	$[DZ+^{107}Ag]^+$	410.9	411.0
	$[DZ-C_2H_4+^{107}Ag]^+$	382.9	383.0
	$[DZ-2(C_2H_4)+^{107}Ag]^+$	354.8	354.9
	$[C_8H_{12}N_2O+H_2O+^{107}Ag]^+$	276.8	277.0
	$[C_8H_{12}N_2O+^{107}Ag]^+$	259.1	259.0
	$[C_8H_{12}N_2O+H]^+$	153.2	153.1
	$^{107}Ag^+$	107.0	106.9
$DZ+Cu^{2+}$			
	$[DZ+^{63}Cu]^+$	367.0	367.0
	$[DZ-C_2H_4+^{63}Cu]^+$	339.0	339.0
	$[DZ-2(C_2H_4)+^{63}Cu]^+$	310.9	311.0
	$[C_8H_{12}N_2O+H_2O+^{63}Cu]^+$	232.9	233.0
	$[C_8H_{12}N_2O+^{63}Cu]^+$	215.1	215.0
	$[C_8H_{12}N_2O+H]^+$	153.2	153.1
	$^{63}Cu^+$	63.5	63.5

If the thiono-thionol rearrangement observed for protonated diazinon $[DZ+H]^+$ is also occurring in $[DZ+^{107}Ag]^+$, the silver-pyrimidinethiol fragment ion $[C_8H_{12}N_2S+^{107}Ag]^+$ (*m/z* 280) should be observed in the mass spectrum, just as $[C_8H_{12}N_2S+H]^+$ (*m/z* 169) was observed in Figure 3.8a. The silver-pyrimidinethiol ion, $[C_8H_{12}N_2S+^{107}Ag]^+$ (*m/z* 280) is a diagnostic ion of the thiolo isomer of diazinon.[13] The absence of a peak arising from this ion in Figure 3.8b indicates that the thiono-thiolo rearrangement is not favored when silver ion is present. The substitution of copper for silver ion has no effect on the fragmentation pattern, as copper analogues of the fragment ions discussed above for the diazinon-silver complex were observed.

Figure 3.8c shows the product ion spectrum of $[DZ-(C_2H_4)+^{63}Cu]^+$ (*m/z* 339). The fragment ion $[DZ-(C_2H_4)+^{63}Cu]^+$ (*m/z* 339), which was initially formed by the loss of one ethene group from $[DZ+^{63}Cu]^+$ (*m/z* 367) upon CID, loses the second ethene group to give rise to fragment ion $[DZ-2(C_2H_4)+^{63}Cu]^+$ (*m/z* 311). Subsequent fragmentation of $[DZ-2(C_2H_4)+^{63}Cu]^+$ (*m/z* 311) results in loss of PO_2SH to form $[C_8H_{12}N_2O+^{63}Cu]^+$ (*m/z* 215), which then reacts with water to form an adduct at *m/z* 233. The loss of copper ion from $[C_8H_{12}N_2O+^{63}Cu]^+$ (*m/z* 215) followed by protonation gives rise to $[C_8H_{12}N_2O+H]^+$, which is observed at *m/z* 153. The only difference in the product ion spectra of silver and copper-diazinon complexes lies in the relative abundances of the fragment ions (Figure 3.8b and c). Apart from $[DZ-2(C_2H_4)+M]^+$, where the copper-containing ion (*m/z* 311) occurs in higher abundance than its silver analogue at *m/z* 355, all the silver-diazinon fragment ions are always observed in higher relative abundances compared to their copper analogues. This observation, which is consistent with our earlier results discussed in Chapter 2, suggests that the silver ion is much effective in stabilizing the fragment ion than copper. This is thought to

be due to the nature of the interaction between the soft thiophosphoryl sulfur atom and the metal ion. Because of the larger ionic radius of the silver ion (0.067 nm), its interaction with the sulfur atom will be more effective than that of copper, which has a smaller ionic radius (0.057 nm). The fragmentation patterns for diazinon in the absence and presence of silver or copper ion are summarized in Figure 3.9.

3.4 Conclusions

The study here describes the fragmentation patterns of fenitrothion, parathion, malathion and diazinon in the absence and presence of silver and copper ions. My results show that the fragmentation patterns of fenitrothion, parathion, malathion and diazinon in the absence of metal ion is consistent with previously reported results. Phosphorothioate pesticides with R_1 and R_2 = ethyl preferentially lose ethene groups, while sequential losses of methanol are observed if R_1 and R_2 are methyl groups. My results also show evidence of thiono-thiolo rearrangement occurring, as fragment ion peaks due to both thiol and thion were observed during the CID of phosphorothiate pesticides. The only phosphorodithioate compound investigated, malathion shows no sign of such rearrangement, as its fragmentation pattern is completely different from those of the other three pesticides. In the presence of metal ions, the fragmentation patterns of phosphorothioate pesticides investigated were similar to their protonated analogues, as almost the same set of moieties were lost. However, fragment ions resulting from the thiono-thiolo rearrangement were not observed. It thus appears that the presence of metal ion inhibits this unique rearrangement from taking place.

Acknowledgements

Jacob Donton is thanked for his preliminary work on the CID of the pesticides and pesticide-metal complexes.

References

1. Soler, C.; Manes, J.; Pico, Y. The role of the liquid chromatography-mass spectrometry in pesticide residue determination in food. *Crit. Rev. Anal. Chem.* **2008,** *38*, 93-117.
2. Malik, A. K.; Blasco, C.; Pico, Y. Liquid chromatography-mass spectrometry in food safety. *J. Chromatogr. A* **2010,** *1217*, 4018-4040.
3. Pico, Y.; Blasco, C.; Font, G. Environmental and food applications of LC-tandem mass spectrometry in pesticide-residue analysis: An overview. *Mass Spectrom. Rev.* **2004,** *23*, 45-85.
4. Ortiz, D.; Salpin, J.-Y.; Song, K.; Spezia, R. Galactose-6-Sulfate collision induced dissociation using QM plus MM chemical dynamics simulations and ESI-MS/MS experiments. *Int. J. Mass Spectrom.* **2014,** *358*, 25-35.
5. Kovacevic, B.; Schorr, P.; Qi, Y.; Volmer, D. A. Decay mechanisms of protonated 4-quinolone antibiotics after electrospray ionization and ion activation. *J. Am. Soc. Mass Spectrom.* **2014,** *25*, 1974-1986.
6. Crotti, A. E. M.; Bronze-Uhle, E. S.; Nascimento, P. G. B. D.; Donate, P. M.; Galembeck, S. E.; Vessecchi, R.; Lopes, N. P. Gas-phase fragmentation of gamma-lactone derivatives by electrospray ionization tandem mass spectrometry. *J. Mass Spectrom.* **2009,** *44*, 1733-1741.
7. Di Marco, V. B.; Bombi, G. G. Electrospray mass spectrometry (ESI-MS) in the study of metal-ligand solution equilibria. *Mass Spectrom. Rev.* **2006,** *25*, 347-379.
8. Amorim Madeira, P. J.; Florencio, H. M. Applications of tandem mass spectrometry: From structural analysis to fundamental studies. In *Tandem Mass Spectrometry - Applications and Principles*, Prasain, J. K., Ed. InTech: Croatia, **2012**; pp 3-32.
9. de Hoffmann, E. Tandem mass spectrometry: A primer. *J. Mass Spectrom.* **1996,** *31*, 129-137.
10. Kuivalainen, T.; Kostiainen, R.; Bjork, H.; Uggla, R.; Sundberg, M. R. Fragmentation of protonated *O,O*-dimethyl *O*-aryl phosphorothionates in tandem mass spectral analysis. *J. Am. Soc. Mass Spectrom.* **1995,** *6*, 488-497.

11. Kuivalainen, T.; Kostiainen, R.; Uggla, R.; Sundberg, M. R.; Bjork, H. Fragmentation of protonated *O,O*-diethyl *O*-aryl phosphorothionates in tandem mass spectral analysis. *J. Am. Soc. Mass Spectrom.* **1996,** *7*, 189-197.
12. Garcia-Reyes, J. F.; Molina-Diaz, A.; Fernandez-Alba, A. R. Identification of pesticide transformation products in food by liquid chromatography/time-of-flight mass spectrometry via "fragmentation-degradation" relationships. *Anal. Chem.* **2007,** *79*, 307-321.
13. Barr, J. D.; Bell, A. J.; Bird, M.; Mundy, J. L.; Murrell, J.; Timperley, C. M.; Watts, P.; Ferrante, F. Fragmentations and reactions of the organophosphate insecticide diazinon and its oxygen analog diazoxon studied by electrospray ionization ion trap mass spectrometry. *J. Am. Soc. Mass. Spectrom.* **2005,** *16*, 515-23.
14. Banoub, J.; Gentil, E.; Kiceniuk, J. Analysis of organophosphorus pesticide residues by low energy tandem mass spectrometry using electrospray ionization. *Int. J. Environ. Anal. Chem.* **1995,** *61*, 143-167.
15. Schwarzenberg, A.; Ichou, F.; Cole, R. B.; Machuron-Mandard, X.; Junot, C.; Lesage, D.; Tabet, J. C. Identification tree based on fragmentation rules for structure elucidation of organophosphorus esters by electrospray mass spectrometry. *J. Mass Spectrom.* **2013,** *48*, 576-586.
16. Eto, M. *Organophosphorus pesticides: Organic and biological chemistry*. CRC Press: Cleveland OH, **1974**; p 387.
17. Cooks, R. G.; Gerrard, A. F. Electron impact-induced rearrangements in compounds having the P=S bond. *J. Chem. Soc. B* **1968**, 1327-1333.
18. Niessen, W. M. A. Group-specific fragmentation of pesticides and related compounds in liquid chromatography-tandem mass spectrometry. *J. Chromatogr. A* **2010,** *1217*, 4061-4070.
19. Lacorte, S.; Molina, C.; Barcelo, D. Temperature and extraction voltage effect on fragmentation of organophophorus pesticides in liquid chromatography-atmospheric pressure chemical ionization mass spectrometry. *J. Chromatogr. A* **1998,** *795*, 13-26.
20. Bell, A. J.; Despeyroux, D.; Murrell, J.; Watts, P. Fragmentation and reactions of organophosphate ions produced by electrospray ionization. *Int. J. Mass Spectrom.* **1997,** *165*, 533-550.

21. Pearson, R. G. Hard and soft acids and bases. *J. Am. Chem. Soc.* **1963,** *85*, 3533.

22. Niessen, W. M. A. Group-specific fragmentation of pesticides and related compounds in liquid chromatography-tandem mass spectrometry. *J. Chromatogr. A* **2010,** *1217*, 4061-4070.

Chapter 4

Probing Uranyl(VI) Speciation in the Presence of Amidoxime Ligands using Electrospray Ionization Mass Spectrometry[†]

Abstract

Extraction processes using poly(acrylamidoxime) resins are being developed to extract uranium from seawater. The main complexing agents in these resins are thought to be 2,6-dihydroxyiminopiperidine (DHIP) and N^1,N^5-dihydroxypentanediimidamide (DHPD), which form strong complexes with uranyl(VI) at the pH of seawater. It is important to understand uranyl(VI) speciation in the presence of these and similar amidoxime ligands to understand factors affecting uranyl(VI) adsorption to the poly(acrylamidoxime) resins. Experiments were carried out in positive ion mode on a quadrupole ion trap mass spectrometer equipped with an electrospray ionization source. The ligands investigated were DHIP, DHPD, and N^1,N^2-dihydroxyethanediimidamide (DHED). DHED and DHPD differ only in the number of carbons separating the oxime groups. The effects on the mass spectra of changes in uranyl(VI):ligand ratio, pH, and ligand type were examined. My results show that DHIP binds uranyl(VI) more effectively than DHPD or DHED in the pH range investigated, forming ions derived from solution-phase species with

---

[†]Chapter published in *Rapid Commun. Mass Spectrom.* **2013**, *27*, 2135–2142. Reproduced with permission from John Wiley and Sons. See Appendix B for letter of permission to republish this material.

uranyl(VI):DHIP stoichiometries of 1:1, 1:2, and 2:3. The 2:3 uranyl(VI):DHIP complex appears to be a previously undescribed solution species. Ions related to uranyl(VI):DHPD complexes were detected in very low abundance. DHED is a more effective complexing agent for uranyl(VI) than DHPD, forming ions having uranyl(VI):DHED stoichiometries of 1:1, 1:2, 1:3, and 2:3. This study presents a first look at the solution chemistry of uranyl(VI)-amidoxime complexes using electrospray ionization mass spectrometry. The appearance of previously undescribed solution species suggests that the uranyl(VI)-amidoxime system is a rich and relatively complex one, requiring a more in-depth investigation.

4.1 Introduction

Earth's oceans contain an estimated ~4.5 x 10^9 metric tons of uranium,[1] mainly in the form of the uranyl(VI) carbonate complex $UO_2(CO_3)_3^{4-}$. This uranium is derived from, and continually replenished by, the erosion of crustal rocks. The amount of uranium contained in seawater is many times greater than that contained in known terrestrial sources,[2] and it has been recognized since at least the 1940's that seawater would form an important source of uranium if an economically viable extraction process could only be developed.[3] Although various methods for the extraction of uranium from seawater have been evaluated,[4, 5] sorption methods using polymeric materials having functional groups with a high affinity for uranyl(VI) are thought to be the most economically and environmentally feasible.[1, 6] In particular, the amidoxime functional group ($-C(NH_2)=NOH$) has a high affinity for uranyl(VI) in the pH range of seawater (~pH 8), is able to compete with carbonate for uranyl(VI), and can displace preexisting carbonate ligands from the predominant $UO_2(CO_3)_3^{4-}$ complex, even at the pH of seawater.[1, 7] Several types of amidoxime-based

uranyl(VI)-adsorbing materials have been developed and tested over the years.[8-12] While various binding modes have been proposed for uranyl(VI)-amidoxime complexes,[13-15] single-crystal X-ray structures of uranyl(VI)-acetamidoximate and -benzamidoximate complexes and calculations using density functional theory indicate that η^2 coordination to the N-O bond is likely the most stable form of binding for the uranyl(VI) ion.[13]

Only a few studies on uranyl(VI) speciation in the presence of amidoxime ligands in aqueous or organic solvents have been published. Salicylamidoxime, nicotinamidoxime, benzamidoxime, and *N*[1],*N*[2]-dihydroxyethanediimidamide have been investigated for use as reagents in the spectrophotometric determination of uranyl(VI).[16-19] Manoussakis and Kouimtzis[20] used potentiometry to determine metal:ligand ratios and formation constants for uranyl(VI)-benzanilidoxime complexes in an 50% (v/v) solution of dioxane/water. In their study, uranyl(VI)-benzanilidoxime complexes with stoichiometries of 1:1 and 1:2 formed above ~pH 4. Hirotsu et al.[21] used potentiometry and spectrophotometry to investigate uranyl(VI)-acetamidoxime complexes in aqueous solution. Their results showed that both 1:1 and 1:2 uranyl(VI):acetamidoxime complexes formed, with the 1:1 complex predominant at lower pH values and the 1:2 complex predominant at pH > 5.5. However, precipitates were formed above about pH 6. Hirotsu et al.[21] also reported stability constants for the 1:1 and the 1:2 species. Park et al.[22] and Kim et al.[23] used ^{1}H and ^{13}C NMR to study the uranyl(VI)-benzamidoxime complexes in acetone. They reported that a 1:3 uranyl(VI):benzamidoxime complex was formed in acetone in the presence of an excess of benzamidoxime. In more recent studies, Tian et al.[24, 25] performed potentiometric and spectrophotometric titrations to examine the complexation of uranyl(VI) with 2,6-dihydroxyiminopiperidine (DHIP) and *N*[1],*N*[5]-dihydroxypentanediimidamide (DHPD),

thought to be the main complexing agents in poly(acrylamidoxime) resins that have shown to be effective sorbers of uranyl(VI) from seawater.[1, 11, 26] They reported stability constants for 1:1 and 1:2 uranyl(VI) complexes with these ligands.

As sorbents having amidoxime functional groups are increasingly used in schemes for uranium sequestration, it has become more important to understand the complexation chemistry of amidoxime ligands with regards to uranyl(VI). Electrospray ionization mass spectrometry (ESI-MS) has often been used for the study of metal speciation in the presence of organic and inorganic ligands, as well as for determining complex stoichiometries.[27-30] In this work we have used ESI-MS to investigate uranyl(VI) speciation in the presence of three amidoxime ligands, 2,6-dihydroxyiminopiperidine (DHIP), N^1,N^5-dihydroxypentanediimidamide (DHPD), and N^1,N^2-dihydroxyethanediimidamide (DHED). The first two are of interest to us because the solution species are known and stability constants determined.[24, 25] Thus, it is possible to compare the previously described solution complexes to those detected using mass spectrometry. The third ligand, DHED, was chosen to understand the effect of alkyl chain length on uranyl(VI) coordination. The structures of these ligands are shown in Figure 4.1. To the best of our knowledge, there have been no published mass spectrometric studies on the amidoximate-uranyl(VI) system.

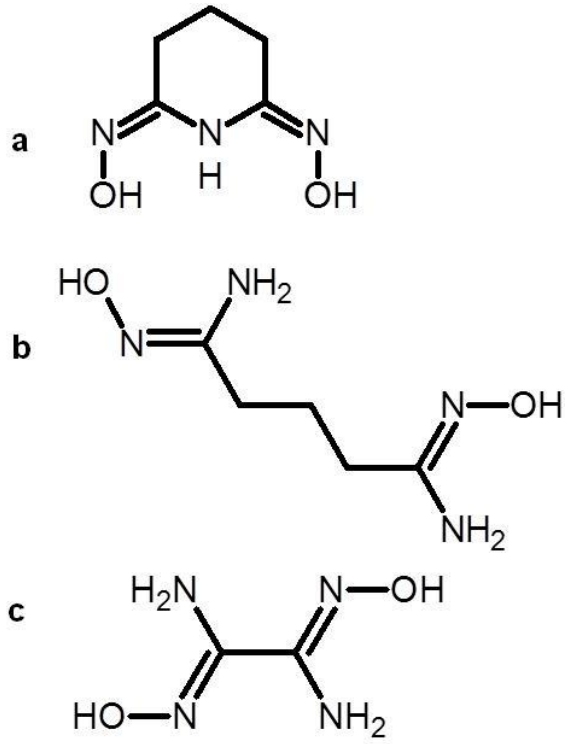

Figure 4.1 Structures of amidoxime ligands. (a) 2,6-dihydroxyiminopiperidine (DHIP), (b) N^1,N^5-dihydroxypentanediimidamide (DHPD), (c) N^1,N^2-dihydroxyethanediimidamide (DHED).

4.2 Experimental

4.2.1 Materials

2,6-Dihydroxyiminopiperidine (DHIP) and N^1,N^5-dihydroxypentanediimidamide (DHPD) were received as gifts from Dr. Linfeng Rao at Lawrence Berkeley National Laboratory (Berkeley, CA, USA). N^1,N^2-dihydroxyethanediimidamide (DHED) (97.5%) was purchased from ThermoFisher Scientific (Pittsburg, PA, USA). Uranyl(VI) nitrate hexahydrate was purchased from International Bio-Analytical Industries, Inc. (Boca Raton, FL, USA). Nitric acid (ACS grade), ammonium hydroxide (ACS grade) and methanol

(Omnisolve) were purchased from EMD Chemicals (Gibbstown, NJ, USA). Water (18 MΩ) was purified with a Milli-Q system (Millipore Corp., Billerica, MA, USA). All chemicals were used as received.

4.2.2 Sample preparation

Stock solutions of 10 mM uranyl(VI) nitrate were prepared in 18 MΩ Milli-Q water, while 10 mM solutions of the ligands were prepared in 20% (v/v) methanol/water. Solutions of N^1,N^5-dihydroxypentanediimidamide were sonicated for ~5 min. to ensure complete dissolution. The 10 mM uranyl(VI) and ligand stock solutions were combined in appropriate ratios and diluted with a 20% (v/v) methanol/water solution to give a final uranyl(VI) concentration of 0.1 mM. The sample pH was adjusted with HNO_3 or NH_4OH. pH measurements of the 20% (v/v) methanol-water solutions were made using an Orion ROSS combination pH electrode (Thermo Fisher Scientific, Pittsburg, PA, USA) standardized against pH 4.0 and 7.0 buffers traceable to the NIST pH activity scale.

4.2.3 Instrumentation

ESI-MS measurements were made with a Deca XP Plus ion trap mass spectrometer (ThermoFinnigan Co., San Jose, CA, USA). Samples were introduced by direct infusion at a flow rate of 3 μL/min. All experiments were performed in positive ion mode at the following electrospray ionization conditions: spray voltage, 4.00 kV; capillary voltage 40 V; capillary temperature, 275 °C; sheath gas (N_2) flow rate, 35 (arbitrary units).

4.3 Results and Discussion

4.3.1 DHIP complexation with uranyl(VI)

ESI-MS spectra of solutions containing uranyl(VI) and DHIP, uranyl(VI) and DHPD, and uranyl(VI) and DHED were acquired at various uranyl(VI):ligand ratios and pH values in order to characterize the uranyl(VI) complexes formed. Changes in the uranyl(VI)/ligand ratio were first monitored at pH 5.5, because 1:1 uranyl(VI)-amidoximate complexes have been observed to form at this pH.[21, 24, 25] The mass spectra are shown in Figure 4.2. Ion assignments are given in Table 4.1. Previous studies on uranyl(VI)-DHIP and -DHPD complexes have suggested that the ligand can be either protonated or deprotonated in aqueous solution, depending on solution pH.[24, 25] However, ligands can also become protonated during electrospray. We are assuming for the purpose of ion assignments that the amidoxime ligand can be either protonated or deprotonated, and that the methanol and water solvent adducts are present as neutral species.

The base peak in the mass spectrum acquired from a 0.1 mM solution of DHIP in 20% (v/v) methanol/water at pH 5.5 can be assigned to protonated DHIP ($[DHIP + H]^+$, *m/z* 144) (Figure 4.2a, Table 4.1). An ion with *m/z* 126 likely results from the loss of water from $[DHIP+H]^+$. Figures 4.2b-e show how changes in the metal/ligand mole ratio at pH 5.5 affect the relative intensities of peaks assigned to uranyl(VI)-DHIP complexes. When uranyl(VI) is added to a solution containing DHIP such that the uranyl(VI):DHIP mole ratio is 1:1, several peaks that can be assigned to 1:1 uranyl(VI):DHIP ions appear in the mass spectrum. Specifically, the mass spectrum shows a small peak at *m/z* 412, assigned to $[UO_2+(DHIP-H)]^+$, and more intense peaks at *m/z* 430, *m/z* 444, and *m/z* 540 assigned to

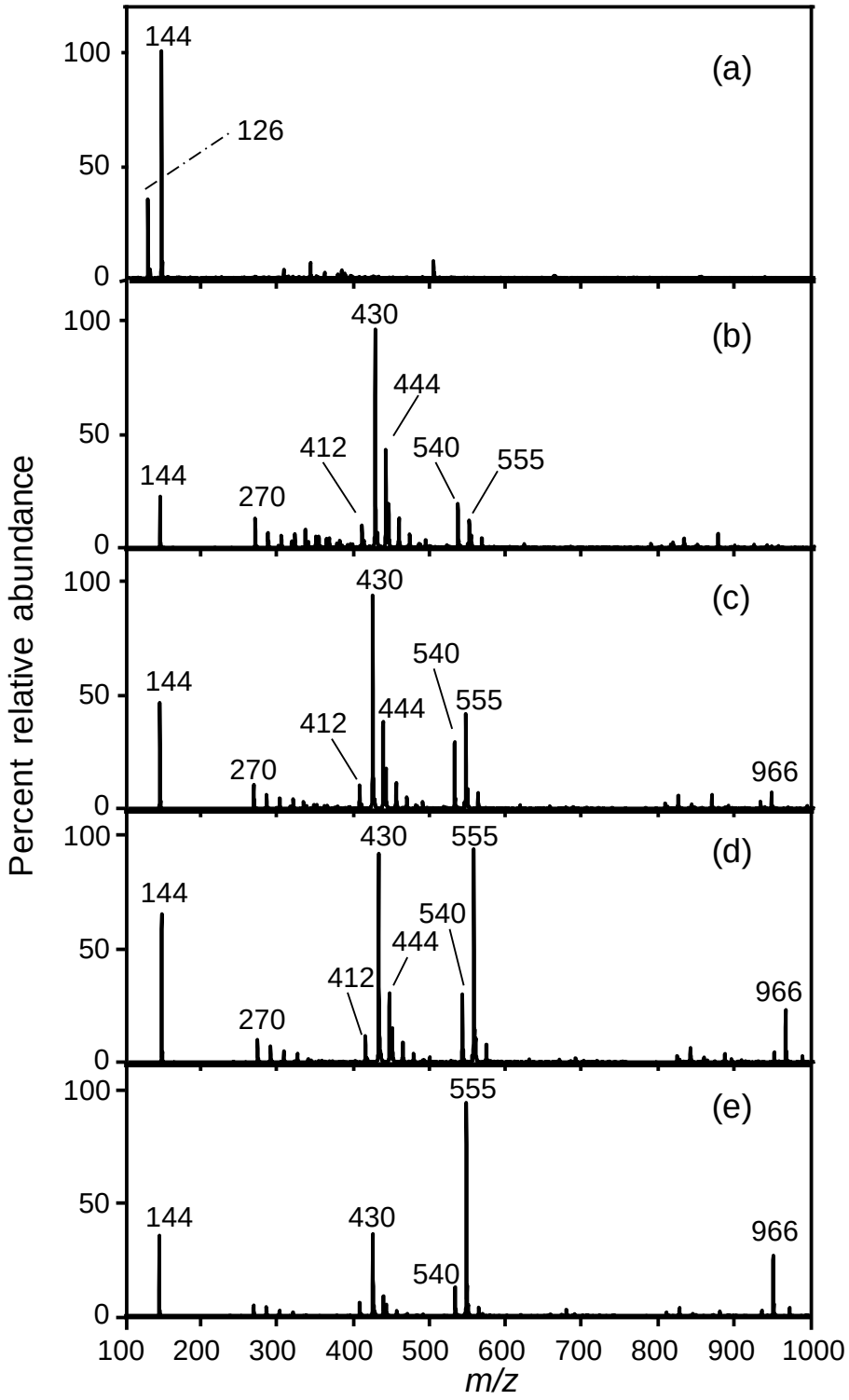

Figure 4.2 Positive-ion ESI mass spectra of solutions containing a) 0.1 mM DHIP, b) 0.1 mM uranyl(VI) and 0.1 mM DHIP, c) 0.1 mM uranyl(VI) and 0.2 mM DHIP, d) 0.1 mM uranyl(VI) and 0.3 mM DHIP, and e) 0.1 mM uranyl(VI) and 0.5 mM DHIP. All samples in 20% CH_3OH / 80% H_2O (v/v) at pH 5.5.

Table 4.1 ESI-MS peak assignments for uranyl(VI) species.

Solution	Species	Observed *m/z*	Theoretical *m/z*
Uranyl(VI)			
	UO_2^+	270.4	270.0
	$[UO_2+OH]^+$	287.4	287.0
	$[UO_2+OH+H_2O]^+$	305.3	305.1
	$[UO_2+OH+CH_3OH]^+$	319.0	319.1
	$[UO_2+OH+2(H_2O)]^+$	323.2	323.1
	$[UO_2+CH_3O+2(H_2O)]^+$	337.2	337.1
	$[UO_2+CH_3O+CH_3OH+H_2O]^+$	351.1	351.1
	$[UO_2+CH_3O+2(CH_3OH)]^+$	365.1	365.1
	$[UO_2+CH_3O+CH_3OH+2(H_2O)]^+$	369.1	369.1
	$[UO_2+CH_3O+2(CH_3OH)+H_2O]^+$	383.0	383.1
	$[UO_2+CH_3O+3(CH_3OH)]^+$	397.1	397.1
	$[UO_2+NO_3+2(CH_3OH)+H_2O]^+$	413.9	414.1
Uranyl(VI)/DHIP			
	$[(DHIP-H_2O)+H]^+$	126.1	126.1
	$[DHIP+H]^+$	144.2	144.1
	$[UO_2+(DHIP-H)]^+$	412.5	412.1
	$[UO_2+(DHIP-H)+H_2O]^+$	430.2	430.1
	$[UO_2+(DHIP-H)+CH_3OH]^+$	444.3	444.1
	$[UO_2+(DHIP-H)+4(CH_3OH)]^+$	540.1	540.2
	$[UO_2+(DHIP-H)+DHIP]^+$	555.3	555.2
	$[UO_2+Na+2(DHIP-H)]^+$	577.2	577.2
	$[UO_2+K+2(DHIP-H)]^+$	593.1	593.1
	$[2(UO_2)+3(DHIP-H)]^+$	966.3	966.3
	$[2(UO_2)+Na+(DHIP-2H)+2(DHIP-H)]^+$	988.2	988.2
	$[2(UO_2)+K+(DHIP-2H)+2(DHIP-H)]^+$	1004.2	1004.2
Uranyl(VI)/DHPD			
	Unassigned	128.1	-------
	$[DHPD+H]^+$	161.2	161.1
	$[DHPD+Na]^+$	183.1	183.1
	$[2(DHPD)+H]^+$	321.2	321.2
	$[2(DHPD)+Na]^+$	343.1	343.2
	$[2(DHPD)+(DHPD+H)+CH_3OH+2(H_2O)]^+$	549.3	549.3
	$[UO_2+(DHPD-H)+H_2O]^+$	447.2	447.1
	Unassigned	556.1	-------
	$[UO_2+(DHPD-H)+3(CH_3OH)+2(H_2O)]^+$	561.3	561.2
	$[UO_2+(DHPD-H)+DHPD]^+$	589.4	589.2
	$[UO_2+Na+2(DHPD-H)]^+$	611.1	611.2
	$[2(UO_2)+(DHPD-2H)+(DHPD-H)]^+$	857.4	857.2
	Unassigned	984.1	-------
	$[2(UO_2)+3(DHPD-H)]^+$	1017.4	1017.3
	$[2(UO_2)+Na+2(DHPD-2H)+DHPD]^+$	1039.4	1039.3

Table 4.1 continued. ESI-MS peak assignments for uranyl(VI) species.

Solution	Species	Observed *m/z*	Theoretical *m/z*
Uranyl(VI)/DHED			
	$[DHED+H]^+$	119.1	119.1
	$[2(Na)+DHED+(DHED-H)+2(H_2O)+2(CH_3OH)]^+$	381.3	381.1
	$[UO_2+(DHED-H)+2(H_2O)]^+$	423.1	423.1
	$[UO_2+(DHED-H)+H_2O+CH_3OH]^+$	436.9	437.1
	$[UO_2+(DHED-H)+2(CH_3OH)]^+$	450.9	451.1
	$[UO_2+DHED+NO_3+H_2O]^+$	468.0	468.1
	$[Na+3(DHED)+2(CH_3OH)+2(H_2O)]^+$	477.1	477.2
	$[UO_2+(DHED-H)+DHED]^+$	505.0	505.1
	$[UO_2+(DHED-H)+DHED+H_2O]^+$	523.0	523.1
	$[UO_2+2(DHED)+NO_3]^+$	568.1	568.1
	$[UO_2+(DHED-H)+2(DHED)]^+$	623.1	623.2
	$[2(UO_2)+3(DHED-H)]^+$	891.1	891.2
	$[2(UO_2)+2(DHED-H)+DHED+NO_3]^+$	954.1	954.2

$[UO_2+(DHIP-H)+H_2O]^+$, $[UO_2+(DHIP-H)+CH_3OH]^+$, and $[UO_2+(DHIP-H)+4(CH_3OH)]^+$, respectively (Figure 4.2b, Table 4.1). A peak corresponding to a 1:2 uranyl(VI):DHIP species, $[UO_2+(DHIP-H)+DHIP]^+$ (*m/z* 555), can also be observed. In addition to the uranyl(VI)-DHIP complexes, UO_2^+ (*m/z* 270) and several low-abundance uranyl(VI)-hydroxide and -methoxide species can be seen in the mass spectrum (Figure 4.2b, Table 4.1). UO_2^+ results from the reduction of UO_2^{2+} during electrospray,[31, 32] while uranyl(VI)-hydroxide and methoxide ions are commonly observed during ESI-MS of uranyl(VI) solutions containing methanol.[33]

When the concentration of DHIP was increased first to 0.2 and then to 0.3 mM, the relative intensity of the peak assigned to $[UO_2+(DHIP-H)+DHIP]^+$ (*m/z* 555) increased significantly (Figures 4.2c and d). When the concentration of DHIP was increased to 0.5

mM, the peak assigned to $[UO_2+(DHIP-H)+DHIP]^+$ (*m/z* 555) became the dominant peak in the mass spectrum (Figure 4.2e). This may indicate that the 1:2 uranyl:DHIP species is predominant in solution when DHIP is in excess at pH 5.5. Previous studies have suggested that amidoxime ligands can coordinate to uranium in a 1:2 uranyl(VI):ligand ratio.[24, 25] When DHIP is in excess relative to uranyl(VI), an ion appears at *m/z* 966 (Figures 4.2c-e). This ion can be assigned to $[2(UO_2)+3(DHIP-H)]^+$. The presence of a 2:3 uranyl(VI):DHIP complex in our spectra is interesting, as to our knowledge, previous studies on the uranyl(VI)-amidoxime system have not described this complex.[13, 24, 25]

As a general observation, the abundances of UO_2^+ (*m/z* 270) and the uranyl(VI)-hydroxide and -methoxide species decreased as the uranyl(VI):DHIP mole ratio was changed from 1:1 to 1:5, suggesting that a higher proportion of uranyl(VI) in the solution phase is held in the form of DHIP complexes when the ligand is present in excess.

As noted by Steppert et al.,[34] some ions detected in ESI mass spectra may actually be artifacts that arise during the electrospray process. In order to determine whether the 2:3 uranyl(VI):DHIP species was due to a solution complex or was simply an artifact, we examined the effect of solution pH on uranyl(VI)-DHIP complex formation when DHIP was in excess. It is common in solutions containing uranyl(VI) and some chelating ligands for uranyl(VI)-ligand oligomers to form as solution pH increases.[35] Thus, if the 2:3 species is indeed a solution species, its relative abundance in the mass spectrum should change as the solution pH changes, whereas the relative abundance of a peak due to an artifact of the ESI process would be expected to remain constant. Figures 4.3a-e show mass spectra acquired from solutions containing 0.1 mM uranyl(VI) and 0.5 mM DHIP at pH values ranging from

3.2 to 9.2. At pH 2.5, an intense peak assigned to $[DHIP+H]^+$ (*m/z* 144) was observed (spectrum not shown). As the pH was increased to 3.2, low abundance ions at *m/z* 430 and *m/z* 444 also appeared, although $[DHIP+H]^+$ (*m/z* 144) remained the most abundant species (Figure 4.3a). Peaks at *m/z* 430 and *m/z* 444 were previously assigned to $[UO_2+(DHIP-H)+H_2O]^+$ and $[UO_2+(DHIP-H)+CH_3OH]^+$, respectively. When the pH was increased to 4.2, these ions increased in abundance, and the 1:2 uranyl(VI):DHIP complex $[UO_2+(DHIP-H)+DHIP]^+$ (*m/z* 555) appeared (Figure 4.3b). A small peak at *m/z* 540 can be assigned to the methanol adduct $[UO_2+(DHIP-H)+4(CH_3OH)]^+$. When the pH was further increased to pH 5.9, $[UO_2+(DHIP-H)+DHIP]^+$ (*m/z* 555) increased in abundance, while the abundance of $[DHIP+H]^+$ decreased fairly significantly (Figure 4.3c). In addition, the 2:3 uranyl(VI):DHIP species $[2(UO_2)+3(DHIP-H)]^+$ was observed at *m/z* 966.

When the solution pH was increased to 7.9, the relative abundance of $[DHIP+H]^+$ (*m/z* 144) increased dramatically, although peaks assigned to the major uranium-containing ions were still observed (Figure 4.3d). Sodium and potassium adducts of the 1:2 complex were also seen at *m/z* 577 and *m/z* 593, respectively. Ions derived from the 2:3 uranyl(VI):DHIP complex ($[2(UO_2)+3(DHIP-H)]^+$ (*m/z* 966), $[2(UO_2)+Na+2(DHIP-H)+(DHIP-2H)]^+$ (*m/z* 988), and $[2(UO_2)+K+2(DHIP-H)+(DHIP-2H)]^+$ (*m/z* 1004)) increased in abundance. The fact that the relative abundances of ions assigned to the 2:3 uranyl:DHIP complex are pH dependent, appearing above pH ~4, indicates that these ions are unlikely to be artifacts. Thus, a previously undescribed 2:3 uranyl(VI):DHIP species forms in solution at higher pH values. An ion of *m/z* 397 also appears in the mass spectrum at this pH and was assigned to $[UO_2+CH_3O+3(CH_3OH)]^+$.

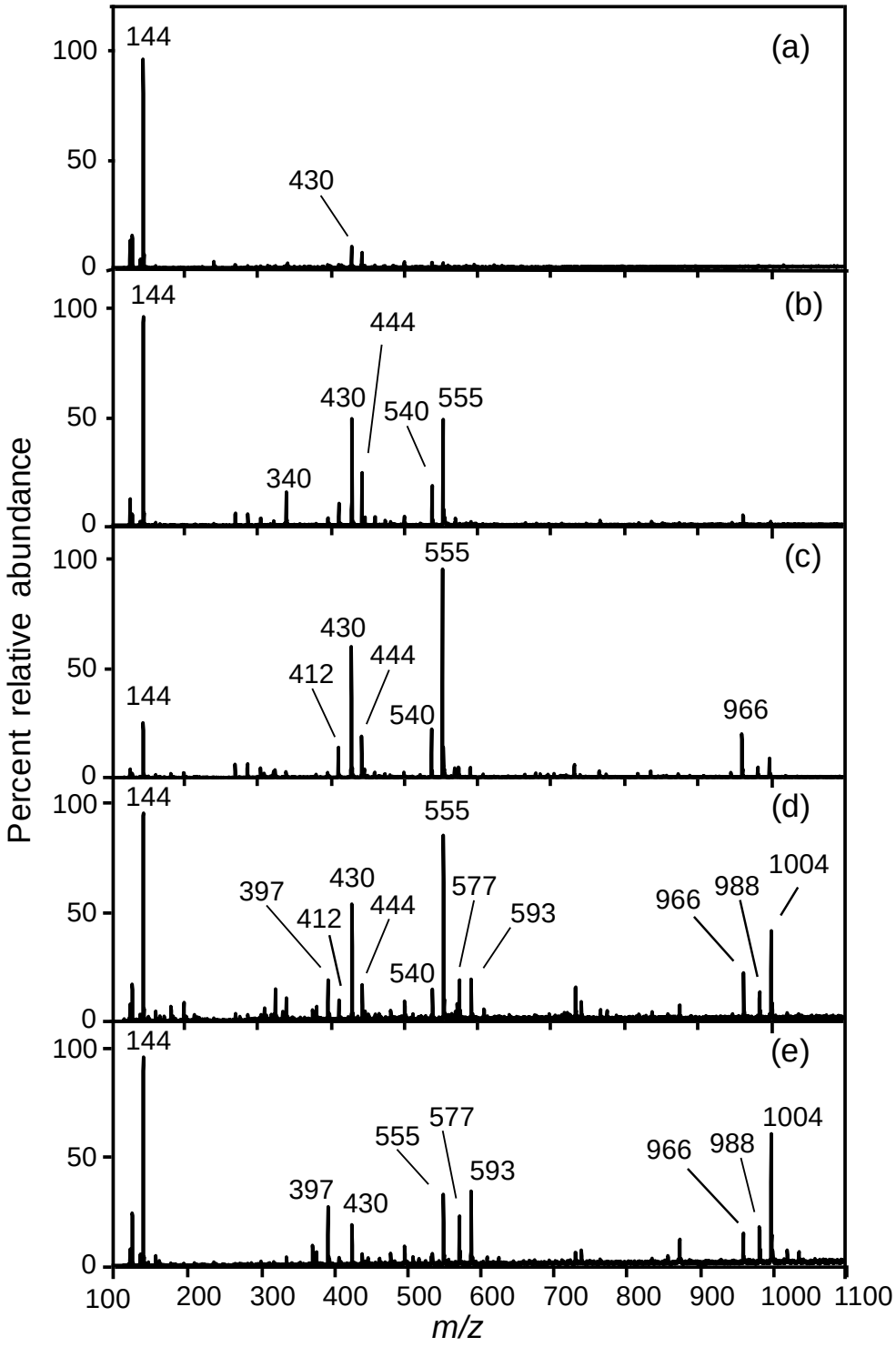

Figure 4.3 Positive-ion ESI mass spectra of solutions containing 0.1 mM uranyl(VI) and 0.5 mM DHIP in 20% CH_3OH/80% H_2O (v/v) at pH a) 3.2, b) 4.2, c) 5.9, d) 7.9, and e) 9.2.

The increase in the abundance of ions arising from uncomplexed DHIP is interesting and may indicate that OH^- is competing with the DHIP for uranyl(VI). This would lead to the formation of uranyl(VI) hydroxide complexes and insoluble uranyl oxyhydroxides, leaving behind the ligand in solution. Uranyl(VI) hydroxide complexes, such as those described by Steppert et al.,[34] were not detected. At a solution pH of 9.2, ions related to the 1:2 uranyl(VI):DHIP complex decrease in abundance relative to those related to the 2:3 complex (Figure 4.3e), suggesting an equilibrium between the 1:2 species and the 2:3 species, with the formation of the more oligomerized species favored at higher pH.

4.3.2 DHPD complexation with uranyl(VI)

Uranyl(VI) complexation with DHPD, an open ring form of DHIP (Figure 4.1), was also studied. In order to make comparisons with the DHIP system easier, mass spectra of solutions containing uranyl(VI) and DHPD in various uranyl(VI):ligand mole ratios were acquired at pH 5.5 (Figure 4.4a-e). The mass spectrum of a solution containing only 0.1 mM DHPD shows an intense peak due to protonated DHPD ($[DHPD+H]^+$, *m/z* 161) as well as other major peaks which were identified as $[DHPD+Na]^+$ (*m/z* 183), $[2(DHPD)+Na]^+$ (*m/z* 343), and $[2(DHPD)+(DHPD+H)+CH_3OH+2(H_2O)]^+$ (*m/z* 549). The peak at *m/z* 128 is thought to be a fragmentation product of DHPD (Figure 4.4a). $[DHPD+H]^+$ gives rise to the base peak in all spectra acquired from solutions containing uranyl(VI) and DHPD (Figure 4.4b-e). Various low abundance uranium-containing species are evident in the mass spectrum shown in Figure 4.4b, which was acquired from a solution containing a 1:1 mole ratio of uranyl(VI):DHPD. These species include UO_2^+ (*m/z* 270) and uranyl(VI)-hydroxide and -methoxy species, which appear between *m/z* 287 and 414 (Figure 4.4b, Table 4.1). The

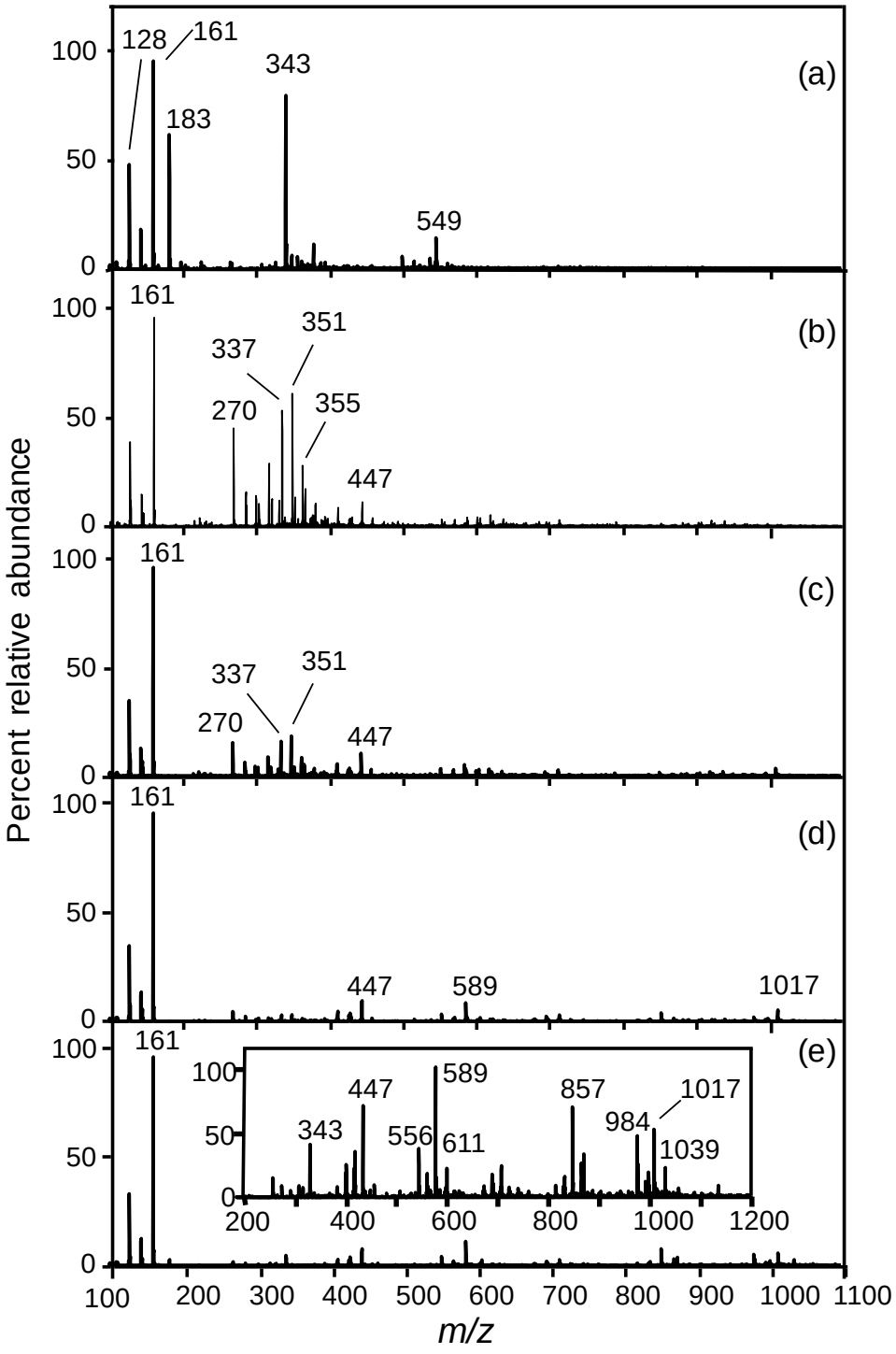

Figure 4.4 Positive-ion ESI mass spectra of solutions containing a) 0.1 mM DHPD, b) 0.1 mM uranyl(VI) and 0.1 mM DHPD, c) 0.1 mM uranyl(VI) and 0.2 mM DHPD, d) 0.1 mM uranyl(VI) and 0.3 mM DHPD, e) 0.1 mM uranyl(VI) and 0.5 mM DHPD (the inset shows uranyl(VI):DHPD ions for *m/z* >200). All samples in 20% CH_3OH / 80% H_2O (v/v) at pH 5.5.

small peak at *m/z* 447 is assigned to a water adduct of the 1:1 uranyl(VI):DHPD complex, $[UO_2+(DHPD-H)+H_2O]^+$. Peaks assigned to uranyl(VI)-containing ions decreased in intensity relative to the base peak at *m/z* 161 as the ligand concentration in solution increased (Figures 4.4b-e).

Uranyl(VI)-DHPD ions were detected only in very low abundance, even at the higher ligand concentrations, possibly indicating that DHPD does not compete with hydroxide as effectively as DHIP in this pH range.[25] Nevertheless, an expanded view of the region between *m/z* 200 and *m/z* 1200 in Figure 4.4e (a uranyl(VI):DHPD mole ratio of 1:5) shows the presence of several uranyl(VI)-containing ions (Figure 4.4e, inset). Peaks at *m/z* 447, 589 and 611 were assigned to $[UO_2+(DHPD-H)+H_2O]^+$, $[UO_2+(DHPD-H)+DHPD]^+$, and $[UO_2+Na+2(DHPD-H)]^+$, respectively, while *m/z* 857 was assigned to a 2:2 complex, $[2(UO_2)+(DHPD-2H)+(DHPD-H)]^+$. 1:1 and 1:2 uranyl(VI):DHPD complexes have been described by Tian et al.[25] A peak at *m/z* 343 was earlier assigned to $[2(DHPD)+Na]^+$ (Figure 4.4e, Table 4.1). Peaks arising from a 2:3 uranyl(VI):DHPD species $[2(UO_2)+3(DHPD-H)]^+$ (*m/z* 1017) and its sodium adduct (*m/z* 1039) were also observed. Peaks at *m/z* 556 and 984 remained unassigned.

The pH of a solution containing a 1:5 mole ratio of uranyl(VI):DHPD was varied to determine if pH has an effect on complex formation (spectra not shown). The results are consistent with the fact that DHPD is a less effective complexing agent than DHIP. At low pH (~2.5), no uranyl(VI)-DHPD complexes were observed, but as the pH was increased to 3.2, and then to pH 5.5, the intensities of the peaks assigned to the ion $[UO_2+(DHPD-H)+H_2O]^+$ (*m/z* 447) increased. The intensity of $[UO_2+(DHPD-H)+DHPD]^+$

(*m/z* 589) did not systematically increase over the same pH range, perhaps an indication that it is formed from $[UO_2+(DHPD-H)]^+$ by adduction of DHPD, and is not a true solution-phase species. The ion $[2(UO_2)+(DHPD-2H)+(DHPD-H)]^+$ (*m/z* 857) consistently appears in spectra acquired from pH 5 solutions of uranyl(VI) and DHPD; additional investigation will be necessary to determine whether or not this ion results from a solution-phase species. At pH values greater than ~7, no peaks arising from uranyl(VI)-DHPD species were observed in the mass spectrum, again possibly due to competition from OH^- for uranyl(VI) and the formation of insoluble uranyl(VI) species. The peaks seen in the mass spectrum could be assigned to DHPD-salt adducts.

4.3.3 DHED complexation with uranyl(VI)

It has been suggested that uranyl(VI) is coordinated by both oxime groups in both the 1:1 and the 1:2 uranyl(VI):DHPD complexes.[25] In DHPD, the two oxime groups are separated by four C−C bonds. Thus, the resulting structure of the uranyl(VI)-ligand complex can be either cyclic (for the 1:1 complex), or bicyclic (for the 1:2 complex). We selected DHED (Figure 4.1), the third ligand under investigation, to examine the effect of alkyl chain length on uranyl(VI) coordination. In DHED, the two oxime groups are separated by only one C−C bond.

The mass spectrum acquired from a pH 5.5 solution containing 0.5 mM DHED shows an intense peak that is assigned to protonated DHED ($[DHED+H]^+$, *m/z* 119) (Figure 4.5a). Peaks assigned to a DHED dimer, $[2(Na)+(DHED-H)+DHED+2(H_2O)+2(CH_3OH)]^+$ (*m/z* 381), and to a trimer, $[Na+3(DHED)+2(CH_3OH)+2(H_2O)]^+$ (*m/z* 477), are also observed.

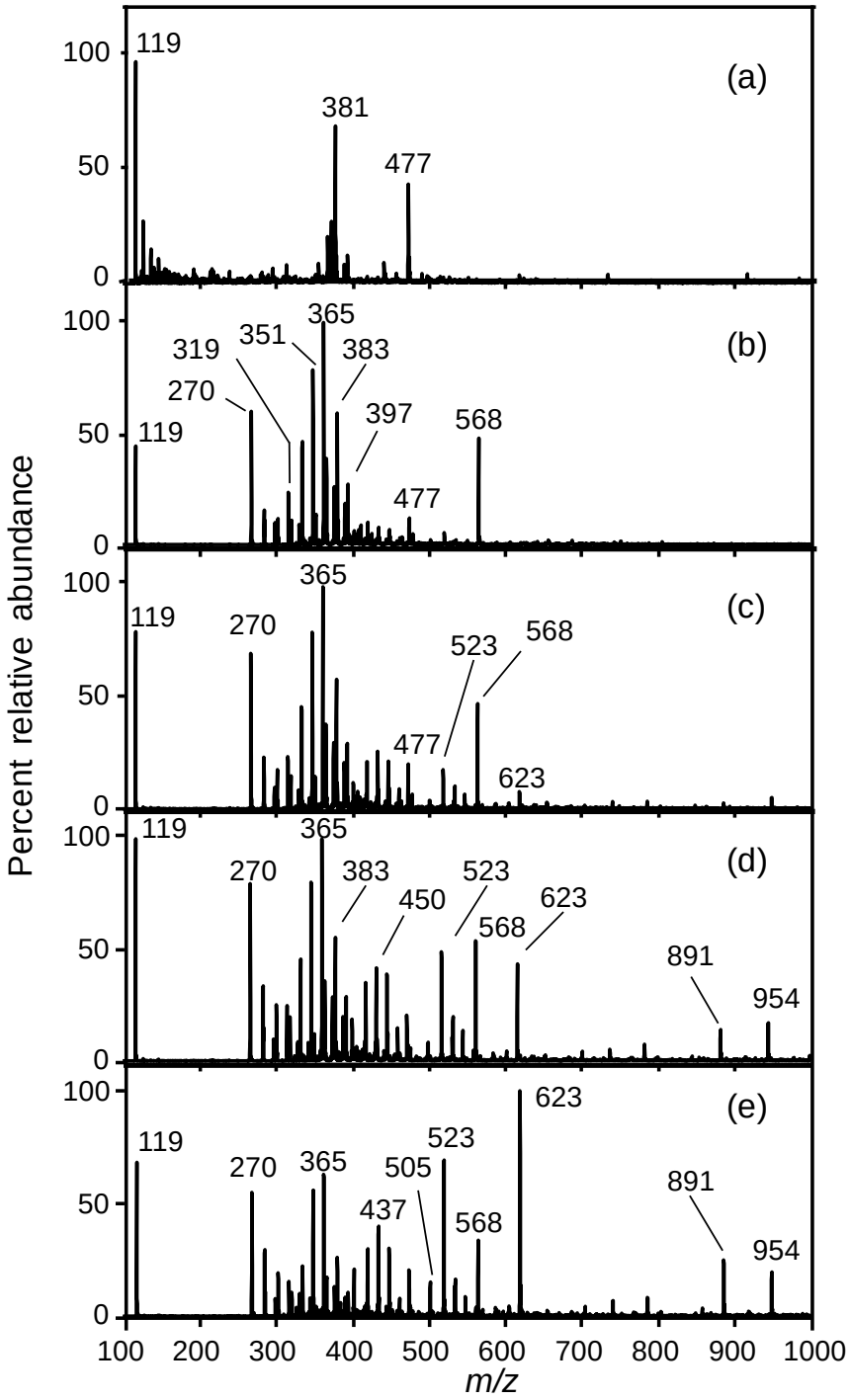

Figure 4.5 Positive-ion ESI mass spectra of solutions containing a) 0.1 mM DHED, b) 0.1 mM uranyl(VI) and 0.1 mM DHED, c) 0.1 mM uranyl(VI) and 0.2 mM DHED, d) 0.1 mM uranyl(VI) and 0.3 mM DHED, and e) 0.1 mM uranyl(VI) and 0.5 mM DHED. All samples in 20% CH_3OH / 80% H_2O (v/v) at pH 5.5.

A spectrum was also acquired from a pH 5.5 solution containing 0.1 mM uranyl(VI) and 0.1 mM DHED. Peaks assigned to UO_2^+ (*m/z* 270) and to the previously described uranyl(VI) hydroxide and methoxide complexes (Figure 4.5b, Table 4.1) were quite prominent in this spectrum. Ions having a general composition of $[UO_2+(DHED-H)+2A]^+$, where A = H_2O or CH_3OH, were observed at *m/z* 423, 437, and 451. A nitrate-containing ion $[UO_2+(DHED)+(NO_3)+H_2O]^+$ was observed at *m/z* 468. A peak assigned to $[UO_2+2(DHED)+NO_3]^+$ was also observed at *m/z* 568 (Figure 4.5b, Table 4.1). When the ligand concentration increased to 0.2 mM, a new peak at *m/z* 623, assigned to $[UO_2+(DHED-H)+2(DHED)]^+$, was observed in the mass spectrum (Figures 4.5c, Table 4.1). As the concentration of DHED in the electrosprayed solutions increased still further, $[UO_2+(DHED-H)+2(DHED)]^+$ increased in abundance and peaks at *m/z* 891 and 954 appeared (Figures 4.5d and e). These latter peaks were assigned to $[2(UO_2)+3(DHED-H)]^+$ and $[2(UO_2)+2(DHED-H)+DHED+NO_3]^+$, respectively. Assignments for other major ions are shown in Table 4.1.

When the pH of a solution containing a 1:5 mole ratio of uranyl(VI):DHED was varied from pH 3.0 to pH 7.0, peaks at *m/z* 568, 623, 891, and 954, assigned to the uranyl(VI):DHED species described above, increased in intensity (spectra not shown). Uranyl(VI)-DHED complexes were not observed at pH >7, again possibly due to the formation of hydrolyzed uranyl(VI) species.

4.3.4 Comparison of ligand-uranyl(VI) binding affinities

In order to compare uranyl(VI)-DHIP, -DHPD, and -DHED binding, total ion abundances for ions resulting from 1) free ligand, 2) uranyl(VI) not complexed by an

amidoxime ligand, and 3) urany(VI)-amidoxime complexes were compared for mass spectra acquired from pH 5.5 solutions containing 1:3 mole ratios of uranyl(VI):DHIP, uranyl(VI):DHPD, and uranyl(VI):DHED. The spectra are shown in Figures 4.2d, 4.4d, and 4.5d, respectively. Ion abundances were calculated by summing ion intensities for related ions (e.g. those related to free ligand, uranyl(VI) not complexed by an amidoxime ligand, and uranyl(VI)-amidoxime species). The resulting ion intensities for a particular spectrum were normalized to the total ion intensity in that spectrum. Three replicates were acquired for each system studied. The results are shown in Figure 4.6.

It can be observed from Figure 4.6 that the percentage of ions in the form of a uranyl(VI)-amidoxime complex at pH 5.5 is greatest in the uranyl(VI)/DHIP system and least in the uranyl(VI)/DHPD system. In fact, ~80% of the ions in the uranyl(VI)/DHIP system result from uranyl(VI)-DHIP complexes, whereas ~5% of the ions in the uranyl(VI)/DHPD system result from uranyl(VI)-DHPD complexes. In the uranyl(VI)/DHED system, ~40% of the ions result from uranyl(VI)-DHED complexes. This difference is very likely due to differences in stability constants for the various uranyl(VI)-amidoxime species formed at this pH. Tian et al.[24, 25] determined stability constants for 1:1 and 1:2 uranyl(VI)-DHIP and -DHPD complexes, but neither a literature review nor a search of the NIST Standard Reference Database turned up stability constants for the uranyl(VI)/DHED system. However, from the results of our analysis, we can conclude that the effectiveness of the ligand in complexing with uranyl(VI) at pH 5.5 is as follows: DHIP > DHED > DHPD.

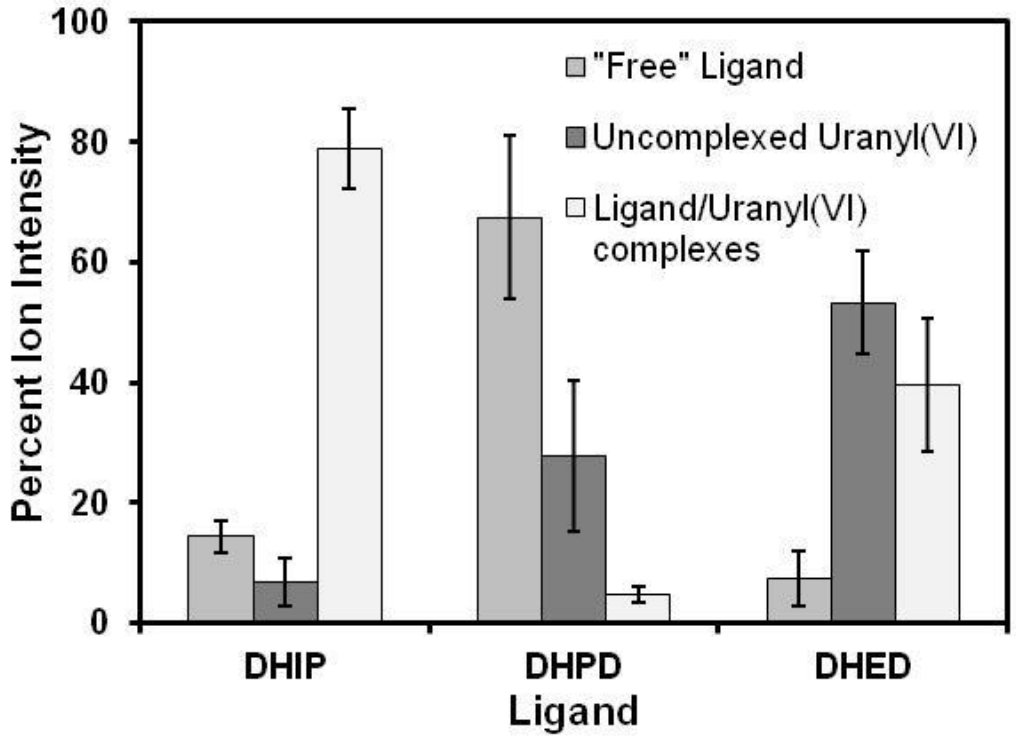

Figure 4.6 Comparison of total ion abundances of ions resulting from 1) free ligand, 2) uranyl(VI) not complexed to any amidoxime ligand, and 3) urany(VI)-amidoxime complexes in spectra acquired from solutions 0.1 mM in uranyl(VI) and 0.3 mM in ligand at pH 5.5.

Our results confirm that, of the three ligands used in this study, DHIP is probably more effective in binding uranyl(VI) than either of the other two ligands because it can form tridentate complexes with uranyl(VI), with binding through the two oxime oxygens and the imide nitrogen atom.[24] DHPD, in which the two amidoxime groups are separated by four C–C bonds, is the least effective ligand for uranyl(VI). This may be due to the nature of its coordination to uranyl(VI), with binding either through the oxime oxygens only,[36] or through η^2 coordination to the N-O bond.[13] DHPD and DHED differ only in chain length

(Figures 4.1b and c), yet DHED forms more stable complexes at pH 5.5. The reason for the difference in uranyl(VI) binding ability between these two ligands remains to be elucidated.

4.4 Conclusions

The effect of changes in uranyl(VI):ligand mole ratio and solution pH on the speciation of uranyl(VI) in solutions containing the amidoxime ligands DHIP, DHPD, and DHED was investigated using ESI-MS. DHIP and DHPD are thought to be the main complexing agents in poly(acrylamidoxime) resins developed to sorb uranyl(VI) from seawater. DHED, which differs from DHPD only in having vicinal amidoxime groups, was chosen to examine whether the distance between amidoxime groups has an effect on the formation of uranyl(VI)-amidoxime complexes. DHIP was found to bind uranyl(VI) more effectively than DHPD or DHED, forming uranyl(VI):DHIP complexes with stoichiometries of 1:1, 1:2, 2:2 and 2:3. The 2:2 and 2:3 complexes became more important at pH > 6. Ions related to the 1:1, 1:2, 2:2, and 2:3 uranyl(VI):DHPD complexes were also detected, but were present in very low abundance, suggesting that DHPD binds uranyl(VI) less effectively than does DHIP. DHED, with its vicinal amidoxime groups, proved to be a more effective binding agent than DHPD, in which the amidoxime groups are separated by a three-carbon alkyl chain. Mass spectra acquired from solutions containing uranyl(VI) and DHED showed the presence of ions having uranyl(VI):DHED stoichiometries of 1:1, 1:2, 1:3, and 2:3.

Acknowledgements

This work was supported by the U. S. Department of Energy Office of Nuclear Energy's Nuclear Energy University Programs, Subcontract # 00042246. SPP and AMM

thank Dr. Linfeng Rao of Lawrence Berkeley National Laboratory for providing the 2,6-dihydroxyiminopiperidine and the N^1,N^5-dihydroxypentanediimidamide.

References

1. Schenk, H. J.; Astheimer, L.; Witte, E. G.; Schwochau. K. Development of sorbers for the recovery of uranium from seawater. 1. Assessment of key parameters and screening studies of sorber materials. *Sep. Sci. Technol.* **1982**, *17*, 1293.
2. Bodansky, D., *Nuclear energy: Principles, practices, and prospects*, 2nd ed., Springer-Verlag, New York, **2003**.
3. Davies, R. V.; Kennedy, J.; McIlroy, R. W.; Spence, R.; Hill, K. M. Extraction of uranium from seawater. *Nature* **1964**, *203*, 1110.
4. Rao. L., Lawrence Berkeley National Laboratory Paper LBNL-4034E, Berkeley, **2011**.
5. Kim, J.; Tsouris, C.; Mayes, R. T.; Oyola, Y.; Saito, T.; Janke, C. J.; Dai, C. J.; Schneider, E.; Sachde, D. Recovery of uranium from seawater: A review of current status and future research needs. *Sep. Sci. Technol.* **2013**, *48*, 367.
6. Tian, G.; Geng, J.; Jin, Y.; Wang, C.; Li, S.; Chen, Z.; Wang, H. Sorption of uranium(VI) using oxime-grafted ordered mesoporous carbon CMK-5. *J. Hazard. Mater.* **2011**, *190*, 442.
7. Das, S.; Pandey, A. K.; Athawale, A. A.; Manchanda, V. K. Exchanges of uranium(VI) species in amidoxime-functionalized sorbents. *J. Phys. Chem.* **2009**, *113*, 6328.
8. Saito, K.; Hori, T.; Furusaki, S.; Sugu, T.; Okamoto, J. Porous amidoxime-group-containing membrane for the recovery of uranium from seawater. *Ind. Eng. Chem. Res.* **1987**, *26*, 1977.
9. Omichi, H.; Katakai, A.; Sugo, T.; Okamoto, J. A new type of amidoxime-group-containing adsorbent for the recovery of uranium from seawater. *J. Sep. Sci. Technol.* **1985**, *20*, 163.
10. Egawa, H.; Harada, H. Recovery of uranium from sea water by using chelating resins containing amidoxime groups. *Nippon Kagaku Kaishi* **1979**, 958.
11. Astheimer, L.; Schenk, H. J.; Witte, E. G.; Schwochau, K. Development of sorbers for the recovery of uranium from seawater. 2. The accumulation of uranium from

seawater by resins containing amidoxime and imidoxime functional groups. *J. Sep. Sci. Technol.* **1983**, *18*, 307.

12. Egawa, H.; Harada, H.; Shuto, T. Studies on selective adsorption resins. 13. Recovery of uranium from sea water by the use of chelating resins containing amidoxime groups. *Nippon Kagaku Kaishi* **1980**, 1773.
13. Vukovic, S.; Watson, L. A.; Kang, S. O.; Custelcean, R.; Hay, B. P. How amidoximate binds the uranyl cation. *Inorg. Chem.* **2012**, *51*, 3855.
14. Zekri, O.; Boutamine, S.; Slaouti, H.; Hank, Z.; Meklati, M.; Vittori, O. Synthesis and characterization of complexes of uranium(VI) with acetone oxime and α-benzoin oxime. *Synth. React. Inorg. Met.* **2002**, *32*, 1471.
15. Beirakhov, A. G.; Orlova, I. M.; Mikhailov, Y. N.; Shchelokov, R. N. Structure of α-dioximes and their coordination modes in uranyl complexes. *Dokl. Chem.* **2001**, *381*, 305.
16. Bandyopadhayay, D. Salicylamidoxime as an analytical reagent. III. Spectrophotometric determination of uranium. *J. Ind. Chem. Soc.* **1956**, *33*, 269.
17. Busev, A. I.; Zholondkovskaya, T. N.; Krysina, L. S.; Korobkina, L. I. The reaction between benzamidoxime and uranyl ions. *Moscow Univ. Chem. Bull.* **1967**, *22*, 108.
18. Tripathi, K. K.; Banerjea, D. Nicotinamidoxime as an analytical reagent. I. Spectrophotometric determination of uranium. *Fresen. Z. Anal. Chem.* **1959**, *168*, 326.
19. Jara, R.; Estela, J. M.; Cerda, V. Analytical properties of the amidoxime group: Spectrophotometric and thermometric behavior of ethanediamidoxime and its Cu(II) and U(VI) complexes. *Thermochim. Acta* **1991**, *177*, 229.
20. Manoussakis, G.; Kouimtzis, T. Study on complexes of Fe^{3+}, Cu^{2+} and UO_2^{2+} with benzanilidoxime. *J. Inorg. Nucl. Chem.* **1969**, *31*, 3851.
21. Hirotsu, T.; Katoh, S.; Sugasaka, K.; Seno, M.; Itagaki, T. Binding ability of acetamide oxime with proton, copper(II), and dioxouranium(VI) in aqueous solutions. *J. Chem. Soc. Dalton Trans.* **1986**, 1609.
22. Park, Y. Y.; Kim, S. Y.; Kim, J. S.; Harada, M.; Tomiyasu, H.; Nogami, M.; Ikeda, Y. Complex formation of U(VI) with benzamidoxime in non-aqueous solvents. *J. Nucl. Sci. Technol.* **2000**, *37*, 344.

23. Kim, S. Y.; Harada, M.; Tomiyasu, H.; Ikeda, Y.; Park, Y. Y. Structure and kinetic studies of U(VI)-benzamidoxime complex in non-aqueous solutions by ^{1}H- and ^{13}C-NMR. *Prog. Nucl. Energy* **2000**, *37*, 399.

24. Tian, G.; Teat, S. J.; Zhang, Z.; Rao, L. Sequestering uranium from seawater: Binding strength and modes of uranyl complexes with glutarimidedioxime. *Dalton Trans.* **2012**, *41*, 11579.

25. Tian, G.; Teat, S. J.; Rao, L. Thermodynamic studies of U(VI) complexation with glutardiamidoxime for sequestration of uranium from seawater. *Dalton Trans* **2013**, *42*, 5690.

26. Kobuke, Y.; Tanaka, H.; Ogoshi, H. Imidedoxime as a significant component in so-called amidoxime resin for uranyl adsorption from seawater. *Polym. J.* **1990**, *22*, 179.

27. Di Marco, V. B.; Bombi, G. G. Electrospray mass spectrometry (ESI-MS) in the study of metal-ligand solution equilibria. *Mass Spectrom. Rev.* **2006**, *25*, 347.

28. Keith-Roach, M. J. A review of recent trends in electrospray ionisation-mass spectrometry for the analysis of metal-organic ligand complexes. *Anal. Chim. Acta* **2010**, *678*, 140.

29. May, C. C.; Worsfold, P. J.; Keith-Roach, M. J. Analytical techniques for speciation analysis of aqueous long-lived radionuclides in environmental matrices. *Trac-Trend. Anal. Chem.* **2008**, *27*, 160.

30. Carlton, D. D.; Schug, K. A. A review on the interrogation of peptide-metal interactions using electrospray ionization-mass spectrometry. *Anal. Chim. Acta* **2011**, *686*, 19.

31. Lavanant, H.; Virelizier, H.; Hoppilliard, Y. Reduction of copper(II) complexes by electron capture in an electrospray ionization source. *J. Am. Soc. Mass. Spectrom.* **1998**, *9*, 1217.

32. Colton, R.; D'Agostino, A.; Traeger, J. C. Electrospray mass spectrometry applied inorganic and organometallic chemistry. *Mass Spectrom. Rev.* **1995**, *14*, 79.

33. Van Stipdonk, M. J.; Chien, W.; Bulleigh, K.; Wu, Q.; Groenewold, G. Gas-phase uranyl-nitrile complex ions. *J. Phys. Chem. A* **2006**, *110*, 959.

34. Steppert, M.; Walther, C.; Fuss, M.; Buchner, S. On the polymerization of hexavalent uranium. An electrospray mass spectrometry study. *Rapid Comm. Mass Spectrom.* **2012**, *26*, 583.

35. Pasilis, S. P.; Pemberton, J. E. Speciation and coordination chemistry of uranyl(VI)-citrate complexes in aqueous solution. *Inorg. Chem.* **2003**, *42*, 6793.

36. Witte, E. G.; Schwochau, K. S.; Henkel, G.; Krebs, B. Uranyl complexes of acetamidoxime and benzamidoxime. Preparation, characterization, and crystal structure. *Inorg. Chim. Acta* **1984**, *94*, 323.

Chapter 5

Gas-Phase Complexes formed between Amidoxime Ligands and Vanadium or Iron Investigated using Electrospray Ionization Mass Spectrometry[‡]

Abstract

Gas-phase complexes of the amidoxime ligands 2,6-dihydroxyiminopiperidine (DHIP) and N^1, N^5-dihydroxypentanediimidamide (DHPD) with iron(III) and vanadium(V) have been characterized using electrospray ionization mass spectrometry (ESI-MS). ESI-MS was also used to examine how the presence of vanadium(V) and iron(III) affects gas-phase complexes formed between uranyl(VI) and each of the two ligands. The effect on the mass spectra of changes in metal, ligand, metal:ligand mole ratio, and pH was examined. My results show that a 1:1 vanadium(V):DHIP complex, $[VO_2+DHIP]^+$, forms when the vanadium(V):DHIP mole ratio in solution is 1:1, while a 1:2 complex, $[VO_2+2(DHIP)-H_2O]^+$, is formed when the DHIP concentration is higher than the concentration of vanadium(V). DHPD, unlike DHIP, forms only a 1:2 complex, $[VO_2+2(DHPD)-H_2O]^+$, at all vanadium(V):DHPD mole ratios investigated. Changes in solution pH have no effect on the gas phase complexes formed in the vanadium/DHIP or the vanadium/DHPD system. Iron(III) forms only a 1:2 complex with DHIP, $[Fe+2(DHIP-H)]^+$,

---

[‡]Chapter to be submitted for publication in *Rapid Commun. Mass Spectrom.*

irrespective of pH or ligand concentration, while it forms both 1:2 and 1:3 complexes with DHPD ($[Fe+2(DHPD-H)+2(CH_3OH)]^+$ and $[Fe+3(DHPD)-2H]^+$). Gas-phase uranyl(VI)-DHIP complexes are less likely to form when either iron(III) or vanadium(V) is present in solution at pH 8.3, as vanadium and iron gas-phase complexes preferentially form. Results from a competitive interaction study reveal that the metals form gas-phase complexes with DHIP in the following order of preference: iron(III) > vanadium(V) > uranyl(VI).

5.1 Introduction

The extraction of uranium from seawater has attracted a great deal of interest since the 1940's because of the importance of the metal for nuclear power generation.[1, 2] Uranium is the main component in nuclear fuel rods used in most nuclear reactors, and there is fear that the 63 million metric tons currently present in terrestrial deposits worldwide may not last beyond this century. Recycling of the nuclear fuel rods is not economical and cannot meet the high demand for uranium in the nuclear energy sector. This has led to a search for an alternative source of the metal. The amount of uranium present in the earth's oceans is estimated to be ~4.5 billion metric tons. However, uranium is present in seawater only at very low concentrations (~3ppb). This uranium exists mainly in the form of uranyl(VI) carbonate complexes, the most important of which is $[(UO_2)(CO_3)_3]^{4-}$.[3] Various methods for the extraction of uranium from seawater have been investigated over the years, but sorption methods using amidoxime-functionalized sorbents have been shown to be the most effective.[4, 5] As discussed in Chapter 4, the amidoxime functional groups ($-C(NH_2)NOH$) are stable at seawater pH (pH 8.3, on average), have a high affinity for uranyl(VI), and can

effectively displace carbonate from the stable $[(UO_2)(CO_3)_3]^{4-}$complex to form uranyl(VI)-amidoxime complexes.

The sorbent is usually prepared by copolymerization of polyacrylonitrile on to a polyethylene polymer via a radiation-induced grafting process. The nitrile groups of the polyacrylonitrile are then converted to amidoxime derivatives by reacting them with hydroxylamines, followed by treatment with potassium hydroxide. The sorbents, which can be in the form of braided fibers or bundles, are lowered into the ocean and held in place using an anchor.[6] The efficiency of the amidoxime-functionalized sorbent in extracting uranyl(VI) from seawater was first demonstrated in the 1990's by a group of scientists in Japan, where ~1.5 g of uranium per 1 kg of sorbent was collected after 30 days in seawater.[7] A similar amidoxime-based polymeric sorbent fiber, which was developed at Oak Ridge National Laboratory (ORNL) and tested at Pacific Northwest National Laboratory (PNNL) in the United States in 2014, showed a small improvement in the uranyl(VI) uptake, as ~3.3 g of uranium per 1 kg of sorbent was adsorbed by the sorbent when immersed in seawater for 8 weeks.[8]

The main challenge of this uranyl(VI) extraction methodology is the economic feasibility of the process on a large scale. Uranyl(VI) extraction using amidoxime-based sorbents will cost ~$600 – $1000 per 1 kg of uranium recovered when implemented on a large scale. This is more than the current cost for uranium extraction from terrestrial sources, ~$260 per 1 kg of uranium.[8-10] To reduce this cost and make uranyl(VI) extraction using amidoxime-functionalized sorbents economically competitive, scientists in both Japan and the United States are looking at both fundamental and practical ways of improving the

selectivity, sorption efficiency and reusability of the sorbents. The selectivity and sorption efficiency can be improved by first understanding the interactions of the amidoxime functional groups with uranyl(VI) and other metal ions in seawater. Table 5.1 shows the concentration of metal ions present in seawater that can bind to the uranyl(VI) binding sites on the amidoxime-functionalized sorbents. The binding of these metal ions to the sorbent reduces the number of sorption sites available for uranyl(VI) binding, leading to low uranyl(VI) uptake and contributing to the high overall cost of uranium collection.

Table 5.1 List of common metal ions and their concentrations in seawater. Table reproduced from Reference 11.

Element	Concentration (ppb)
Uranium	3.3
Vanadium	1.6
Iron	3.4
Potassium	3.92×10^5
Magnesium	1.29×10^6
Calcium	4.11×10^5
Copper	0.9
Nickel	6.6
Lead	0.03
Sodium	1.08×10^7

In order to fully understand the mechanism by which uranyl(VI) is adsorbed by amidoxime-functionalized sorbents, the interactions between uranyl(VI) and various ligands having amidoxime functional groups have been investigated.[4, 5, 12-17] In one study using density functional theory calculations, Vukovic et al.[16] showed that amidoxime compounds interact with uranyl(VI) through three different modes. These include 1) monodentate binding to the oxygen atom of the oxime group, 2) bidentate binding to both the oxime oxygen atom and amide nitrogen atom, and 3) η^2 binding to the N-O bond (Figure 5.1). The

η^2 binding mode was later shown to be the most stable and preferential mode of uranyl(VI)-amidoxime binding.[16] The various binding modes are shown in Figure 5.1.

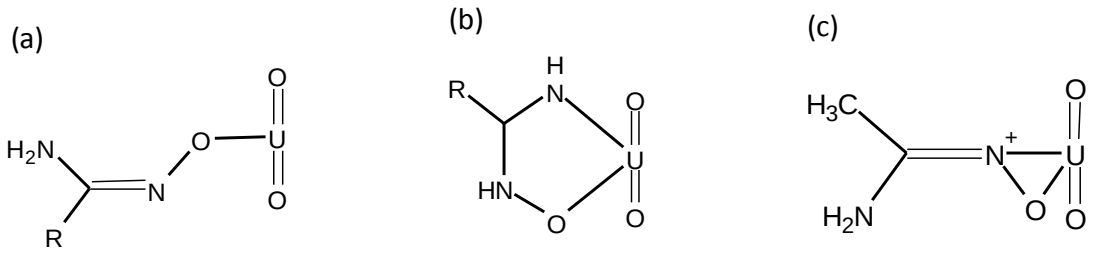

Figure 5.1 Different ways by which the amidoxime group can bind uranyl(VI). (a) Monodentate binding, (b) bidentate binding, and (c) η^2 binding. Figure adapted from Reference 16.

The main active complexing agents in the amidoxime-functionalized sorbents are thought to be cyclic 2,6-dihydroxyiminopiperidine (DHIP) and acyclic N^1,N^5-dihydroxypentanediimidamide (DHPD). The structures of these compounds are shown in Figure 4.1. Rao et al.[13, 14, 18] determined the formation constants for DHIP and DHPD complexes with uranyl(VI). These formation constants are given in Table 5.2. Examination of this table shows that the formation constants for the uranyl(VI)-DHIP complexes (UO_2A, $UO_2A_2^{2-}$, and $UO_2HA_2^-$, A = DHIP−2H) are slightly higher than those for the corresponding DHPD analogues (UO_2B, $UO_2B_2^{2-}$, and $UO_2HB_2^-$, B = DHPD−2H), suggesting that the cyclic isomer forms a slightly stronger solution complex with uranyl(VI) than the acyclic isomer. A recent study by our group (discussed in Chapter 4), in which we used ESI-MS to compare uranyl(VI) binding with DHIP and DHPD, showed that gas-phase uranyl(VI)-DHIP complexes form more readily than gas-phase uranyl(VI)-DHPD complexes.[19]

Table 5.2 Formation constants for DHIP and DHPD complexes with metal ions commonly found in seawater. n is the charge on the metal ion. Table produced using data from References 11, 13, 14, and 18.

DHIP (H_2A)	log K						
Reactions	UO_2^{2+}	Fe^{3+}	Cu^{2+}	Pb^{2+}	Ni^{2+}	Ca^{2+}	Mg^{2+}
$M^{n+} + A^{2-} = MA^{n-2}$	17.8	---	18.9	14.3	10.3	2.28	----
$M^{n+} + H^+ + A^{2-} = M(HA)^{n-1}$	22.7	25.7	22.7	21.8	----	14.5	14.4
$M^{n+} + 2A^{2-} = MA_2^{n-4}$	27.5	36.0	24.5	19.4	16.7	----	----
$M^{n+} + H^+ + 2A^{2-} = MHA_2^{n-3}$	36.8	43.9	35.8	30.0	27.1	17.3	18.5
$M^{n+} + 2H^+ + 2A^{2-} = M(HA)_2^{n-2}$	43.0	49.7	----	----	----	----	----
$M^{n+} + H_2O + 2A^{2-} = M(OH)A_2^{n-5} + H^+$	----	25.7	----	----	----	----	----

DHPD (H_2B)	log K
Reactions	UO_2^{2+}
$M^{n+} + B^{2-} = MB^{n-2}$	17.3
$M^{n+} + 2H^+ + B^{2-} = M(H_2B)^{n+}$	29.2
$M^{n+} + 2B^{2-} = MB_2^{n-4}$	26.1
$M^{n+} + H^+ + 2B^{2-} = MHB_2^{n-3}$	36.4
$M^{n+} + 4H^+ + 2B^{2-} = M(H_2B)_2^{n+}$	56.3

Rao et al.[11, 18] also investigated the binding interactions between DHIP and iron(III), copper(II), lead(II), and nickel(II), calcium(II), and magnesium(II) present in seawater. They determined the formation constants of complexes formed by some of these metal ions with DHIP. These formation constants are also given in Table 5.2. Rao et al. observed that iron(III) forms much stronger complexes with DHIP than do the other metal ions investigated. The binding strength of the metal ions toward DHIP was observed to follow the order: $Fe^{3+} > UO_2^{2+} \sim Cu^{2+} > Pb^{2+} > Ni^{2+} > Ca^{2+} > Mg^{2+}$.[11, 18] The position of vanadium(V) (VO_2^+) or vanadium (IV) (VO^{2+}) within this order is not yet known, because the formation constants of vanadium(V)-DHIP conplexes have not yet been reported. While the DHIP complexes with metal ions such as Ni^{2+}, Ca^{2+}, and Mg^{2+} have lower formation

constants than the uranyl(VI)-DHIP complexes, the high concentrations of these metals in seawater means they may readily compete with uranyl(VI) for binding sites on the sorbent. Formation constants for DHPD complexes with metal ions other than uranyl(VI) have not been reported. Formation constants for uranyl(VI)-DHPD complexes are given in Table 5.1. Rao et al.[11] concluded that the strong iron(III)-DHIP interaction will greatly affect the extraction of uranyl(VI) from seawater, as iron(III) will compete with uranyl(VI) for sorption sites on the amidoxime-functionalized sorbents.

Vanadium, iron, nickel, and copper are metals that are present in seawater at concentrations approximately comparable to that of uranyl(VI). Vanadium, which exists in the +4 (as VO^{2+}) and +5 (as VO_2^{+}) oxidation states in seawater, has been observed to bind strongly to the amidoxime-functionalized sorbent, reducing the sorption sites available for uranyl(VI) binding.[2, 20] In order to understand the competition between uranyl(VI) and vanadium(V) for amidoxime functional groups on the functionalized sorbents, Kelley et al.[21] compared structures of uranyl(VI)- 4,5-di(amidoximyl)imidazole complexes and vanadium(V)- 4,5-di(amidoximyl)imidazole complexes. The authors observed that both metals formed 1:2 metal-ligand complexes with the 4,5-di(amidoximyl)imidazole ligand, though with different coordination chemistries. Uranyl(VI) coordinates the 4,5-di(amidoximyl)imidazole ligand through the two oxime oxygens via η^2 binding, while vanadium(V) coordinates to the ligand via an interaction with only one oxime oxygen and with the imidazole nitrogen.[21] This difference in interaction means that each metal-ligand complex has a different geometry.

There have been many studies in which ESI-MS has been used to study vanadium complexes with various ligands. Van Stipdonk and coworkers[22] investigated the gas-phase

complexes formed from solutions containing $VOSO_4$ and organonitrile compounds such as acetonitrile, propionitrile, butyronitrile, and benzonitrile. Gas phase-ions containing nitrile ligands and vanadyl cations, such as vanadyl (VO^{2+}), vanadyl hydroxide ($VOOH^{+}$), and vanadium(V)dioxide (VO_2^{+}) were observed. The dominant species in the spectrum were doubly-charged complexes with the general formula $[VO(L)_n]^{2+}$, where L is the nitrile ligand and n = 4 and 5. Kaczorowska et al.[23] used ESI-MS to investigate the complexes of vanadium(V) formed with three organic acids: fumaric acid, maleic acid, and succinic acid. Using methanol as a solvent, they observed that the acids formed complexes with vanadium having the general formula $[VO+(C_2H_{2n}(COO)_2)+(CH_3OH)]^{+}$, where n is either 1 or 2 depending if the organic acid contains an unsaturated or saturated alkyl chain. They proposed that the acids coordinate to vanadium in a bidentate fashion, using two oxygen atoms from two different carboxylic groups. Apart from these two studies examining vanadium-ligand complexes,[22, 23] there have also been some ESI-MS studies investigating the gas-phase oxovanadium species. In the presence of suitable precursors, these oxovandium species can be generated using electrospray. Feyel et al.[24] generated bare vanadium cluster cations having the general formula $[V_nO_m]^{+}$ (m = 1-4, n = 1-10), by electrospraying a solution containing hexanuclear (methoxido)oxidovanadium ($V_6O_7(OCH_3)_{12}$) as a precursor compound. Using ESI-MS and CID, Al Hasan et al.[25] generated both singly- and multiply-charged polyoxovanadate anions from a solution prepared using a tetradecavanadate compound, $V_{14}O_{36}Cl(L)_5$, ($L = (CH_2CH_3)_4N^{+}$).

ESI-MS studies of solutions containing iron(III) and various ligands have also been reported. Pakchung et al.[26] characterized the gas-phase complexes formed in a solution containing suberodihydroxamic acid and either iron(III), gallium(III), indium(III),

cesium(III), europium(III), or ytterbium(III) at various metal:ligand mole ratios. Pakchung et al. observed that suberodihydroxamic acid formed gas-phase complexes with iron(III) of various stoichiometric ratios, including 1:1, 1:2, 2:2, 2:3, and 3:4 iron(III):suberodihydroxamic acid complexes. Bertoli et al.[27] also used ESI-MS techniques to investigate the interaction between iron(III) and copper(II) with a physiologically relevant ligand, citrate. It was shown that the ligand formed gas-phase 1:1 and 1:2 metal:citrate complexes of with each of the metals, with the 1:1 complexes being preferentially formed. Using tobramycin instead of citric acid as the ligand, Sekar et al.[28] investigated the gas phase complexes formed with iron(III) and copper(II). Both 1:1 and 1:2 complexes were observed.

Iron(III) and vanadium(V) are among the main metals in seawater that compete with uranyl(VI) for binding sites on amidoxime-functionalized sorbents. They are of interest to us because of their strong interactions with amidoxime ligands. As previously mentioned, iron(III) formed the strongest complexes with DHIP, while adsorption of vanadium(V) to the amidxoime-functionalized sorbent during extraction of uranyl(VI) from seawater has previously been observed.[2, 20] The solution chemistry of iron(III) in the presence of DHIP has been investigated using potentiometry, and the structure of a vanadium(V) - 4,5-di(amidoximyl)imidazole complex has been determined using crystallography.[11, 21] To the best of our knowledge, the gas-phase interactions of iron(III) and vanadium(V) with the amidoxime ligands DHIP and DHPD have not been investigated. In the study reported here, we characterize the gas-phase complexes that iron(III) and vanadium(V) form with the amidoxime ligands DHIP and DHPD. We also investigate how the presence of iron(III) and vanadium(V) affects the formation of gas-phase uranyl(VI)-DHIP complexes.

5.2 Experimental

5.2.1 Materials

DHIP and DHPD used for this study were received as gifts from Dr. Chien Wai (University of Idaho). The ligands were synthesized by Dr. Horng-Bin Pan using a previously described procedure.[14] Uranyl(VI) nitrate hexahydrate was purchased from International Bio-Analytical Industries, Inc. (Boca Raton, FL, USA), while iron(III) nitrate nonahydrate (99.4%) and vanadium(V) pentaoxide (99.6%) were purchased from Fisher Scientific (Fair Lawn, NJ, USA) and Alfa Aesar (Ward Hill, MA, USA), respectively. Nitric acid (ACS grade), ammonium hydroxide (ACS grade), and methanol (Omnisolve), were purchased from EMD Chemicals (Gibbstown, NJ, USA). Water (18 MΩ) was purified with a Milli-Q system (Millipore Corp., Billerica, MA, USA). All chemicals were used as received.

5.2.2 Sample preparation

10 mM stock solutions of DHIP, DHPD, iron(III) nitrate, and uranyl(VI) nitrate were prepared by dissolving the appropriate amount of each compound in 20% (v/v) methanol:water and bringing the solution to volume in a 10 mL volumetric flask. A 5 mM solution of vanadium pentoxide was prepared in the same way. The dissolution of vanadium pentoxide was facilitated by adding 1.6 mL of 1% ammonium hydroxide to the volumetric flask containing the material. The metal and ligand stock solutions were combined in appropriate ratios and diluted with 20% (v/v) methanol:water to give a final metal concentration of 1 mM. The solution pH was measured using an Orion ROSS combination

pH electrode (Thermo Fisher Scientific) standardized against pH 4.0 and 7.0 buffers traceable to the NIST pH activity scale. The solution pH was adjusted with HNO_3 or NH_4OH as appropriate. Stock solutions and samples were prepared on the day of use.

5.2.3 Instrumentation

ESI mass spectra were collected using a Finnigan LCQ Deca XP plus ion trap mass spectrometer (ThermoFinnigan Corporation, San Jose, CA). The sample solutions were infused at a flow rate of 3 µL/min. The spray needle voltage was maintained at +4.00 kV, while the nitrogen sheath gas flow rate was set to 35 (arbitrary units). A capillary voltage of 15 V was applied. The capillary temperature was maintained at 200 $^{\circ}$C. The ion trap mass analyzer was operated at a pressure of 1.5×10^{-5} torr. The instrument was set to detect ion species in the *m/z* range of 100 – 1000. Spectra were acquired in positive ion mode and processed using Xcalibur software (Thermo Electron, San Jose, CA).

5.3 Results and Discussion

5.3.1 DHIP complexes with vanadium(V) and iron(III)

In order to compare the effect of vanadium(V) and iron(III) on uranyl(VI) complexation by DHIP, we have characterized the complexes that these metals form with DHIP. Gas-phase uranyl(VI)-DHIP complexes have been discussed in Chapter 4 and in Reference 19. Vanadium(V)-DHIP and iron(III)-DHIP complexes are discussed below.

Figure 5.2 shows mass spectra acquired from pH 5.5 solutions of vanadium(V) and DHIP at various metal:ligand mole ratios. Peak assignments are given in Table 5.3. At a 1:1

vanadium(V):DHIP molar ratio, a peak due to a 1:1 vanadium(V)-DHIP complex, $[VO_2+DHIP]^+$, can be observed at *m/z* 226 (Figure 5.2a, Table 5.3). A 1:2 vanadium(V)-DHIP complex, $[VO_2+2(DHIP)-H_2O]^+$ (*m/z* 351) is also observed, but at a very low relative abundance. A peak at *m/z* 129, is thought to be a fragment ion formed by the loss of an NH group from DHIP. The peak is assigned as $[(DHIP-NH)+H]^+$ (*m/z* 129). The peak at *m/z* 433 is believed to be due to an oxovanadium(V) ion and is assigned as $[V_4O_{12}+CH_3OH+5H]^+$, while the peaks at *m/z* 336 and 722 are unassigned. The presence of this oxovanadium(V) ion at high relative abundance in the spectrum shown in Figure 5.2a shows that its formation is favored over the formation of vanadium(V)-DHIP complexes when the vanadium(V) concentration is equal to or lower than the ligand concentration.

However, when the ligand concentration was increased such that the vanadium(V):DHIP mole ratio was 1:3, the complex $[VO_2+2(DHIP)-H_2O]^+$ (*m/z* 351), which was earlier observed in relatively low abundance, became the most dominant ion in the spectrum (Figure 5.2b). The mechanism of the H_2O loss is not yet understood, but complex formation is clearly favored when the ligand concentration is in excess of vanadium(V) concentration in solution. The peak at *m/z* 433, which arises from $[V_4O_{12}+CH_3OH+5H]^+$, is observed to decrease dramatically. This is because the excess ligand causes a shift in the equilibrium favoring the formation of vanadium(V)-DHIP complexes. No change in the mass spectrum was observed when the vanadium(V):DHIP mole ratio was changed to 1:5, as the same set of ions are observed, with $[VO_2+2(DHIP)-H_2O]^+$ (*m/z* 351) still the most dominant ion in the spectrum (Figure 5.2c). The peak at *m/z* 144 arises from $[DHIP+H]^+$.

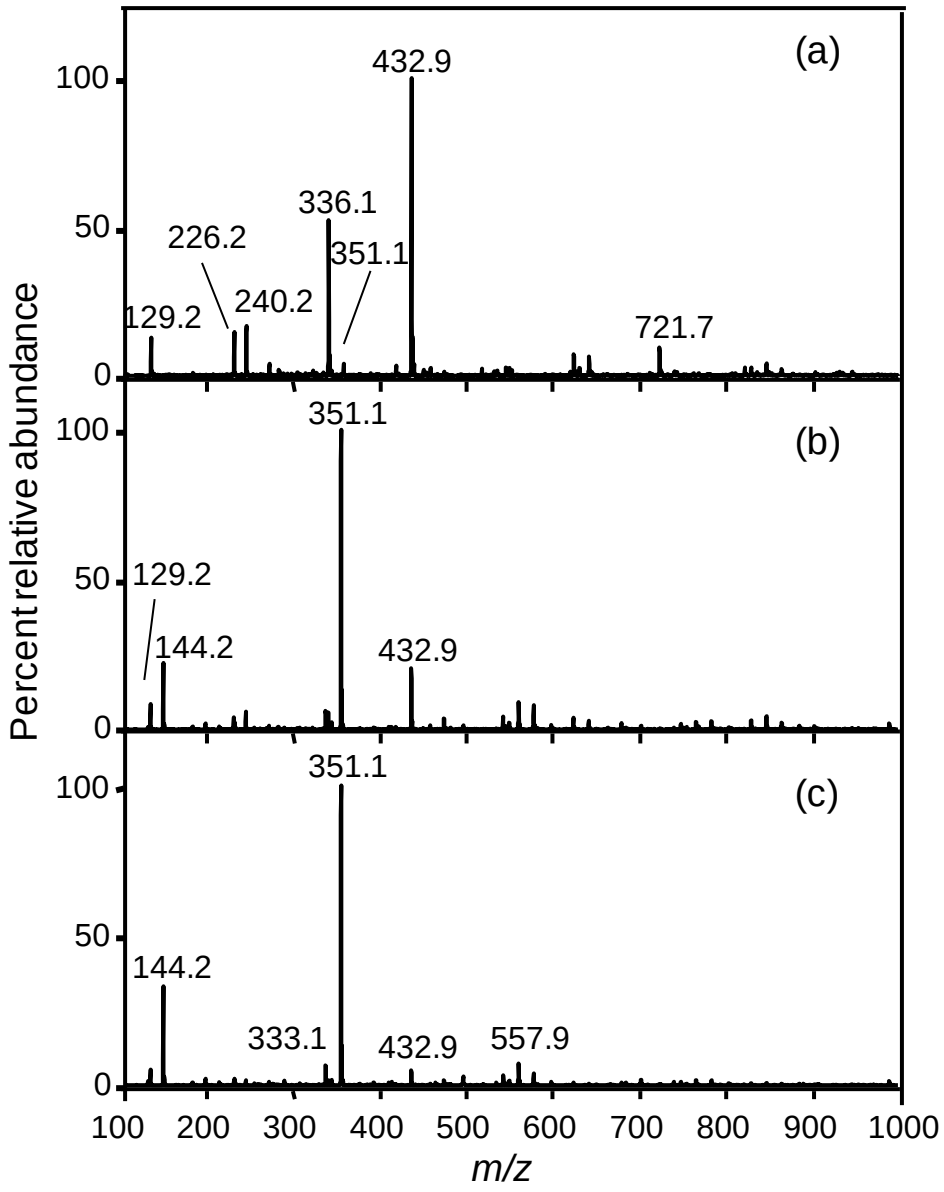

Figure 5.2 Positive ion mass spectra acquired from solutions containing 0.1 mM vanadium(V) and a) 0.1 mM DHIP, b) 0.3 mM DHIP, and c) 0.5 mM DHIP. All samples in 20% (v/v) methanol:water at pH 5.5.

Table 5.3 ESI-MS peak assignments for DHIP and DHPD complexes of vanadium(V), iron(III), and uranyl(VI).

Solution	Species	Observed *m/z*	Theoretical *m/z*
DHIP System ($C_5H_9N_3O_2$)			
Vanadium(V)/DHIP	$[(DHIP-NH)+H]^+$	129.2	129.1
	$[DHIP+H]^+$	144.2	144.1
	$[VO_2+DHIP]^+$	226.2	226.2
	$[VO_2+DHIP+CH_3OH-H_2O]^+$	240.2	240.1
	$[VO_2+2(DHIP)-2(H_2O)]^+$	333.1	333.1
	Unassigned	336.1	------
	$[VO_2+2(DHIP)-H_2O]^+$	351.1	351.1
	$[V_4O_{12}+CH_3OH+5H]^+$	432.9	432.7
	$[VO_2+K+2(DHIP)-2(H_2O)-H]^+$	371.0	371.0
	$[VO_2+K+2(DHIP)-H_2O-H]^+$	389.0	389.0
	$[2(VO_2)+K+2(DHIP)-(H_2O)-2H]^+$	470.9	470.9
	$[VO_2+3(DHIP)+2(CH_3OH)-H_2O]^+$	557.9	558.1
	$[VO_2+K+3(DHIP)+2(CH_3OH)-H_2O]^+$	595.8	596.1
	$[2(VO_2)+K+4(DHIP)-4(H_2O)-2H]^+$	702.8	703.0
	Unassigned	721.7	------
Iron(III)/DHIP	$[Fe+2(DHIP-H)]^+$	340.1	340.0
	$[Fe+(DHIP-H)]^+$	198.1	198.0
Uranyl(VI)/DHIP	See Table 4.1	------	------
DHPD System ($C_5H_{12}N_4O_2$)			
Vanadium(V)/DHPD	$[DHPD-2(NH_2)]^+$	128.2	128.1
	$[VO_2+2(DHPD)-H_2O]^+$	385.1	385.0
	$[VO_2+2(DHPD)+2(CH_3OH)]^+$	466.9	467.1
Iron(III)/DHPD	$[Fe+2(DHPD-H)+2(CH_3OH)]^+$	437.9	438.1
	$[Fe+3(DHPD)-2H]^+$	533.9	534.0
Uranyl(VI)/DHPD	See Table 4.1	------	------

Table 5.3 continued. ESI-MS peak assignments for DHIP and DHPD complexes of vanadium(V), iron(III), and uranyl(VI).

Solution	Species	Observed *m/z*	Theoretical *m/z*
Mixed Metal Complexes			
	$[Fe+UO_2+3(DHIP-H)]^+$	751.1	751.0
	$[Fe+VO_2+3(DHIP-H)-H_2O]^+$	546.9	547.0
	$[Fe+2(VO_2)+3(DHIP)-H_2O-2H]^+$	753.7	753.9
	$[VO_2+UO_2+3(DHIP)-H_2O-2H]^+$	762.0	762.2
	$[Fe+UO_2+3(DHIP-H)]^+$	751.1	751.0

The dependence on solution pH of the various vanadium(V)-DHIP complexes was also investigated. Figure 5.3 shows the mass spectra acquired from solutions containing a 1:5 mole ratio of vanadium(V):DHIP at different pH values. Peak assignments are given in Table 5.4. At pH 3.5, species observed include $[VO_2+2(DHIP)-H_2O]^+$ (*m/z* 351) and $[VO_2+2(DHIP)-2H_2O]^+$ (*m/z* 333). The potassium adducts $[VO_2+K+2(DHIP)-2(H_2O)-H]^+$ (*m/z* 371), $[VO_2+K+2(DHIP)-H_2O-H]^+$ (*m/z* 389), $[2(VO_2)+K+2(DHIP)-H_2O-2H]^+$ (*m/z* 471), and $[2(VO_2)+K+4(DHIP)-4H_2O-2H]^+$ (*m/z* 703) were also observed (Figure 5.3a and Table 5.3).

When the pH was increased to 5.9, $[VO_2+2(DHIP)-H_2O]^+$ (*m/z* 351) and $[VO_2+2(DHIP)-2(H_2O)]^+$ (*m/z* 333) were still observed, with the peak at *m/z* 351 still the most abundant in the spectrum (Figure 5.3b). Potassium adducts of the complexes were conspicuously absent. Increasing the pH further, to 7.0 and finally to 8.3 (seawater pH), does not cause any important changes in the gas-phase complexes observed, except for the disappearance of peaks due to the potassium adducts at *m/z* 389, 471 and 596. The presence of the complex $[VO_2+2(DHIP)-H_2O]^+$ (*m/z* 351) as the most abundant ion in the spectra at all pH values shows that this 1:2 complex of vanadium(V):DHIP is easily formed and stable

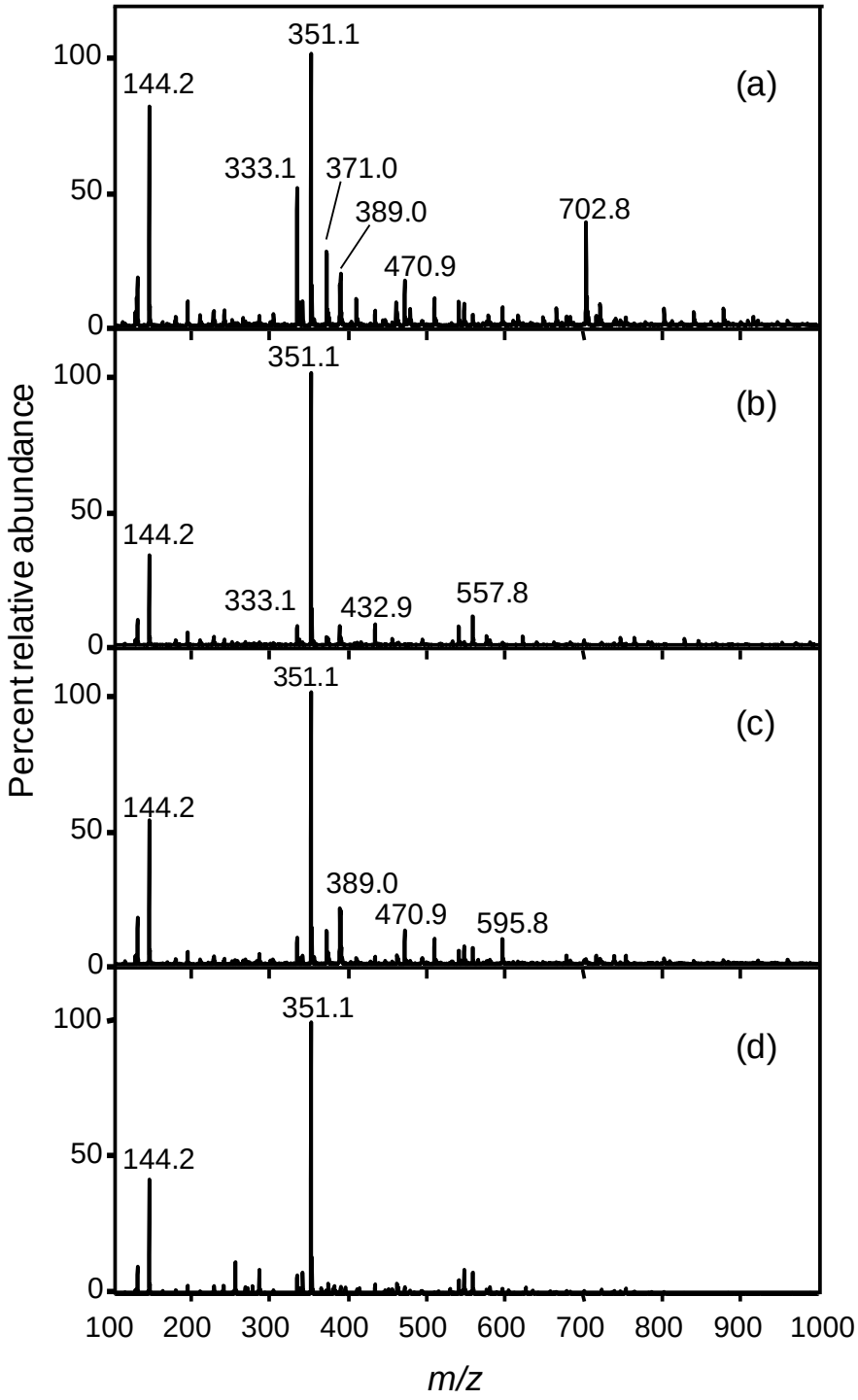

Figure 5.3 Positive ion mass spectra acquired from solutions containing 1 mM vanadium(V) and 5 mM DHIP in 20% (v/v) methanol:water at pH a) 3.5, b) 5.9, c) 7.0, and d) 8.3.

at all pH values. This is observation is consistent with the work of Kelley et al,[21] who showed that VO_2^+ can be complexed by two amidoxime molecules. Thus, $[VO_2+2(DHIP)-H_2O]^+$ (*m/z* 351) is not an artifact but an ion arising from a complex that is formed in solution and undergoes little or no perturbation (except for the loss of H_2O) during the ESI process to form a gas-phase ion.

Iron(III)-DHIP complexes were also investigated. A mass spectrum acquired from a solution containing 1 mM iron(III) and 1 mM DHIP at pH 5.5 shows peaks at *m/z* 144 and 340 (Figure 5.4). The peak at *m/z* 144 has previously been assigned as $[DHIP+H]^+$ while the peak at 340 is due to the iron(III)-DHIP complex $[Fe+2(DHIP-H)]^+$ (Table 5.3). No changes in the mass spectra were observed when the ligand concentration was increased first to 3 mM and then to 5 mM (spectra not shown). Thus, the 1:2 complex is the only complex formed in the iron(III)/DHIP system, unlike the vanadium(V) and uranyl(VI)/DHIP systems.

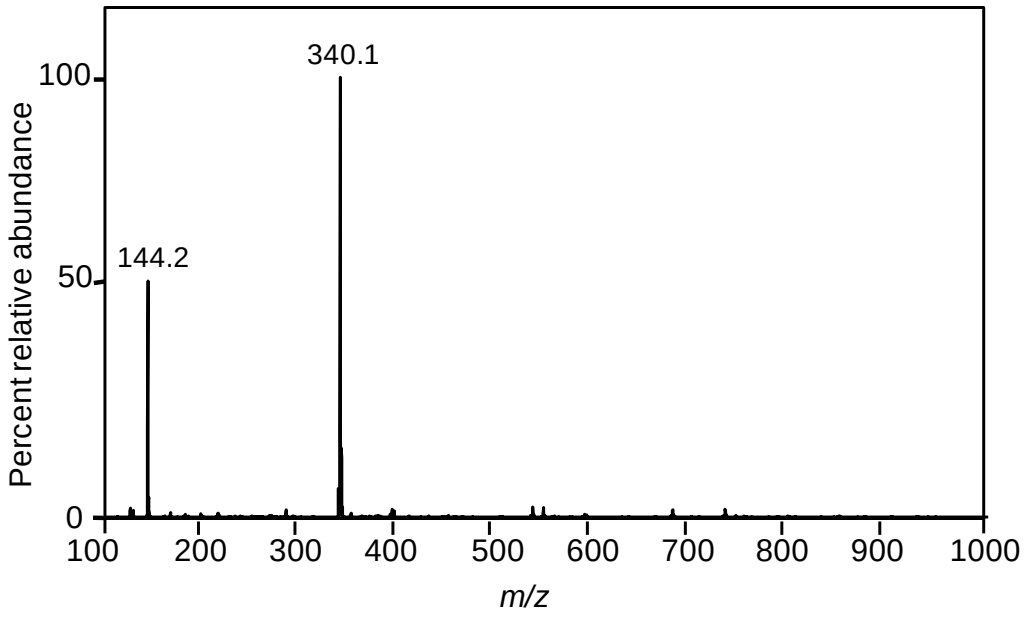

Figure 5.4 Positive ion mass spectrum acquired from a solution containing 1 mM iron(III) and 1 mM DHIP in 20% (v/v) methanol:water at pH 5.5.

The effect of pH on iron(III)-DHIP complex formation was investigated as well. Spectra acquired at various pH values (pH 3 – 8) from solutions containing iron(III) and DHIP in a 1:5 mole ratio show only the presence of $[Fe+2(DHIP-H)]^+$ (*m/z* 340) (spectra not shown). It is well known that metal ions form hydroxides at high pH. The absence of any peaks that can be assigned to hydroxide ions such as $[Fe+2(OH)]^+$ or $[Fe+OH]^{2+}$ suggests that DHIP is a stronger competitor for iron(III) than hydroxide.

Rao et al.[11] reported that iron(III) can form both 1:1 and 1:2 metal:ligand complexes with DHIP (Table 5.3). Thus, it is surprising that only the 1:2 metal:ligand complex $[Fe+2(DHIP-H)]^+$ (*m/z* 340) was observed in this gas-phase study regardless of mole ratio and pH. As discussed in Chapter 1, solution perturbations during the ESI process are thought to be the major reason for the differences in the species observed in the gas phase vs. in the solution phase. Both 1:1 and 1:2 metal:ligand complexes are believed to be present in the solution phase, as predicted by Rao et al., but the 1:1 metal:ligand complex $[Fe+(DHIP-2H)]^+$ can potentially react with a second DHIP molecule to form an adduct with the same *m/z* as the 1:2 iron(III):DHIP complex. In both cases, the ion assignment is $[Fe+2(DHIP-H)]^+$ (*m/z* 340).

As previously explained in Chapter 4 and shown in Figure 4.2 and Table 4.1, uranyl(VI) forms 1:1, 1:2 and 2:3 gas-phase uranyl(VI)-DHIP complexes with DHIP when the uranyl(VI):DHIP mole ratio in solution is 1:5. At this same mole ratio, vanadium(V) and iron(III) form only 1:2 metal:ligand gas-phase complexes with DHIP. (Figures 5.2 and 5.4, respectively). In addition, neither vanadium(V) nor iron(III) forms a 2:3 metal:ligand gas-phase complex with DHIP at any metal:ligand mole ratio or pH investigated, unlike

uranyl(VI), which form a 2:3 gas-phase metal:ligand complex with DHIP at high pH and high DHIP concentration relative to uranyl(VI) concentration. This difference has to do with differences in binding mechanism. This difference, which also determines the relative stability of the complexes formed, will be discussed in detail in section 5.3.3.

5.3.2 DHPD complexes with vanadium(V) and iron(III)

DHPD is an acyclic isomer of DHIP and it is interesting to compare the complexes DHPD forms with iron(III) and vanadium(V) with those formed by DHIP. Our group[19] and other research goups[13, 14] have recently reported the complexation of uranyl(VI) by DHPD and compared the relative binding affinities of DHIP and DHPD for uranyl(VI). It has been shown that DHPD forms complexes with uranyl(VI) less effectively than does DHIP. This is based on the formation constants of the resulting species[13, 14] as well as on the relative abundances of uranyl(VI)-DHPD complexes vs. relative abundances of uranyl(VI)-DHIP complexes in ESI mass spectra.

The mass spectrum acquired from a solution containing 1 mM each of DHPD and iron(III) at pH 7.1 is shown in Figure 5.5a. Iron(III) forms 1:2 and 1:3 metal:ligand complexes with DHPD to give peaks at *m/z* 438 and 534. These can be assigned as $[Fe+2(DHPD-H)+2(CH_3OH)]^+$ and $[Fe+3(DHPD)-2H]^+$, respectively. Peaks due to uncomplexed ligand, $[DHPD+H]^+$ (*m/z* 161) and $[2(DHPD)+H]^+$ (*m/z* 321), were also observed in the spectrum. The peak at *m/z* 128 is also believed to be due to a fragment ion arising from the loss of two amino groups from DHPD. This peak is assigned as $[DHPD-2(NH_2)]^+$ (*m/z* 128). Unlike in the iron(III)/DHIP system (Figure 5.4), where

$[DHIP+H]^+$ was low in abundance compared to the iron-DHIP complex, $[DHPD+H]^+$ (*m/z* 161) appears as the most prominent ion in the iron(III)/DHPD system (Figure 5.5a).

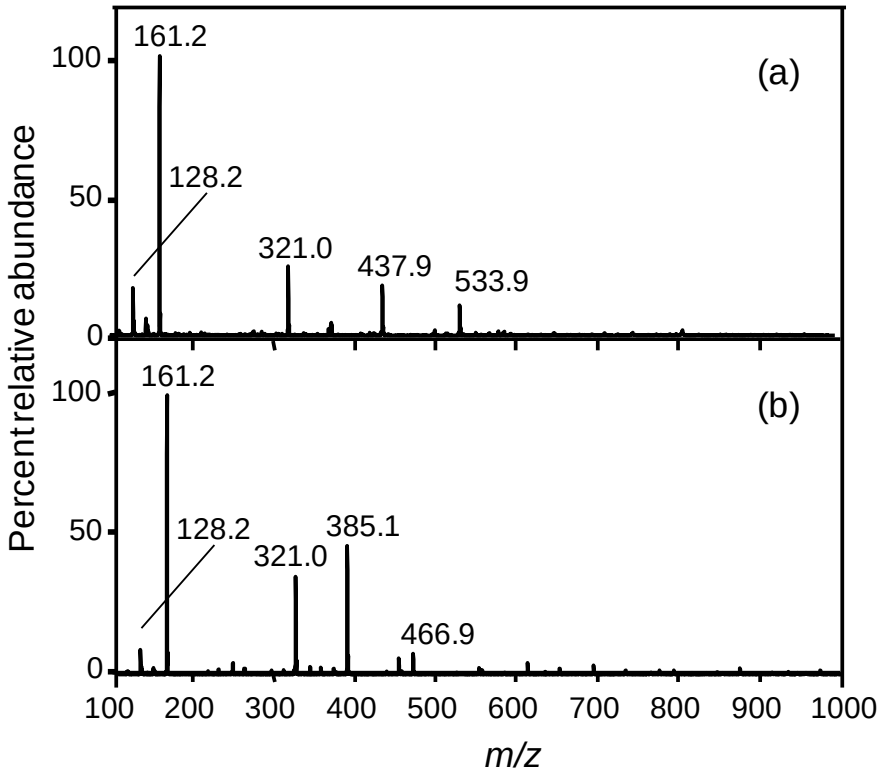

Figure 5.5 Positive ion mass spectra acquired from solutions containing a) 1 mM iron(III) and 1 mM DHPD, and b) 1 mM vanadium(V) and 1 mM DHPD. All samples in 20% (v/v) methanol:water at pH 7.1.

However, as the metal:ligand mole ratio was changed from 1:1 to 1:3, the relative abundances of ions assigned to iron(III)-DHPD complexes ($[Fe+2(DHPD-H)+2(CH_3OH)]^+$ (*m/z* 438), and $[Fe+3(DHPD)-2H]^+$ (*m/z* 534)) decreased, and at a 1:5 metal:ligand mole ratio, they were not observable (spectra not shown). This observation may be due to the increase in ion intensity of $[DHPD+H]^+$ with increasing DHPD concentration, resulting in

signal suppression of the iron(III)-DHPD complexes. This is in contrast to the iron(III)/DHIP system, where the relative abundance of the only iron(III) complex formed, $[Fe+2(DHIP-H)]^+$, was unaffected by increases in the DHPD concentration. Similarly to the uranyl(VI)/DHPD system, iron(III) appears to form gas-phase complexes with DHPD less effectively than with DHIP. We were not able to confirm our results with those obtained using other techniques, as an extensive literature search did not turn up other studies on the iron(III)/DHPD system.

Similar studies to those described above were carried out for solutions containing DHPD and vanadium(V). A spectrum acquired from a solution containing 1 mM each of DHPD and vanadium(V) at pH 7.1 is shown in Figure 5.5b. Vanadium(V) forms complexes with DHPD that give rise to peaks at *m/z* 385 and 467. These are assigned as $[VO_2+2(DHPD)-H_2O]^+$ (*m/z* 385) and $[VO_2+2(DHPD-H)+2(CH_3OH)]^+$ (*m/z* 467). Other peaks in the spectrum are due to uncomplexed DHPD, as previously described. Similarly to the mass spectrum acquired from a solution containing iron(III) and DHPD shown in Figure 5.5a, uncomplexed DHPD dominates the spectrum, with $[DHPD+H]^+$ (*m/z* 161) being the most prominent peak. Increasing either the ligand concentration or the pH has no effect on the species detected but does increase the relative abundance of $[VO_2+2(DHPD)-H_2O]^+$ (*m/z* 385) (spectra not shown). Again, this is contrary to what is observed in the iron(III)/DHPD system, where increasing either the ligand concentration or pH reduces the relative abundance of the iron(III)-DHPD complexes. Since a literature search did not uncover other investigations of the vanadium(V)/DHPD system using other techniques, we could not compare our results with those of other researchers.

5.3.3 Competition between uranyl(VI), vanadium(V) and iron(III) for DHIP

Data presented in the previous sections have shown that vanadium(V) and iron(III) form complexes with DHIP and DHPD. It is of interest to see how these two metal ions can affect the extraction of uranium from seawater using amidoxime-functionalized sorbents. A competitive binding study was therefore carried out to determine the relative affinities of uranyl(VI), iron(III), and vanadium(V) towards DHIP. DHIP was chosen instead of DHPD because it binds more effectively with each metal, as has been previously shown.[14] A competitive study was carried out in a fashion similar to one previously described by Keith-Roach et al.[29] Using the model described by Keith-Roach et al., a solution containing 5 mM DHIP and 1 mM each of the following metal ion pairs were prepared: iron(III) and uranyl(VI), uranyl(VI) and vanadium(V), and iron(III) and vanadium(V). The pH of each solution, which was initially in the range of pH 2.0 – 3.5, was thereafter increased to ~pH 8.3. The solution containing DHIP, iron(III), and vanadium(V) was observed to form a reddish brown colloid. The solution was sonicated until the colloid disappeared, and a clear solution formed. Solutions containing iron(III), uranyl(VI), and DHIP, or vanadium(V), uranyl(VI), and DHIP formed no colloidal material.

A mass spectrum acquired from a solution containing iron(III), uranyl(VI), and DHIP in a 1:1:5 mole ratio is shown in Figure 5.6a. Peak assignments are given in Table 5.3. Peaks due to both iron(III)-DHIP complexes and uranyl(VI)-DHIP complexes were observed, along with the peak due to uncomplexed DHIP at *m/z* 144. The dominant peak in the spectrum is that arising from the previously described iron(III) complex,

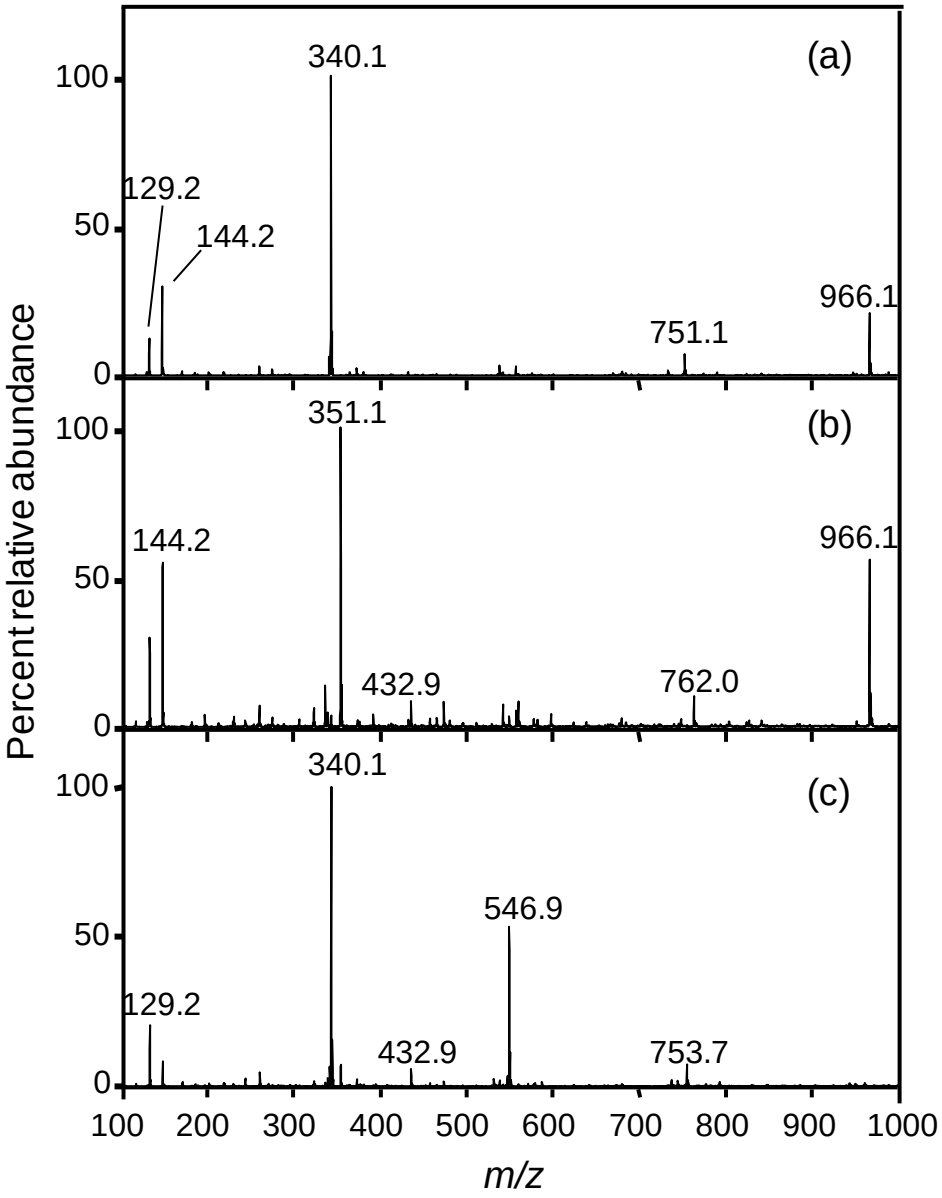

Figure 5.6 Positive ion mass spectra acquired from solutions containing 5 mM of DHIP and 1 mM of a) iron(III) and uranyl(VI), b) uranyl(VI) and vanadium(V), and c) iron(III) and vanadium(V) at pH 8.3.

$[Fe+2(DHIP-H)]^+$ (*m/z* 340), while the uranyl(VI) complex, $[2(UO_2)+3(DHIP-H)]^+$ (*m/z* 966), occurs in relatively low abundance (20%). The presence of an iron(III)-containing ion as the dominant ion in the spectrum suggests that iron(III) has a greater affinity for DHIP than does uranyl(VI). A small peak observed at *m/z* 751 is due to the formation of a mixed metal complex, $[Fe+UO_2+3(DHIP-H)]^+$. The higher affinity of iron(III) for DHIP, compared to the affinity of uranyl(VI) for DHIP, has previously been attributed to the higher binding strength of the metal towards the ligand. The formation constants of DHIP complexes with some common metal ions present in seawater have earlier been reported and are shown in Table 5.2.[11]

As previously mentioned, Rao et al. observed that the formation constants for iron(III)-DHIP complexes are higher than those for the uranyl(VI)-DHIP complexes.[11] The high formation constants of iron(III)-DHIP complexes compared to those of the uranyl(VI)-DHIP complexes is believed to be due to the nature of binding between each metal and DHIP.[11] In the iron(III)-DHIP complexes, the metal *d*-orbital interacts with the orbitals of DHIP donor atoms (i.e. oxygen and nitrogen), resulting in a relatively large overlap. This large overlap is what leads to strong covalent bonds and thus high formation constants. In the uranyl(VI)-DHIP complexes, on the other hand, it is the less extended *f*-orbital of the metal that interacts with the ligand donor atoms, forming a covalent bond weaker than the bond for iron(III)-DHIP complexes. This difference in the metal orbital interacting with the ligand donor atoms is what is responsible for the differences in binding strength.

The relative affinities of uranyl(VI) and vanadium(V) for DHIP were also investigated. Figure 5.6b shows the mass spectrum acquired from a solution containing 1

mM of each metal ion and 5 mM DHIP. While the uranyl(VI) complex, $[2(UO_2)+3(DHIP-H)]^+$ (*m/z* 966), was observed at a much higher relative abundance (55%) compared what was observed for the iron(III)/uranyl(VI) system (20%, Figure 5.6a), a peak due to the vanadium(V) complex, $[VO_2+2(DHIP)-H_2O]^+$ (*m/z* 351) was the most dominant peak in the spectrum. This suggests that vanadium(V) has a higher affinity for DHIP than uranyl(VI) at the pH investigated. This observation is consistent with results from an earlier study by Kelley et al. in which they investigated the structures of amidoxime complexes of uranyl(VI) and vanadium(V).[21] Kelley et al. observed that both uranyl(VI) and vanadium(V) bind to the amidoxime ligand 4,5-di(amidoximyl)imidazole via different coordination modes, which results in different geometries for the resulting complexes.[21] As previously reviewed in section 5.2, vanadium(V) coordinates to the amidoxime ligand via the imidazole nitrogen, and it is expected that the imide nitrogen in DHIP will also interact with vanadium. Kelly et al. then concluded that if this imide nitrogen of DHIP is involved in the bonding, then the vanadium(V)-DHIP complex will be more stable than the uranyl(VI)-DHIP complex.[21]

The final system investigated was a solution containing vanadium(V), iron(III), and DHIP. The mass spectrum (Figure 5.6c) acquired from that solution shows that iron(III) has a higher affinity for DHIP than vanadium(V). This conclusion can be made because the dominant ion in the spectrum is the iron(III)-DHIP complex, $[Fe+2(DHIP-H)]^+$ (*m/z* 340), whereas the vanadium(V)-DHIP complex, $[(VO_2+2(DHIP)-H_2O]^+$ (*m/z* 351) has almost completely disappeared. Mixed complexes were also observed at *m/z* 547 ($[Fe+VO_2+3(DHIP-H)-H_2O]^+$) and *m/z* 754 ($[Fe+2(VO_2)+3(DHIP)-H_2O-2H]^+$). The higher binding affinity of iron(III) towards DHIP compared to vanadium(V) could be due to

the relative differences in the metal ionic radii and/or bond lengths between each metal and the ligand. The formation constants of iron(III)-DHIP complexes have been reported (Table 5.2), but those of vanadium(V)-DHIP complexes have not. Thus, we cannot compare our results from our gas-phase study on competition between iron(III) and vanadium(V) for DHIP discussed here with results from any solution studies.

Figure 5.7 summarizes the results of the competition study discussed earlier. It shows the relative percentage of each type of complex formed when two different metal ions are added to a solution of DHIP at pH 8.3. For a given metal ion pair and a given mass spectrum, the normalized relative abundance was calculated by dividing the ion abundance of a given complex by the sum of all ion abundances of the complexes in the spectrum. This normalized relative abundance gives us an idea of the relative affinity of each metal towards DHIP. In the iron(III)/uranyl(VI) system, for example, ~63% of the complexes observed were due to iron(III) while ~13% were due to uranyl(VI). The mixed metal iron(III)-uranyl(VI)-DHIP complex accounts for <5% of the total, while uncomplexed DHIP accounts for slightly less than ~20% of the total ion abundance observed in the spectrum. As discussed earlier, iron(III) has a higher affinity for DHIP than uranyl(VI). This can be clearly seen in Figure 5.7. In the vanadium(V)/uranyl(VI) system, vanadium(V)-DHIP complexes accounted for ~45% of the ions observed in the spectra, while uranyl(VI)-DHIP complexes accounted for ~30% of the ions. The remaining ions were due to uncomplexed DHIP, and mixed metal complexes. About 60% of the ions observed in the iron(III)/vanadium(V) system were due to iron(III)-DHIP complexes, while vanadium(V)-DHIP complexes accounted for <5%. Mixed metal complexes were favored in this system compared to the other two systems, and accounted for ~20% of the ions observed in the

spectrum. In summary, the relative affinities of these metal ions towards DHIP follow the order iron(III) > vanadium(V) > uranyl(VI). This gas-phase study suggests that the sequestration of uranyl(VI) from seawater at pH 8.3 using amidoxime-functionalized sorbents will be greatly affected by the presence of vanadium(V) and iron(III). It will be of interest to see if similar results will be obtained from studies investigating iron(III), vanadium(V), and uranyl(VI) competition for DHIP binding in aqueous solution.

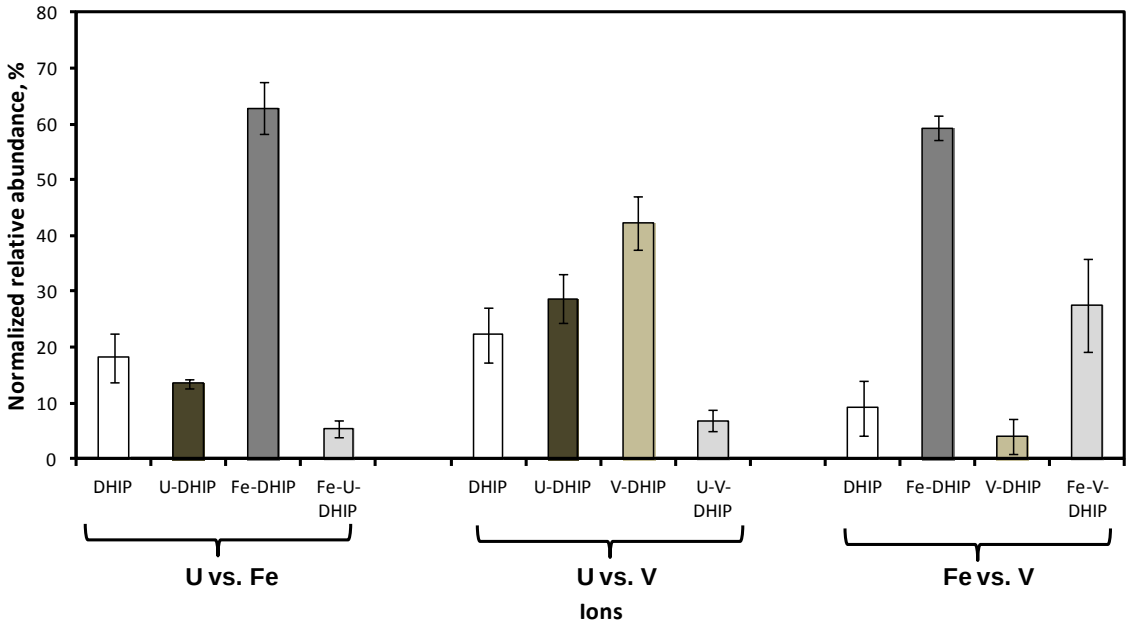

Figure 5.7 Normalized relative abundances of metal-DHIP complexes formed from solutions containing two metal ions and DHIP. U = uranyl(VI), Fe = iron(III), and V = vanadium(V).

5.4 Conclusions

The gas phase complexes of iron(III) and vanadium(V) with the amidoxime ligands DHIP and DHPD were characterized using ESI-MS. The effect of changes in metal:ligand mole ratio and solution pH on these iron(III) and vanadium(V)-amidoxime gas-phase complexes was also investigated. Iron(III) was observed to form only a 1:2 metal:ligand

complex with DHIP at all metal:ligand mole ratios and pH values investigated. However, it forms both 1:2 and 1:3 metal:ligand complexes with DHPD. These complexes decrease in relative abundance as ligand concentration increases and as solution pH increases from pH 6 to 9. Vanadium(V) forms a 1:1 metal:ligand complex with DHIP at low ligand concentrations, but the 1:2 metal ligand complex is favored when the ligand concentration is higher than the metal concentration. However, vanadium(V) forms a 1:2 metal:ligand complex with DHPD at all metal:ligand mole ratios investigated here. Changes in solution pH have no effect on speciation in the vanadium/DHIP or vanadium/DHPD systems. The relative binding affinities of the metal ions towards DHIP follow the order iron(III) > vanadium(V) > uranyl(V). Based on this study of gas-phase chemistry, we can draw the conclusion that iron(III) and vanadium(V) will adversely affect uranyl(VI) extraction from seawater using amidoxime-functionalized sorbents.

Acknowledgements

I thank Dr. Chien Wai and Dr. Horng-Bin Pan for the gift of the 2,6-dihydroxyiminopiperidine and N^1, N^5-dihydroxypentanediimidamide used in this study.

References

1. OECD. *Uranium 2009: Resources, production and demands*. OECD NEA Publication 6891, **2010,** 456.
2. Kim, J.; Tsouris, C.; Mayes, R. T.; Oyola, Y.; Saito, T.; Janke, C. J.; Dai, S.; Schneider, E.; Sachde, D. Recovery of uranium from seawater: A review of current status and future research needs. *Sep. Sci. Technol.* **2013,** *48*, 367-387.
3. Davies, R. V.; Kennedy, J.; Hill, K. M.; McIlroy, R. W.; Spence, R. Extraction of uranium from seawater. *Nature* **1964,** *203*, 1110.
4. Astheimer, L.; Schenk, H. J.; Witte, E. G.; Schwochau, K. Development of sorbers for the recovery of uranium from seawater. 2. The accumulation of uranium from seawater by resins containing amidoxime and imidoxime functional-groups. *Sep. Sci. Technol.* **1983,** *18*, 307-339.
5. Schenk, H. J.; Astheimer, L.; Witte, E. G.; Schwochau, K. Development of sorbers for the recovery of uranium from seawater. 1. Assessment of key parameters and screening studies of sorber materials. *Sep. Sci. Technol.* **1982,** *17*, 1293-1308.
6. DOE Office of Nuclear Energy, *Fuel resources: Uranium from seawater program*; **2013**; pp 1-31.
7. Tamada, M.; Seko, N.; Kasai, N.; Shimizu, T. Cost estimation of uranium recovery from seawater with system of braid type adsorbents. *Trans. At. Energ. Soc. Japan* **2006,** *5*, 358-363.
8. Kim, J.; Tsouris, C.; Oyola, Y.; Janke, C. J.; Mayes, R. T.; Dai, S.; Gill, G.; Kuo, L. J.; Wood, J.; Choe, K. Y.; Schneider, E.; Lindner, H. Uptake of uranium from seawater by amidoxime-based polymeric adsorbent: Field experiments, modeling, and updated economic assessment. *Ind. Eng. Chem. Res.* **2014,** *53*, 6076-6083.
9. Lindner, H.; Schneider, E. Review of cost estimates for uranium recovery from seawater. *Energ. Econ.* **2015,** *49*, 9-22.
10. Schneider, E.; Sachde, D. The cost of recovering uranium from seawater by a braided polymer adsorbent system. *Sci. Global Secur.* **2013,** *21*, 134-163.

11. Sun, X.; Xu, C.; Tian, G.; Rao, L. Complexation of glutarimidedioxime with Fe(III), Cu(II), Pb(II), and Ni(II), the competing ions for the sequestration of U(VI) from seawater. *Dalton Trans.* **2013,** *42*, 14621-14627.

12. Sun, X. Q.; Tian, G. X.; Xu, C.; Rao, L. F.; Vukovic, S.; Kang, S. O.; Hay, B. P. Quantifying the binding strength of U(VI) with phthalimidedioxime in comparison with glutarimidedioxime. *Dalton Trans.* **2014,** *43*, 551-557.

13. Tian, G. X.; Teat, S. J.; Rao, L. F. Thermodynamic studies of U(VI) complexation with glutardiamidoxime for sequestration of uranium from seawater. *Dalton Trans.* **2013,** *42*, 5690-5696.

14. Tian, G. X.; Teat, S. J.; Zhang, Z. Y.; Rao, L. F. Sequestering uranium from seawater: Binding strength and modes of uranyl complexes with glutarimidedioxime. *Dalton Trans.* **2012,** *41*, 11579-11586.

15. Kang, S. O.; Vukovic, S.; Custelcean, R.; Hay, B. P. Cyclic imide dioximes: Formation and hydrolytic stability. *Ind. Eng. Chem. Res.* **2012,** *51*, 6619-6624.

16. Vukovic, S.; Watson, L. A.; Kang, S. O.; Custelcean, R.; Hay, B. P. How amidoximate binds the uranyl cation. *Inorg. Chem.* **2012,** *51*, 3855-3859.

17. Endrizzi, F.; Melchior, A.; Tolazzi, M.; Rao, L. Complexation of uranium(VI) with glutarimidoxioxime: Thermodynamic and computational studies. *Dalton Trans.* **2015,** *44*, 13835-44.

18. Leggett, C. J.; Rao, L. Complexation of calcium and magnesium with glutarimidedioxime: Implications for the extraction of uranium from seawater. *Polyhedron* **2015,** *95*, 54-59.

19. Mustapha, A. M.; Pasilis, S. P. Probing uranyl(VI) speciation in the presence of amidoxime ligands using electrospray ionization mass spectrometry. *Rapid Commun. Mass Spectrom.* **2013,** *27*, 2135-2142.

20. Suzuki, T.; Saito, K.; Sugo, T.; Ogura, H.; Oguma, K. Fractional elution and determination of uranium and vanadium adsorbed on amidoxime fiber from seawater. *Anal. Sci.* **2000,** *16*, 429-432.

21. Kelley, S. P.; Barber, P. S.; Mullins, P. H. K.; Rogers, R. D. Structural clues to UO_2^{2+}/VO_2^{+} competition in seawater extraction using amidoxime-based extractants. *Chem. Commun.* **2014,** *50*, 12504-12507.

22. Parsons, Z.; Leavitt, C.; Duong, T.; Groenewold, G. S.; Gresham, G. L.; Van Stipdonk, M. J. Generation of gas-phase VO^{2+}, $VOOH^{+}$, and VO_2^{+}-nitrile complex ions by electrospray ionization and collision-induced dissociation. *J. Phys. Chem. A* **2006,** *110*, 11627-11635.

23. Kaczorowska, M.; Schwarz, H.; Schroder, D. Gas-phase fragmentation behavior of vanadium(V) complexes containing one molecule of a C-4-dicarboxylic acid. *Eur. J. Inorg. Chem.* **2007,** *21*, 3335-3341.

24. Feyel, S.; Schroeder, D.; Schwarz, H. Gas-phase chemistry of vanadium oxide cluster cations $V_{(m)}O_{(n)}^{(+)}$ (m=1-4; n=1-10) with water and molecular oxygen. *Eur. J. Inorg. Chem.* **2008,** *31*, 4961-4967.

25. Al Hasan, N. M.; Johnson, G. E.; Laskin, J. Gas-phase synthesis of singly and multiply charged polyoxovanadate anions employing electrospray ionization and collision-induced dissociation. *J. Am. Soc. Mass Spectrom.* **2013,** *24*, 1385-1395.

26. Pakchung, A. A. H.; Lifa, T.; Codd, R. Solution species of Fe(III), Ga(III), In(III) or Ln(III) and suberodihydroxamic acid from electrospray ionization mass spectrometry. *RSC Adv.* **2013,** *3*, 16051-16059.

27. Bertoli, A. C.; Carvalho, R.; Freitas, M. P.; Ramalho, T. C.; Mancini, D. T.; Oliveira, M. C.; de Varennes, A.; Dias, A. Structural determination of Cu and Fe-Citrate complexes: Theoretical investigation and analysis by ESI-MS. *J. Inorg. Biochem.* **2015,** *144*, 31-37.

28. Sekar, R.; Kailasa, S. K.; Abdelhamid, H. N.; Chen, Y. C.; Wu, H. F. Electrospray ionization tandem mass spectrometric studies of copper and iron complexes with tobramycin. *Int. J. Mass Spectrom.* **2013,** *338*, 23-29.

29. Reinoso-Maset, E.; Worsfold, P. J.; Keith-Roach, M. J. Evaluation of electrospray ionisation mass spectrometry as a technique for the investigation of competitive interactions: A case study of the ternary Th-Mn-EDTA system. *Rapid Commun. Mass Spectrom.* **2012,** *26*, 2755-2762.

Chapter 6

Conclusions and Future Work

6.1 Conclusions

Chemical knowledge of metal-ligand systems is important to many areas of research, including protein chemistry, drug development, and environmental chemistry, to name a few. Techniques such as potentiometry, and UV-Visible, infrared, Raman, and NMR spectroscopies are commonly used to investigate such interactions. ESI-MS is another valuable technique that can be used to investigate metal-ligand interaction chemistry because it is a relatively straightforward way to determine stoichiometric ratios of metal-ligand complexes.

In this dissertation, I used ESI-MS to investigate metal-ligand complexes in two very different systems of environmental importance, and from two different angles. In general terms, the first study pertained to the analytical utility of gas-phase complexes, and the second to the characterization of metal-ligand complexes in a complicated system. Thus, my dissertation is divided into two parts, with Chapters 2 and 3 comprising the first part, and Chapters 4 and 5 comprising the second part.

In Part I, Chapter 2, I discussed how the formation of silver and copper organophosphorus pesticide complexes affected the detection of this type of pesticide during ESI-MS analysis. In Part I, Chapter 3, I detailed the effect that copper and silver have on the pesticide fragmentation patterns. In Part II, Chapter 4, I discussed how I used ESI-MS to

characterize the gas-phase complexes formed in the uranyl(VI)/DHIP, uranyl(VI)/DHPD, and uranyl(VI)/DHED systems, and in Part II, Chapter 5, I characterized the gas-phase complexes formed in vanadium(V)/DHIP, iron(III)/DHIP, vanadium(V)/DHPD, and iron(III)/DHPD systems, and discussed the effect of vanadium(V) and iron(III) on uranyl(VI)-DHIP complex formation. Following are the major conclusions I drew from my investigations.

6.1.1 Part I

Organophosphorus pesticides are used to control pests in fruits and vegetables, but are poorly ionized, making their detection in mass-spectrometry-based analyses a challenge. The addition of silver or copper ions to a solution containing fenitrothion (FN), parathion (PT), malathion (MT), or diazinon (DZ) increases the signal-to-background ratio (S/B) and limit of detection (LOD) of the pesticides during ESI-MS analysis due to the formation of charged metal complexes. This increase in the S/B is dependent on the pesticide structure and the metal. Pesticides such as diazinon and malathion, which have more than one coordination site, tend to form a more stable complex with silver and copper, and thus have higher S/B than fenitrothion or parathion, which each have only one coordination site. In addition, the atomic radius of the interacting metal ion is also crucial to the improved detection of the pesticides. Silver has a larger atomic radius than copper. Thus, the addition of silver to a pesticide-containing solution led to a more significant improvement in pesticides S/B than did the addition of copper. The addition of silver to pesticide-containing solutions improved the LOD by ten times, suggesting the formation of silver complexes improved their ionization during ESI process.

I also investigated the fragmentation patterns of organophosphorus pesticides in the absence and presence of silver or copper ions (Chapter 3). During CID of the protonated phosphorothioate pesticides $[FN+H]^+$, $[PT+H]^+$, and $[DZ+H]^+$, thiono-thiolo rearrangement reactions take place, and fragment ions due to both thiono and thiolo isomers are observed. The fragmentation patterns of the metal-pesticide complexes are essentially the same as fragmentation patterns for the protonated pesticide ions, as metal-containing analogues of the fragment ions observed during CID of the protonated ions are observed. However, the presence of the metal ion is believed to inhibit the thiono-thiolo rearrangement, as the thiono isomer of fragment ions resulting from CID of the metal-pesticide complexes is not observed in the mass spectra.

Based on my results, I can conclude that metal ions, especially soft metal ions, have the potential of improving the analytical detection of poorly ionized pesticides during mass spectral analysis. This conclusion is based on analysis of pesticide-containing solutions prepared in the laboratory, and not "real-world" samples, but I anticipate that similar results will be observed in analyses of environmental or food samples after proper sample preparation and separation steps.

6.1.2 Part II

In the second part of this dissertation, I focused on the use of ESI-MS as a characterization tool for identifying the gas-phase complexes formed between uranyl(VI), vanadium(V), and iron(III), and the amidoxime ligands DHIP, DHPD, and DHED. In Chapter 4, I looked at the effects of the structures of DHIP, DHPD, and DHED on the interactions of these ligands with uranyl(VI). DHIP (cyclic) and DHPD (acyclic) serve as

models for the complexing agents used in amidoxime-functionalized sorbents used for the extraction of uranyl(VI) from seawater. DHED was selected to investigate the effect of carbon chain length on uranyl(VI) complexation. The structures of these ligands are shown in Figure 4.1. My results show that the types of complexes formed depend both on the structures of the amidoxime ligands, and on the metal-ligand mole ratio. The relative binding affinity of the ligand towards uranyl(VI) is observed to follow the order DHIP > DHED > DHIP, suggesting that uranyl(VI) binding is more effective in amidoxime ligands with cyclic structures and shorter chain lengths. I therefore conclude that the rigid structure and short chain length increases the stability of the uranyl(VI)-amidoxime complexes formed.

Vanadium and iron are among many ions present in seawater that can compete with uranium for binding sites on amidoxime-functional sorbents. In Chapter 5, I characterized the gas-phase complexes that vanadium(V) and iron(III) form with DHIP and DHPD in other to gain an understanding of how they might interact with the amidoxime-functionalized sorbents. My results show that vanadium(V) and iron(III) interact differently with DHIP and DHPD, as might be expected. While complexes of various stochiometric ratios are observed in all the systems investigated, complexes with 1:2 stoichiometric ratios (metal:ligand) are common to both the iron- and vanadium-amidoxime systems. A metal competition study revealed that the binding strength of DHIP towards the metal in the gas-phase followed the order iron(III) > vanadium(V) > uranyl(VI). This binding order, which gives an insight into the solution chemistry, suggests that the formation of gas-phase complexes between uranyl(VI) and amidoxime ligands will be greatly affected by the presence of either iron(III) or vanadium(V). These results are very important for the

development of technology for efficient extraction of uranyl(VI) from seawater, because of the need to have a technology that is selective only towards uranyl(VI), and economically competitive with the present uranium mining technology. A comparison of my results with results acquired using other techniques, such as potentiometry, UV-Visible spectroscopy, infrared spectroscopy etc, will provide a more in depth understanding of uranyl(VI), iron(III), and vanadium(V) speciation in the presence of amidoxime ligands. However, ESI-MS is a valuable tool for characterization of amidoxime complexes with metals that could have an effect on the extraction of uranyl(VI) from seawater.

6.2 Future Work

Based on the findings from this dissertation, I suggest the following studies or experiments:

1 A reactive desorption electrospray ionization mass spectrometry (DESI-MS) method should be developed for the analysis of organophosphorus pesticides on fruit and vegetable skins. DESI is an ambient ionization technique for mass spectrometry analysis, where a solvent plume generated using electrospray impacts a sample surface under atmospheric conditions. The solvent plume desorbs and ionizes the analytes from the sample surface. The ions created in this desorption/ionization process are carried into the mass spectrometer, where they are analyzed and detected. In this reactive DESI-MS method, silver or copper ions will be added to the spray solvent. As the spray solvent contacts the sample surface, the metal ion is expected to react with any pesticide or pesticides present to form charged complexes, which will then be a carried into the mass

spectrometer and detected. The formation of charged complexes will improved the ionization of the pesticide during DESI-MS. The development of this reactive-DESI technique will result in improved detection of pesticides on the surfaces of fruits or vegetables, without need for tedious and slow sample preparation steps.

2 My study of silver and copper interactions with organophosphorus pesticides could be extended to other types of metal ions, such as iron, cobalt, nickel, and zinc, and other groups of pesticides such as carbamate, anilide, phenylurea, sulfonylurea, and phenyoxyalkanoic acid pesticides because they all have groups that could potentially interact with metals. Iron, cobalt, nickel, and zinc do not give appreciable improvement in S/N or LOD for the organophosphosrus pesticides I examined in this dissertation, but it should be interesting to see if and how they improve the detection of other types of pesticides. Any pesticides to be investigated using the method I proposed in this dissertation should contain a functional group which has accessible electrons that can interact with the coordinating metal ion. For example, phosphorothioates and phosphorodithioates pesticides have a P=S functional group that can interact with silver or copper ions. Since carbamate, anilide, phenylurea, sulfonylurea, and phenyoxyalkanoic acid pesticides all have functional groups that can interact with metal ions, I expect to see a significant improvement in the pesticides' S/B and LOD.

3. The gas-phase complexes formed between DHIP and DHPD and other major ions present in seawater, such as cobalt(II), nickel(II), gold(I) etc. should also be investigated. This will allow the development of a library of information on the

binding of DHIP and DHPD with the major metal ions present in seawater, and make it easier to determine the potential of using DHIP or DHPD for the extraction for valuable metals (such as gold, nickel) from the seawater.

Appendix A

Short Note

Gas-phase Complexes formed by 2, 6-dihydroxyiminopiperidine and Desferrioxamine B in the Presence of Uranyl(VI): A Ligand Competition Study Investigated using Electrospray Ionization Mass Spectrometry

A.1 Introduction

This short note describes the gas-phase complexes formed from solutions containing uranyl(VI) and DHIP in the absence and presence of desferrioxamine B (DES). DES, shown in Figure A.1, is a siderophore generally produced by bacteria and fungi growing under low-iron conditions. Because this naturally-occurring compound has a high affinity for uranyl(VI), it could potentially be used to strip uranyl(VI) from amidoxime-functionalized sorbents. Although hydrochloric acid and carbonate/peroxide solutions have been shown to be effective in stripping uranyl(VI) from amidoxime-based sorbents, the reusability of the sorbent is of major concern.[1, 2] Amidoxime groups are unstable in the presence of solutions containing HCl, thereby reducing the adsorption capacity of the sorbent.[1] We hope that this preliminary study of the gas-phase chemistry of uranyl(VI)-DHIP in the absence and presence of DES will give us an insight into the solution chemistry of the uranyl(VI)/DHIP/DES system. We anticipate that this information will allow us to determine if DES could indeed be used to strip uranyl(VI) from an amidoxime-functionalized sorbent.

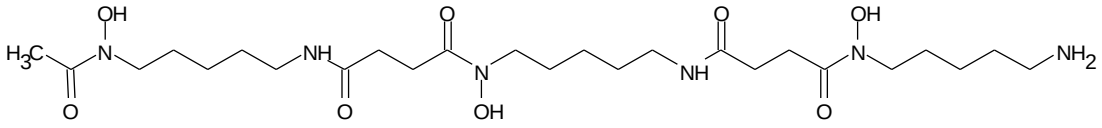

Figure A.1 Molecular structure of desferrioxamine B (DES = $C_{25}H_{48}N_6O_8$).

A.2 Experimental

Desferrioxamine B was purchased from Sigma-Aldrich (St Louis, MO, USA). Other chemicals used have previously been described in Chapters 4 and 5. 10 mM stock solutions of uranyl(VI) and DHIP, and 5 mM of DES were prepared by dissolving the appropriate amount of each compound in 20% (v/v) methanol:water and bringing the volume to 10 mL in a volumetric flask. The solutions containing uranyl(VI) and DHIP, and uranyl(VI), DHIP, and DES were prepared by combining the stock solutions in appropriate ratios and diluting to volume with 20% (v/v) methanol:water in a 10-mL volumetric flask. ESI mass spectra were collected using a Finnigan LCQ Deca XP plus ion trap mass spectrometer (ThermoFinnigan Corporation, San Jose, CA) at the same instrumental settings described in Chapters 4 and 5.

A.3 Results and Discussions

The mass spectrum acquired from a solution containing 0.1 mM each of uranyl(VI) and DES shows peaks corresponding to singly- and doubly-charged 1:1 uranyl(VI):DES complexes at *m/z* 829 ($[UO_2+(DES-H)]^+$) and *m/z* 415 ($[UO_2+(DES-H)]^{2+}$) (Figure A.2, Table A.1). The peaks at *m/z* 561 and 281 are due to $[DES+H]^+$ and $[DES+2H]^{2+}$ respectively.

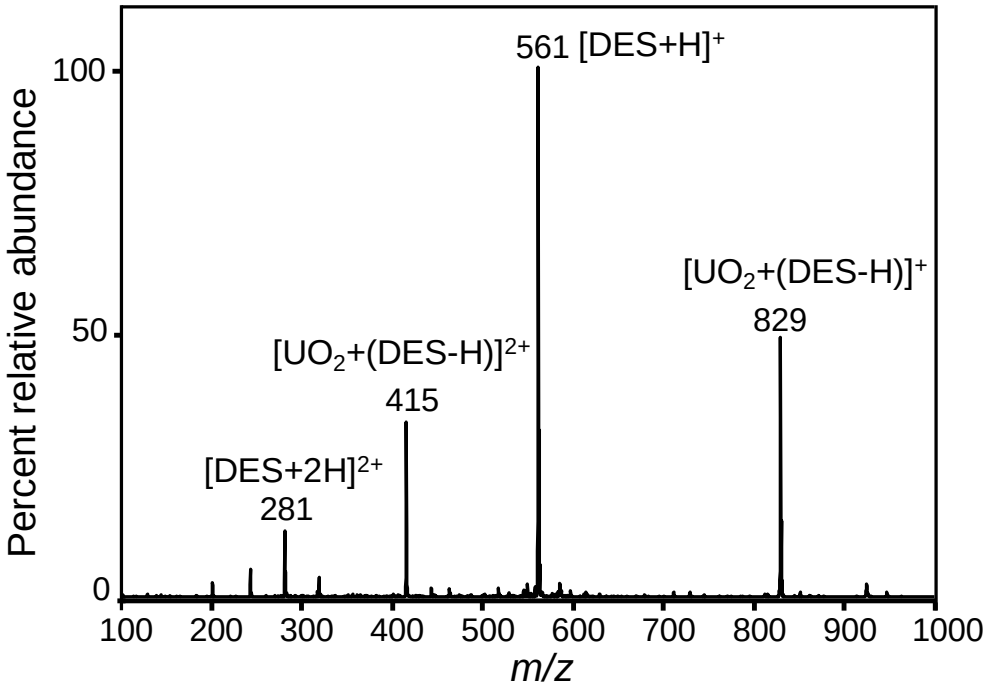

Figure A.2 ESI-MS mass spectrum acquired from a solution containing 0.1 mM each of uranyl(VI) and desferrioxamine B.

Table A.1 ESI-MS peak assignments for DES-containing species.

Solution	**Species**	**Observed** ***m/z***	**Theoretical** ***m/z****
DES			
($C_{25}H_{48}N_6O_8$)	$[DES+2H]^{2+}$	281.2	281.2
	$[DES+H]^{+}$	561.3	561.4
	$[DES+Na]^{+}$	583.3	583.3
Uranyl(VI)-DES			
	$[UO_2+(DES)]^{2+}$	415.3	415.2
	$[UO_2+(DES–H)]^{+}$	829.3	829.4

The competition between DHIP and DES for uranyl(VI) was investigated by monitoring changes in the mass spectra upon addition of a solution containing DES to a solution containing uranyl(VI) and DHIP. The competition between the ligands for

uranyl(VI) was tracked by monitoring the changes in the ion intensities of uranyl(VI)-DHIP-containing ions and uranyl(VI)-DES-containing ions. Figure A.3 shows the effect of DES on the relative abundances of uranyl(VI) and DHIP containing ions. Increasing the concentration of DES resulted in a decrease in the relative abundances of uranyl(VI)-DHIP species. The peaks at *m/z* 412, 430, and 555, which were previously assigned as $[UO_2+(DHIP-H)]^+$, $[UO_2+(DHIP-H)+H_2O]^+$ and $[UO_2+(DHIP-H)+DHIP]^+$ in Table 4.1 were observed to decrease in relative abundance, while the relative abundance of the uranyl(VI)-DES complex, $[UO_2+(DES-H)]^+$ (*m/z* 829) increased with increasing concentration of DES. The peaks at *m/z* 561 and 583 are due to the protonated and sodiated DES ions.

The increase in abundance of $[UO_2+(DES-H)]^+$ (*m/z* 829) and a decrease in the abundances of ions arising from urany(VI)-DHIP complexes seen in Figure A.3 a-e could be taken as an indication that DES strips uranyl(VI) from the uranyl(VI)-DHIP complex. This could indeed be the case. However, the high relative abundance of DES-containing ions in Figure A.3 could also be because DES has a higher response factor than DHIP. As discussed in Chapter 1, response factor is a measure of the amount of the complex in solution that is transferred to gas-phase ion during the ESI process. A high DES response factor could potentially be contributing to the high intensities of uranyl(VI)-DES-containing ions observed in the mass spectra. Investigating the uranyl(VI)/DES/DHIP system using another technique, such as UV-Visible, fluorescence or NMR spectroscopy could help in clarifying the chemistry behind the spectra shown in Figure A.3. However, the preliminary results shown here suggest that DES could potentially be used to strip uranyl(VI) from amidoxime-functionalized sorbents.

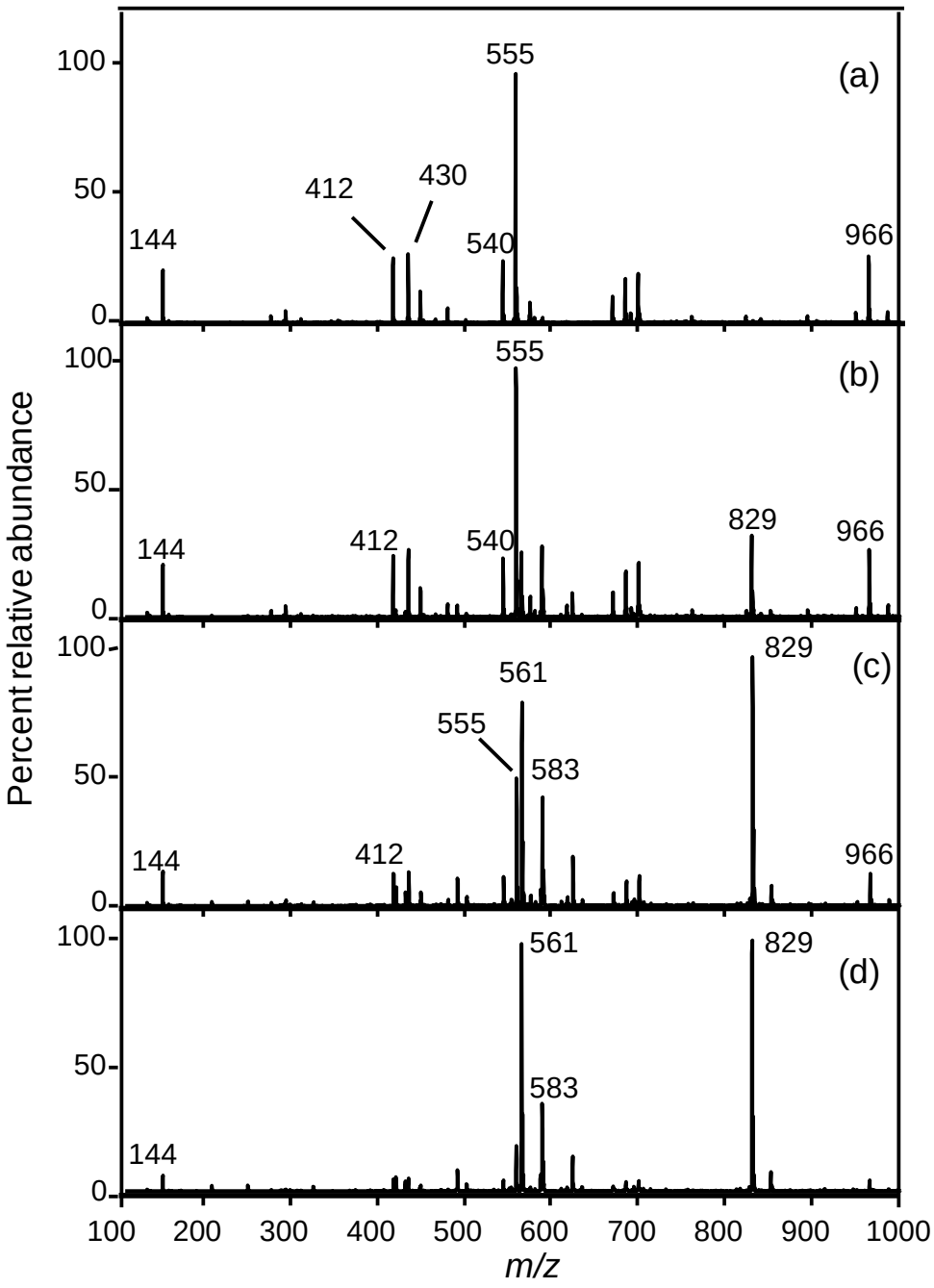

Figure A.3 ESI-MS mass spectra acquired from solutions containing 0.1 mM uranyl(VI), 0.5 mM DHIP, and (a) 0 μM DES, (b) 5 μM DES, (c) 20 μM DES, or (d) 40 μM DES.

References

1. Astheimer, L.; Schenk, H. J.; Witte, E. G.; Schwochau, K. Development of sorbers for the recovery of uranium from seawater. 2. The accumulation of uranium from seawater by resins containing amidoxime and imidoxime functional-groups. *Sep. Sci. Technol.* **1983,** *18* (4), 307-339.
2. Pan, H. B.; Liao, W.; Wai, C. M.; Oyola, Y.; Janke, C. J.; Tian, G.; Rao, L. Carbonate-H_2O_2 leaching for sequestering uranium from seawater. *Dalton Trans.* **2014,** *43* (28), 10713-10718.

Appendix B

Letters of Permission for Copyright Material

Figure 1.1 Copyright Permission

JOHN WILEY AND SONS LICENSE TERMS AND CONDITIONS

Sep 20, 2015

This Agreement between Adetayo M Mustapha ("You") and John Wiley and Sons ("John Wiley and Sons") consists of your license details and the terms and conditions provided by John Wiley and Sons and Copyright Clearance Center.

License Number	3711560505530
License date	Sep 17, 2015
Licensed Content Publisher	John Wiley and Sons
Licensed Content Publication	Mass Spectrometry Reviews
Licensed Content Title	Practical implications of some recent studies in electrospray ionization fundamentals
Licensed Content Author	Nadja B. Cech, Christie G. Enke
Licensed Content Date	May 1, 2002
Pages	26
Type of use	Dissertation/Thesis
Requestor type	University/Academic
Format	Print and electronic
Portion	Figure/table
Number of figures/tables	1
Original Wiley figure/table number(s)	Figure 1
Will you be translating?	No
Title of your thesis / dissertation	Using Electrospray Ionization Mass Spectrometry for Understanding Metal-Ligand Interactions: Silver and Copper Complexes with Organophosphorus Pesticides, and Uranium, Vanadium and Iron Complexes with Amidoxime Ligands
Expected completion date	Sep 2015
Expected size (number of pages)	200

Requestor Location	Adetayo M Mustapha 875 Perimter Drive MS 2343 MOSCOW, ID 83844 United States Attn: Adetayo M Mustapha
Billing Type	Invoice
Billing Address	Adetayo M Mustapha 875 Perimter Drive MS 2343 MOSCOW, ID 83844 United States Attn: Adetayo M Mustapha
Total	0.00 USD

Terms and Conditions

TERMS AND CONDITIONS

Chapter 2 Copyright Permission

JOHN WILEY AND SONS LICENSE TERMS AND CONDITIONS

Aug 17, 2015

This Agreement between Adetayo M Mustapha ("You") and John Wiley and Sons ("John Wiley and Sons") consists of your license details and the terms and conditions provided by John Wiley and Sons and Copyright Clearance Center.

License Number	3691470652480
License date	Aug 17, 2015
Licensed Content Publisher	John Wiley and Sons
Licensed Content Publication	Journal of Mass Spectrometry
Licensed Content Title	Gas-phase copper and silver complexes with phosphorothioate and phosphorodithioate pesticides investigated using electrospray ionization mass spectrometry
Licensed Content Author	Adetayo M. Mustapha, Sofie P. Pasilis
Licensed Content Date	Jan 19, 2015
Pages	8
Type of use	Dissertation/Thesis
Requestor type	Author of this Wiley article
Format	Print and electronic
Portion	Full article
Will you be translating?	No
Title of your thesis / dissertation	Using Electrospray Ionization Mass Spectrometry for Understanding Metal-Ligand Interactions: Silver and Copper Complexes with Organophosphorus Pesticides, and Uranium, Vanadium and Iron Complexes with Amidoxime Ligands
Expected completion date	Sep 2015
Expected size (number of pages)	200
Requestor Location	Adetayo M Mustapha 875 Perimter Drive MS 2343 MOSCOW, ID 83844 United States Attn: Adetayo M Mustapha

Billing Type	Invoice
Billing Address	Adetayo M Mustapha 875 Perimter Drive MS 2343 MOSCOW, ID 83844 United States Attn: Adetayo M Mustapha
Total	0.00 USD

Terms and Conditions

TERMS AND CONDITIONS

Chapter 4 Copyright Permission

JOHN WILEY AND SONS LICENSE TERMS AND CONDITIONS

Aug 17, 2015

This Agreement between Adetayo M Mustapha ("You") and John Wiley and Sons ("John Wiley and Sons") consists of your license details and the terms and conditions provided by John Wiley and Sons and Copyright Clearance Center.

License Number	3691480262809
License date	Aug 17, 2015
Licensed Content Publisher	John Wiley and Sons
Licensed Content Publication	Rapid Communications in Mass Spectrometry
Licensed Content Title	Probing uranyl(VI) speciation in the presence of amidoxime ligands using electrospray ionization mass spectrometry
Licensed Content Author	Adetayo M. Mustapha, Sofie P. Pasilis
Licensed Content Date	Sep 1, 2013
Pages	8
Type of use	Dissertation/Thesis
Requestor type	Author of this Wiley article
Format	Print and electronic
Portion	Full article
Will you be translating?	No
Title of your thesis / dissertation	Using Electrospray Ionization Mass Spectrometry for Understanding Metal-Ligand Interactions: Silver and Copper Complexes with Organophosphorus Pesticides, and Uranium, Vanadium and Iron Complexes with Amidoxime Ligands
Expected completion date	Sep 2015
Expected size (number of pages)	200

Requestor Location	Adetayo M Mustapha 875 Perimter Drive MS 2343 MOSCOW, ID 83844 United States Attn: Adetayo M Mustapha
Billing Type	Invoice
Billing Address	Adetayo M Mustapha 875 Perimter Drive MS 2343 MOSCOW, ID 83844 United States Attn: Adetayo M Mustapha
Total	0.00 USD

Terms and Conditions

TERMS AND CONDITIONS